ISSN: 2588-5596

JGT

Journal of Gas Technology

Volume 8 . Issue 2. Winter 2023 . www.jgt.irangi.org

Journal of Gas Technology, JGT

Volume 8, Issue 2, Winter 2023

Publisher
Iranian Gas Institute

Contact Information
http://jgt.irangi.org
Email: ijgt.igi@gmail.com

EISSN: 2588-5596

Open Access Journal
Journal of Gas Technology is a peer reviewed, open access journal.

JOURNAL OF GAS TECHNOLOGY

Volume 8, Issue 2, Winter 2023

Annual Names of Reviewers

Ali Vatani
University of Tehran

Mastaneh Hajipour
Islamic Azad University, Science and Research Branch

Saeid Jamshidi
Sharif University of Technology

Morteza Zivdar
University of Sistan and Baluchestan

Amir Hossein Mohammadi
University of KwaZulu-Natal, South Africa

Masoud Aghajani
Petroleum University of Technology

Rahbar Rahimi
University of Sistan and Baluchestan

Leila Moharrery
Islamic Azad University, Robat Karim Branch

Yahya Balouchi
University of Sistan and Baluchestan

Seyed Mohsen Peyghambarzadeh
Islamic Azad University, Mahshahr branch

Sepideh Amiri Tavasoli
Hormozgan Province Gas Company

kamran keynejad
University of Tehran

Mehdi Moayed Mohseni
Islamic Azad University, Science and Research Branch

Ebrahim Biniaz Delijani
Islamic Azad University, Science and Research Branch

Reza Mohebian
University of Tehran

Sahar Amiri
Islamic Azad University, Science and Research Branch

Ashkan Vatandoost
Mapsa Technology center(MTC), MAPSA Company

Table of Contents

JOURNAL OF GAS TECHNOLOGY

Volume 8 /Issue 2/ Winter 2023 / Pages 5-26

Journal Home page: http://jgt.irangi.org

Selection of Candidates and Formation Damage Advisor with an Expert System

Ahmad Rigi[1], Mohamad Norouzi Delaviz[1], Saman Jahanbakhshi[2*]

1. M.Sc. of Petroleum Engineering, Abdal Industrial Projects Management Co., MAPSA Technology Center, Tehran, Iran
2. Assistant Professor, School of Mining Engineering, College of Engineering, University of Tehran, Tehran, Iran

ARTICLE INFO

ORIGINAL RESEARCH ARTICLE

Article History:
Received: 04 November 2023
Revised: 07 December 2023
Accepted: 30 December 2023

Keywords:
Expert systems
Matrix acidizing
Formation damage
Candidate selection
Well productivity

ABSTRACT

In the lifecycle of an oil well, numerous factors such as pressure drop, partial perforation, turbulent flow, and formation damage can adversely affect its productivity. Identifying and addressing these issues, especially formation damage, is crucial. Acid treatment is commonly used to mitigate such formation damage, thereby enhancing well productivity. Traditionally, the selection of wells for acid treatment and the identification of formation damages have relied on extensive geological and engineering analyses. These conventional methods, while thorough, are time-consuming and involve the examination of complex geochemical, geophysical, and geological data. Accordingly, the current study introduces an expert system designed to streamline these processes. Expert systems, capable of automated and rapid data analysis, offer significant advantages by accelerating decision-making and improving efficiency. The expert system developed in this research demonstrates notable proficiency in processing intricate datasets, thus enhancing productivity and reducing the probability of errors. Its predictive capabilities also enable proactive management of wells. This research employs an expert system to analyze ten wells, identifying six as suitable candidates for acidizing. The system effectively detects potential formation damages in these wells, demonstrating its accuracy in diagnosis and decision-making. The adoption of expert systems in high-uncertainty scenarios requiring precise analysis is promising. Utilizing more routine or standard algorithms and mathematical models, these systems can significantly improve decision-making processes, predictive accuracy, and operational efficiency in oil and gas reservoirs. Improved decision-making is a key benefit as these systems, with comprehensive and analyzed data, enable more informed and effective decisions. In this study, an expert system is developed for selecting wells suitable for acid treatment and diagnosing formation damage types. Of the ten wells analyzed, six were deemed suitable for acid treatment. The system's ability to detect potential formation damages in each well highlights its effectiveness. These systems, employing algorithms and mathematical models for event modeling and prediction, aid in enhanced, faster decision-making processes. The use of expert systems in areas with high uncertainty and the need for precise modeling is valuable, contributing to improved operational efficiency and productivity in the oil and gas sector.

DOR: 20.1001.1/JGT.2024.2020698.1033

How to cite this article
A. Rigi, M. Norouzi Delaviz, S. Jahanbakhshi, Selection of Candidates and Formation Damage Advisor with an Expert System. Journal of Gas Technology. 2023; 8(2): 5 -26. (https://jgt.irangi.org/article_712118.html)

* Corresponding author.
E-mail address: jahanbakhshi@ut.ac.ir, (S. Jahanbakhshi).

Available online 31 December 2023

1. Introduction

Improved Oil Recovery (IOR) operations are a fundamental aspect of the oil and gas industry, aimed at increasing the recovery of oil from petroleum reservoirs. Typically, only about 30-40% of the oil in a reservoir is extracted using conventional methods, either naturally or through primary recovery techniques. Consequently, IOR operations, which use methods like acidizing, water flooding, gas injection, and the application of polymers, surfactants, and nanotechnology, are crucial for increasing oil recovery rates. Acidizing, a primary and effective IOR method, is divided into matrix acidizing and acid fracturing. Matrix acidizing, common in Iran and low-permeability formations, is favored for its simplicity and cost-effectiveness. Intelligent acidizing uses reservoir modeling software, acidizing operation simulations, and production data analysis. This approach significantly enhances the efficiency and optimization of acidizing methods and additives. In the oil and gas industry, Artificial Intelligence (AI) techniques like neural networks, fuzzy logic, and evolutionary algorithms are revolutionizing key practices, especially in reservoir simulation and drilling optimization (Braswell 2013). Expert systems are increasingly used in decision-making for balanced or overbalanced drilling (Garrouch and Labbabidi 2003). Three-dimensional convolutional neural networks have demonstrated superiority over human descriptor-based models in accurately predicting catalyzed acid reaction rates (Chew, Jiang et al. 2020). Similarly, AI methods such as fuzzy logic have advanced the prediction of pore pressure during drilling and are more time-efficient in geological and engineering evaluations compared to traditional methods (Abdulmalek, Elkatatny et al. 2018). AI methods require less geological and engineering evaluation time compared to traditional methods. (Zoveidavianpoor, Samsuri and Shadizadeh 2012). Furthermore, AI's role in optimizing reservoir simulation and improving well selection for workover operations has been notably demonstrated (Umoh 2019). This study aims to create an expert advisory system that can identify suitable wells for acidizing operations more accurately and quickly and determine the formation damage more precisely. The main goal of this study is to create and execute an expert system that uses key parameters to identify damaged wells This study aims to develop an expert advisory system for more accurate and rapid identification of suitable wells for acidizing operations and precise determination of formation damage. The primary goal is to create and implement an expert system that uses key parameters to identify damaged wells and assess damage types. By identifying essential attributes and correlating them with observed outcomes in previous instances, this system is applied to acidizing operations, bridging the gap between manual systems and acidizing operations through sophisticated AI integration.

2. Methodology

Prior to initiating the acidizing operation, identifying wells suitable for acid treatment is crucial. A comprehensive understanding of potential formation damages is also essential before embarking on the acidizing process (Xiong, Robinson and Foh 2001). Accordingly, this research has been divided into two primary sections: 1) Selection of candidate wells for acidizing, and 2) Diagnosis of formation damage.

2.1. Selection of Candidate Wells

In the evaluation of well performance, the initial step involves assessing the skin factor, a critical parameter determined through pressure transient analysis. In scenarios lacking pressure data, the skin factor can be estimated by considering various factors such as well characteristics, flow conditions, reservoir properties, and the ratio of actual to ideal flow rate. These elements collectively contribute to the total skin factor. For potential acidizing operations, a general guideline is used: if the sandstone skin factor is greater than or equal to 0, and the carbonate skin factor is greater than or equal to -2, the well qualifies as a candidate for acidizing. It's vital to recognize

that the skin factor derived from pressure data represents the total skin factor, which is calculated as follows (Abobaker, Elsanoose et al. 2022):

$$S = S_M + D \times Q \quad (1)$$

The total skin factor is the aggregate of the mechanical skin factor and the dynamic skin factor. The latter arises from turbulent flow, a common occurrence in gas wells. To calculate the mechanical skin factor, one follows a specific formula (Furui, Zhu and Hill 2005):

$$S_M = S_{pp} + S_\Theta + S_d + S_g + S_p + S_f \quad (2)$$

In the above equation, S_M represents the mechanical skin factor, S_{pp} represents the partial perforation skin factor, S_Θ represents the skin factor resulting from the azimuth, Sd represents the skin factor from the damaged zone, S_g represents the gravel pack skin factor, S_p represents the skin factor from perforations, and S_f represents the frac pack (frac pack is a combination of hydraulic fracturing and sand control techniques used in oil and gas wells, especially in formations with sand issues.) skin factor. Furthermore, the dynamic skin factor is calculated as follows (Yildiz 2006):

$$D = D_d + D_r + D_g + D_C + D_f \quad (3)$$

In the above equation, D represents the total dynamic skin factor, D_d represents the dynamic skin factor from the damaged zone, D_r represents the dynamic reservoir skin factor, D_g represents the dynamic skin factor from the gravel pack, D_c represents the crushed zone, and D_f represents the frac pack. The total skin factor is the sum of the mechanical and dynamic skin factors. The dynamic skin factor, pertinent to turbulent flow conditions, is disregarded if the wellbore fluid flow is laminar. Therefore, before selecting a well for acidizing, addressing any mechanical impediments that might cause well-related issues is crucial. These include factors like perforation, partial perforation, gravel pack, turbulent flow, low reservoir pressure requiring gas lift, chokes, and artificial lift operation challenges. A key goal in sandstone formations is restoring damaged areas, aiming to remove up to 90% of the damage. Assessing the economic viability of the acidizing operation, considering costs, is also essential. Notably, for wells with permeability below 10 md in oil wells and 1 md in gas wells, hydraulic fracturing is typically advised (Figure 1) (Zhang, Guo et al. 2021).

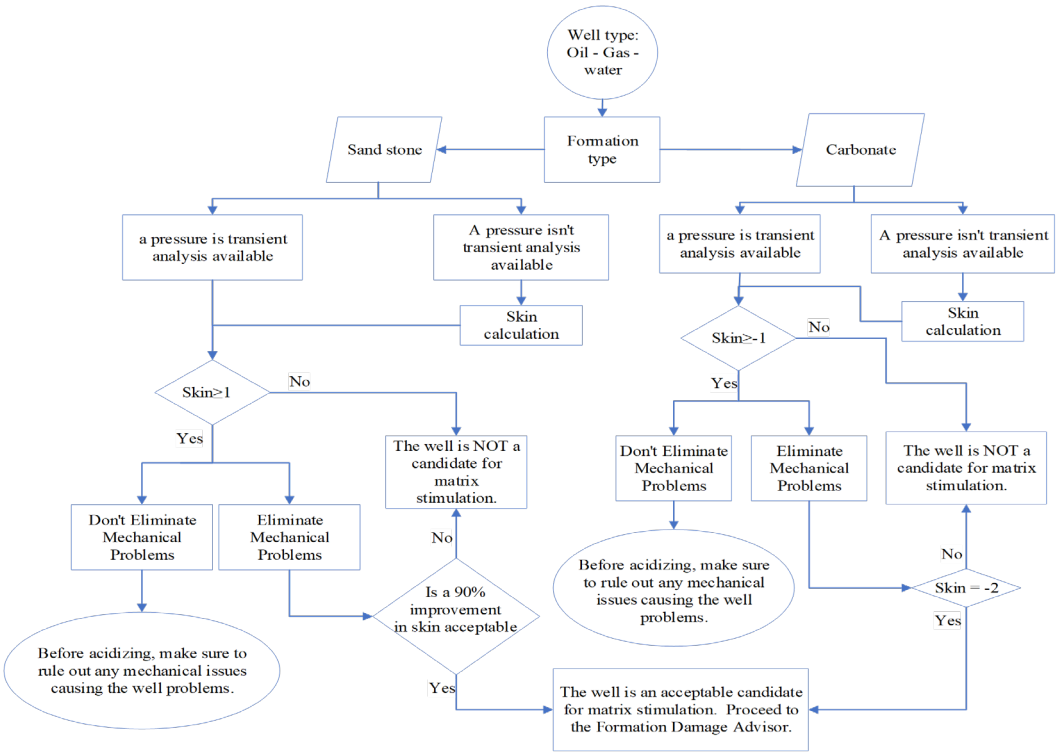

Figure 1. Candidate Selection

2.2. Diagnosis of Formation Damage

Throughout a well's lifecycle, from inception to closure, it undergoes various states such as newly completed, workover/stimulation, huff and puff, continuous operation, steam-enhanced operation, corrosion inhibition, and suspension (wells that are not currently in active production or injection service but have not been permanently abandoned). During these stages, the formation may suffer various damages, including wettability alteration, emulsion blocking, bacterial and organic deposits like asphaltene and paraffin, scale deposits, fine migration, polymer and mixed deposits (presence Scale layered with oil or paraffin), solid mud (excluding filter cake, solid mud damage from drilling mud components plugging formation pores is different from filter cake formed by reservoir fluids), solid completion-workover/stimulation fluid (damage caused by solid particles from well completion fluids, acidizing, and workover operations) residues, precipitates, clay swelling, and water blocking (Xu, Kang et al. 2016). This study leverages insights from scientific articles and existing software in reservoir damage detection to identify potential reservoir damages. The primary objective is to enhance the understanding and effectiveness of acidizing operations.

2.2.1.Wettability Alteration and Emulsion Blocking

Wettability alteration is a common occurrence in newly completed wells, particularly when using oil-based drilling mud with high losses. This phenomenon arises from the interaction between the drilling mud and the rock surface, resulting in a shift in wettability from water-wet to oil-wet. Additionally, wettability alteration may lead to unexpected gradual or sudden declines in well production rates or even total well lockup. These changes are particularly significant when the reduction in well rates cannot be attributed to other factors such as scale deposits or tubing issues but rather to interaction between rock and fluid affinity. Emulsion formation can be diagnosed based on several factors, including the appearance of emulsion at the surface, the tendency of oil to form slugs or emulsions, minimal viscosity differences between oil and water, a high acid number of the oil, and a sudden decline in productivity index after well stimulation. These factors can alter the rock's surface properties, affecting its interaction with different fluids and the probability of particle migration. Therefore, this can lead to the formation of emulsions that obstruct flow pathways within the reservoir or production equipment. Furthermore, the manner of well completion, such as gravel pack completion with perforated casing or pre-packed screens (consisting of a gravel layer between two screens to wellbore stabilization), can also influence emulsion occurrence due to the potential for emulsions to form and obstruct flow within the completion design. During workover operations on gas and oil-producing wells, it is imperative to identify the factors contributing to emulsion formation. During stimulation operations on oil wells, especially when using HCl or HCl-HF acidizing fluids, can heighten the formation's susceptibility to emulsion occurrence. This susceptibility arises from chemical or physical alterations induced by the acidizing fluids, leading to changes in the properties of the oil and reservoir, thereby promoting emulsion formation. Additionally, in the context of sandstone reservoirs, the application of cationic surfactants and observing a sudden reduction in well rate holds the potential to cause wettability alteration damage. The use of cationic surfactants can alter the surface properties of the reservoir, impacting wettability characteristics (Figure 2) (Liew, Gholami et al. 2019).

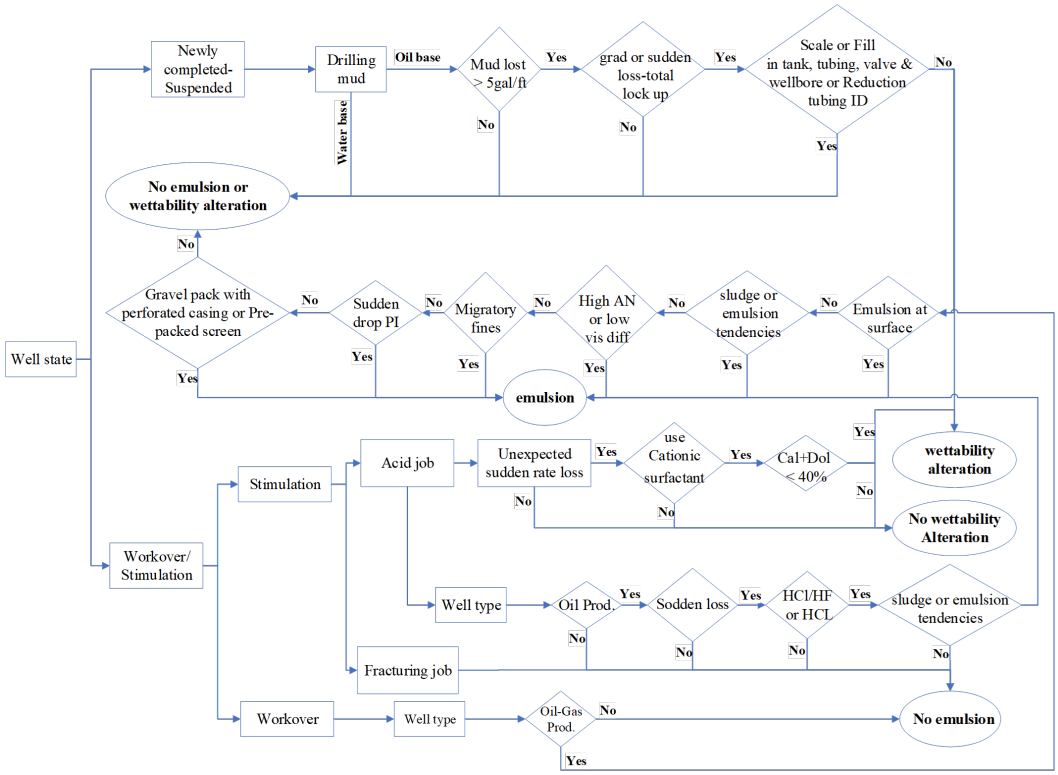

Figure 2. Diagnosis of Wettability Alteration and Emulsion Blocking

2.2.2. Bacteria, Asphaltene and Injection Carryover

Bacterial damage in injection wells can arise from various factors. Continuous operations (uninterrupted production or injection process within a well over an extended period) in these wells often create environments that promote bacterial growth, leading to bacterial damage. In wells located in H_2S-containing reservoirs, increased pressure or reduced injection rates can further exacerbate this damage. These altered conditions are conducive to bacterial proliferation, negatively affecting the well. In non-sour reservoirs, the presence of high levels of bacteria or the use of bacteria treatment operations can also lead to additional well damage. Scientific evidence indicates that these factors significantly influence the occurrence and progression of bacterial damage in oil wells. Asphaltene deposition can arise from alterations in thermodynamic conditions within the reservoir and oil and gas production wells. These changes may encompass fluctuations in temperature, pressure, shifts in the chemical composition of reservoir fluids, or variations in the pH of the reservoir water, all contributing to the formation of asphaltene deposits. Furthermore, factors such as fluid density, the mixing of fluids with diverse compositions, and chemical reactions resulting from changes in temperature and pressure can also contribute to the formation of asphaltene deposits. Observing an unexpected gradual or sudden decrease in well rate, along with the presence of paraffin and asphaltene in reservoir fluid analysis, a resin-to-asphaltene ratio of less than one, or the floatability of solid particles on water, accompanied by solid and sooty burns (solid particles that, when burned, leave a sooty residue) that are soluble in xylene, indicate the potential for asphaltene deposition. The presence of paraffin and asphaltene in reservoir fluid analysis suggests that the reservoir fluid contains components with a tendency to form deposits. A resin-to-asphaltene ratio of less than one indicates a chemical imbalance in crude oil composition, potentially leading to asphaltene precipitation. This imbalance is critical as resins typically stabilize asphaltenes in oil. Insufficient resin levels allow asphaltenes to precipitate, forming

solid deposits that can cause operational issues. The detection of asphaltene deposits can be indicated by the floatability of solid particles on water and the observation of solid, sooty burns soluble in xylene, which are characteristic signs of asphaltene presence. When solid particles can float on water, it suggests that they have a lower density than water, which is characteristic of asphaltene deposits. Additionally, the presence of solid, sooty residues that dissolve in xylene is indicative of organic, carbonaceous materials, commonly associated with asphaltene deposits. Injection carryover damage (injection carryover damage refers to issues in injection wells caused by the injected water's quality or the conditions of injection), a concern in injection wells, is mainly related to the source of the injection water or injection conditions. It can be categorized into three main groups: emulsion, formation solids, and oil damages. Emulsion damage arises when emulsions form due to mixing injection water with reservoir fluids, leading to stable emulsions that damage both the reservoir and the injection system. Formation solid damage is caused by the deposition of solids in the well, impeding injection water flow and affecting well performance. Oil damage occurs when oil is carried into the injection system, potentially causing plugging and reduced injectivity. Monitoring injection pressure and rate is essential, as fluctuations in these can indicate injection carryover damage. The presence of emulsion or oil on injection water filters, incompatible water additives, or oil leaks from injection equipment into the stream are signs of potential oil or emulsion damage (Figure 3).

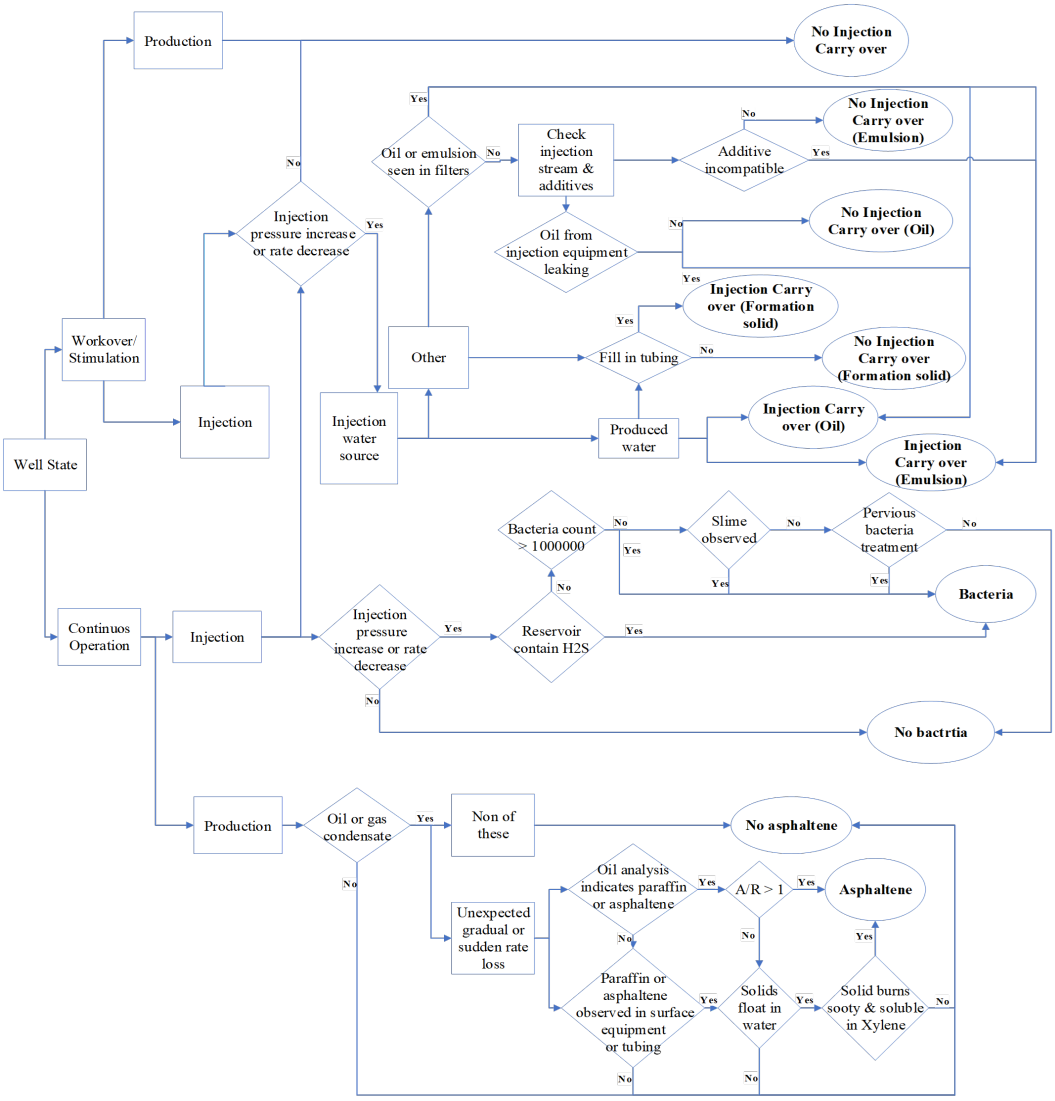

Figure 3. Diagnosis of Bacteria, Carry Over and Asphaltene

2.2.3. Scale Deposition

Scale deposition is a prevalent issue in production wells, particularly during workover, stimulation, continuous operation with steam (This method is used in heavy oil reservoirs to heat the oil with steam, making it easier to extract. It can be cyclic or part of a continuous steam flooding operation), and huff and puff processes. Analyzing produced fluids during workover and stimulation is essential for assessing potential scale damage and reviewing the field history. Even if no water is produced from the well, the potential for scale damage should not be overlooked. Field history analysis plays a crucial role in identifying scale damage in production wells, offering insights into reservoir performance, fluid composition, production rates, and previous pressure maintenance issues. This information is key to understanding reservoir dynamics and potential scale-related problems. During pressure maintenance operations in oil and gas reservoirs, the possibility of scale damage tends to be lower. This is because sustained pressure plays a crucial role in mitigating scale accumulation. Scale formation, often involving minerals like calcium carbonate or barium sulfate, is a common issue in reservoirs and production equipment. It leads to reduced flow efficiency and potential damage to equipment. Pressure maintenance, achieved through methods such as water flooding (Moghadasi, Jamialahmadi et al. 2004) or gas injection, helps to maintain reservoir pressure at levels that deter the chemical conditions necessary for scale precipitation. This happens because a decrease in pressure can trigger changes in fluid temperature and composition, which promotes mineral supersaturation and subsequent scale deposition. In assessing scale deposition in fields where pressure is maintained, factors such as wellhead pressure (WHP) are critical. Changes in WHP without operator intervention may indicate scale deposition, as scale can restrict fluid flow in the wellbore, thereby altering WHP. Monitoring and analyzing changes in WHP are vital for identifying and addressing potential scale issues. Accumulating scale can constrict the flow area, leading to an increase in pressure drop and potentially affecting production rates. Significant changes in production conditions, such as flow rates or fluid compositions, can influence the probability of scale formation. For instance, variations in temperature, pressure, or chemical composition can encourage the precipitation of scale-forming minerals. A sudden increase in water cuts could signal scale issues, as scale deposits can disrupt fluid separation processes, leading to higher water production. Water flooding in the field can alter the reservoir's chemical and physical environment, potentially promoting scale formation due to changes in water chemistry and rock-fluid interactions. Crossflow between different reservoir layers can lead to changes in pressure and fluid composition, which may influence scale deposition. Additionally, scale deposits reducing the tubing's inner diameter can result in flow restrictions and increased pressure drops. The presence of scale in production equipment is a clear indication of potential scale damage. Thus, monitoring these factors is vital

for identifying and addressing scale deposition. Regular monitoring and analysis of production well conditions are crucial for mitigating scale deposition. Implementing scale inhibition treatments and chemical squeeze programs can help in preventing and controlling scale formation. Periodic well cleanouts and scale removal operations are important to maintain optimal production rates. Continuous monitoring of WHP, fluid composition, and production conditions enables operators to proactively address potential scale issues, ensuring efficient and smooth production operations. Furthermore, the use of advanced modeling and predictive analytics can assist in forecasting and managing scale-related challenges, optimizing reservoir performance and maximizing production efficiency. After considering the above factors to identify scale deposits and meeting at least one of them in the field of pressure maintenance, the probability of scale formation is high. If any of the following factors are observed, scale deposits are present: an increase in gamma-ray levels can indicate the presence of Scale-$BaSO_4$ and $SrSO_4$ due to the natural radioactive properties of these scale-forming substances. This phenomenon allows Scale-$BaSO_4$ and $SrSO_4$to absorb and emit gamma rays, which can be detected by specialized equipment. When the pH of produced water drops below 6, it suggests that the water is turning acidic and can cause the breakdown of carbonate minerals in the formation, like limestone (primarily composed of calcium carbonate, $CaCO_3$) (Qazvini, Golkari et al. 2021). This breakdown can lead to the formation of calcium carbonate scale or $CaCO_3$. High CO_2 levels in produced water may also suggest the possible existence of carbonate scales, like $CaCO_3$ and $MgCO_3$, as carbon dioxide (CO_2) reacts with calcium and magnesium ions in the water to create carbonate scale, The detection of sour gas in a reservoir, typically containing hydrogen sulfide (H_2S), can indicate the potential for forming iron sulfide (FeS) scale. When hydrogen sulfide is present in the reservoir fluids and contacts iron compounds, like iron ions (Fe^{2+}), it can lead to the formation of an iron sulfide scale, A NaCl (sodium chloride) concentration above 50,000 ppm (parts per million) may suggest the possibility of sodium chloride (NaCl) scale formation. Elevated NaCl levels in water can result in solution saturation and the subsequent precipitation of NaCl as scale in production equipment and reservoir formations, The absence of inhibitors for tubular can indeed lead to the possibility of scale Fe_2O_3 (iron oxide) deposition. Without the use of appropriate inhibitors, tubular and other production equipment can be more susceptible to corrosion, which can result in the formation of iron oxide scale. If pressure maintenance operations are not conducted in the field, the observation of any of these indicative factors mentioned above indicates a significant risk of scale deposition damage. SiO_2 scale, commonly found in oil-producing wells during continuous operations with steam and huff and puff, is identified by a reduction in the tubing's inner diameter, which leads to decreased well productivity. This damage is associated with the accumulation of SiO_2 compounds in the wellbore, particularly during steam injection processes (Figure 4) (Khurshid, Al-Shalabi and Alameri 2020) (Moghadasi, Jamialahmadi et al. 2004).

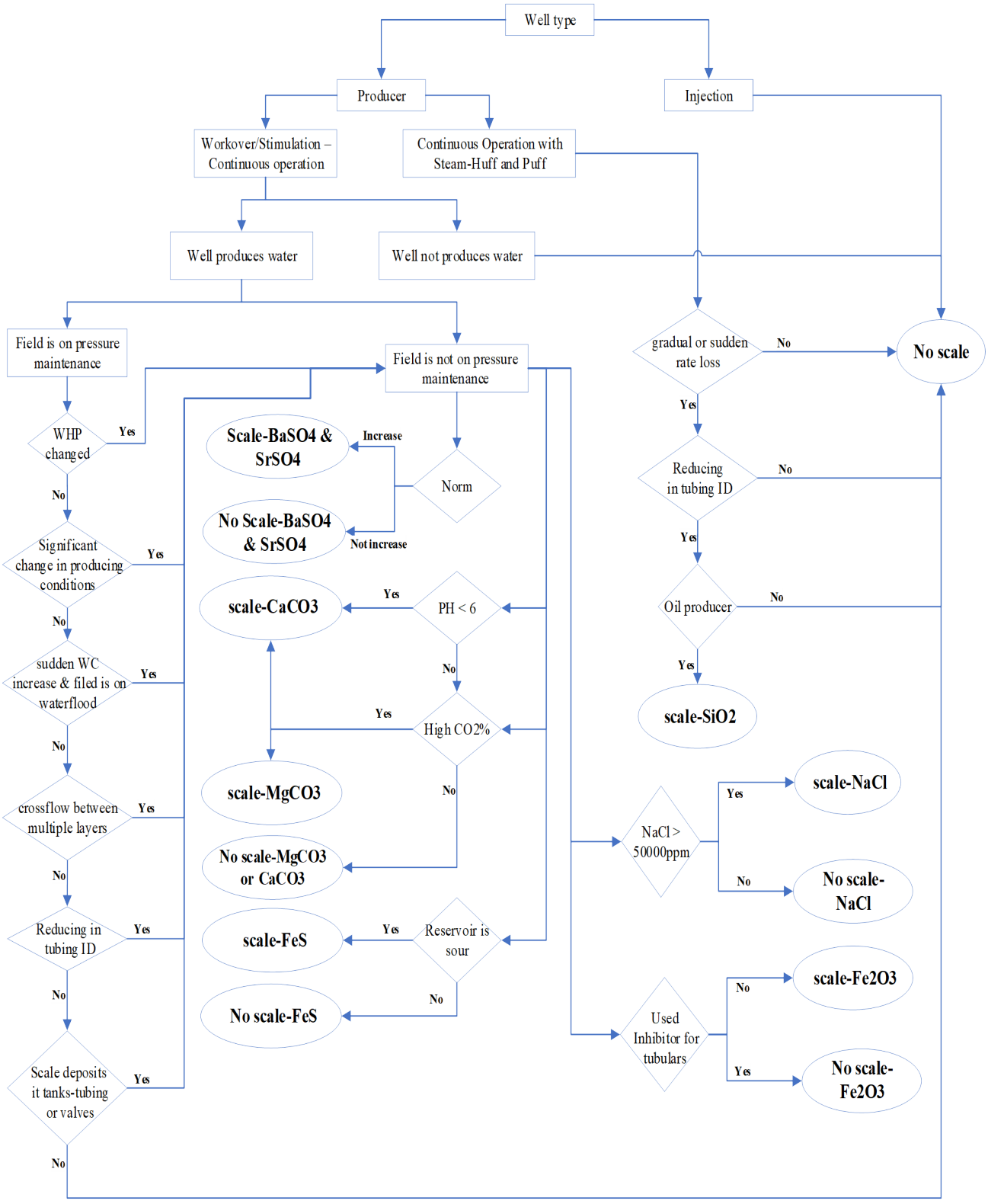

Figure 4. Diagnosis of Scale Deposition

2.2.4. Fine Migration, Polymer and Mixed Deposits

In all well states, potential issues such as polymer damage, fine migration, and mixed deposits must be considered. In a newly completed well, it is important to monitor for signs of polymer damage, particularly if a polymer-based fluid was used during the completion operation. This issue may be indicated by a gradual or sudden decrease in the well rate, in the absence of observed fill or scaling in the production equipment. If fill or scale deposits are observed in the production equipment, or if the well is not newly completed, the potential for pumping fluids into the damaged zone should be investigated. Furthermore, if the inability of fluid pumps is observed and a polymer-based fluid was used in the completion operation, polymer damage is likely to have occurred. Mixed deposit damage in oil-producing wells is characterized by a gradual or sudden decrease in the well rate, accompanied by the presence of scale layered with oil or paraffin. This type of damage suggests a mix of deposits including scale, oil, and paraffin, which can decrease well productivity and cause operational issues in all well states. The presence of Illite, chlorite, and kaolinite minerals in sandstone reservoirs makes them susceptible to fine migration damage. These clay minerals can become mobilized within the reservoir, leading to the migration of fine particles, potentially blocking pore throats, reducing permeability, and causing damage to the reservoir (Wang, Li et al. 2021). Additionally, the mineral composition of sandstone reservoirs, particularly the presence of calcite and dolomite, plays a significant role in determining susceptibility to fine migration damage. Formations with less than 40% of calcite and dolomite are classified as sandstone (Tan, You et al. 2021). These compositions can influence the propensity for fine migration. The factors mentioned can exacerbate the risk of fine migration damage in sandstone reservoirs containing Illite, chlorite, and kaolinite minerals due to their influence on the mobilization and migration of fine particles within the reservoir. Specific well completion techniques can disrupt the formation and increase the possibility of fine particle migration. For example, the use of a gravel pack with a perforated liner or pre-packed screen can introduce stress and disturb the formation, leading to the mobilization of fine particles. Filling of the production equipment can create pressure differentials that may cause the migration of fine particles, potentially leading to blockages and reduced permeability. High production rates can induce changes in reservoir pressure and flow dynamics, potentially mobilizing fine particles and causing migration within the reservoir. Excessive drawdown rates during production can exert stress on the formation, leading to the release and migration of fine particles. Significant changes in production conditions, such as increased water cuts or unexpected shut-ins caused by surging, can alter the flow dynamics within the reservoir, potentially leading to the migration of fine particles. Lastly, the solubility of minerals such as Illite, chlorite, and kaolinite in acids like hydrochloric acid (HCl) or hydrofluoric acid (HF) can lead to the dissolution and release of fine particles, contributing to migration and potential damage within the reservoir. (Figure 5) (Radwan, Wood et al. 2022).

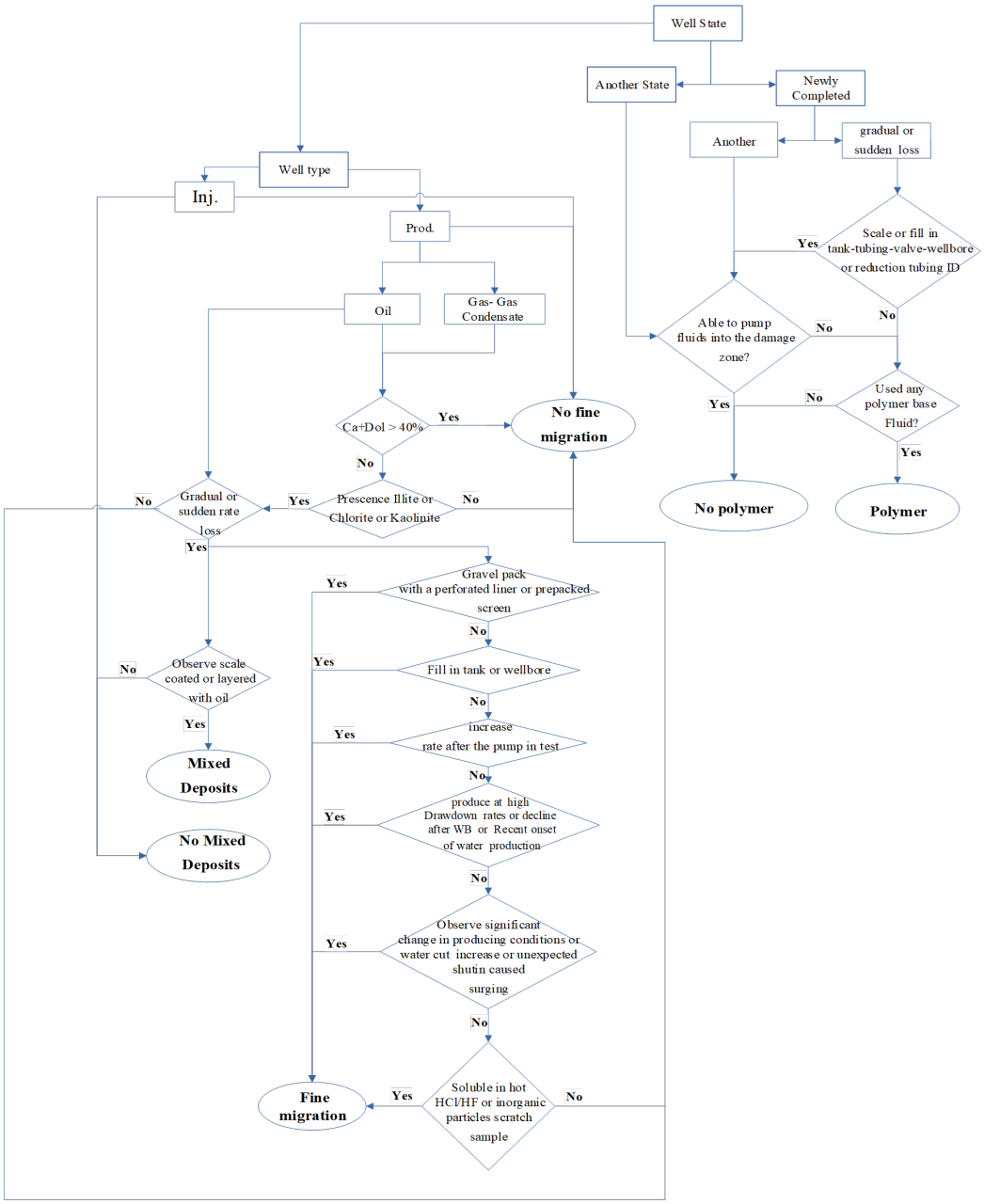

Figure 5. Diagnosis of Fine Migration, Polymer and Mixed Deposits

2.2.5. Solid Mud (Not Filter Cake)

Solid mud damage in oil and gas wells can result from various factors, including the invasion of drilling fluids into the formation, which leads to pore plugging and reduced permeability. This type of damage typically occurs in newly completed or suspended wells. High mud losses indicate an excessive intake of drilling fluid by the formation, causing decreased well productivity. A sudden or gradual decrease in well rate, or total well lock-up without observed scale or fill in the production equipment, suggests the possibility of this damage. The presence of a horizontal or heavily deviated well can increase the risk of solid mud damage due to the potential for uneven distribution and settling of drilling fluids within the wellbore, which can lead to blockages and reduced permeability. Inadequate cleaning of drilling mud before running the casing can result in residual drilling fluid and solid particles within the wellbore, potentially causing formation damage and reduced well productivity. Perforations in the

mud system can allow the migration of solid particles into the formation, leading to pore plugging and reduced permeability, ultimately resulting in well damage. In naturally fractured reservoirs, the presence of fractures can act as pathways for drilling fluids and solid particles to enter the formation, potentially causing damage through pore plugging and reduced permeability. Inaccurate or poor cement bonding, and variable density logs, can result in inadequate zonal isolation, allowing for the migration of drilling fluids and solid particles into the area behind the pipe, and contributing to potential damage. Lower well performance compared to open hole logs, and unproductive zones observed in production logs, may indicate potential issues such as solid mud damage (Figure 6).

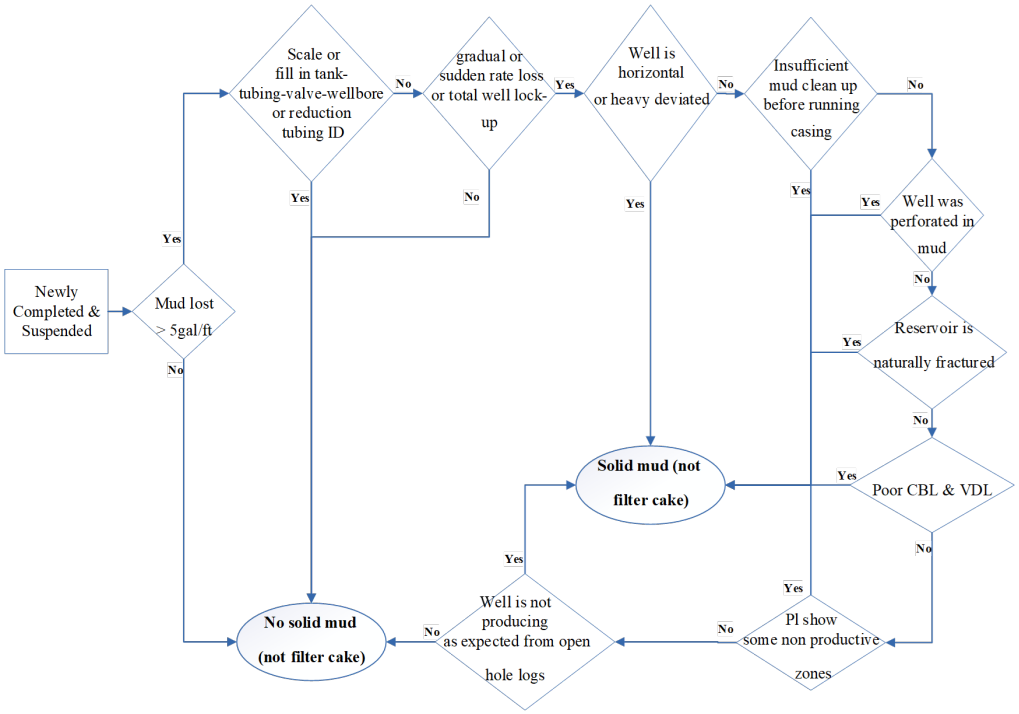

Figure 6. Diagnosis of Solid Mud (Not Filter Cake)

2.2.6. Solid-Completion-Workover/Stimulation Fluids

Damage of this kind is associated with the solid particles found in well-completion fluid and workover/stimulation fluids, warranting investigation in two distinct scenarios. In the case of solid completion fluids, in newly completed wells that are completed with a cased-hole or gravel pack (type of sand control technique in oil and gas wells to prevent the migration of formation sand into the wellbore) along with a perforated casing, insufficient underbalanced perforation can lead to the accumulation of perforation debris, solid particles, and other formation materials near the wellbore. This situation can also arise if the well was not perforated underbalanced, or if the underbalanced pressure used during perforation is less than the minimum required, potentially resulting in incomplete cleaning of the perforation tunnels and leaving solid particles and debris (unwanted material blocking fluid flow) within the wellbore, which may cause formation damage. When it comes to workover/stimulation fluids, using a dirty water-based fluid in the killing job introduces solid particles, contaminants, and other debris into the wellbore and near the completion zone. These contaminants can accumulate in the formation, near the perforations, or within the completion equipment, leading to

reduced permeability, formation damage, and blockage within the wellbore, thus impacting the productivity and performance of the well. During the fill clean-out operation (clear obstructions in wellbores), the well's production may be hindered due to the presence of solid particles, contaminants, and debris within the wellbore and near the completion zone, which can manifest as a decrease in well rate or total well lockup, indicating potential formation damage and blockage. In acidizing operations, if the string is not cleaned sufficiently, there can be a rapid decline (Steady decrease in flowrate for two or three days) in well rate or total well lockup. The accumulation of solid particles and debris in the wellbore and near the completion zone can decrease permeability, leading to reduced productivity. Therefore, a sudden decrease in well rate or total well lockup following these operations is a strong indicator of potential formation damage and blockage, and this risk is also present when using a clean water-based or polymer-based fluid during the kill job, or when cleaning the string before the acidizing operation, particularly if a lost circulation mud pill with solids has been used (Figure 7).

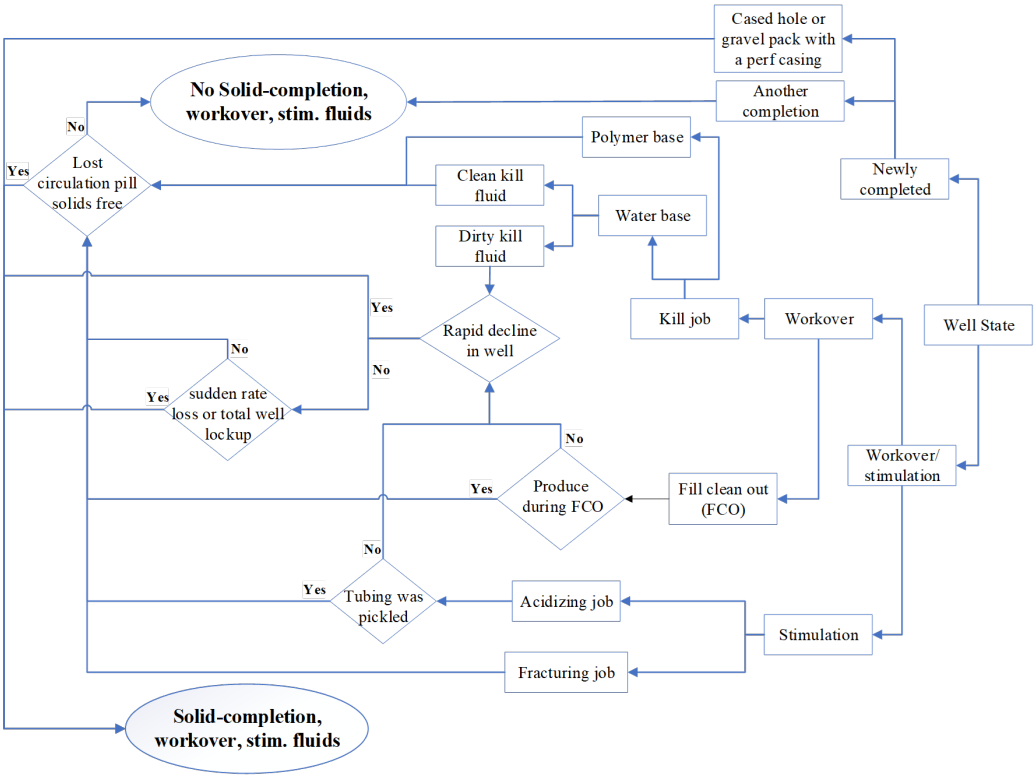

Figure 7. Diagnosis of Solid-Completion, Workover, Stimulation, Fluids

2.2.7. Precipitate

When a well undergoes acid treatment, it can lead to precipitation-induced damage. This damage occurs when the acid reacts with minerals in the formation, resulting in the formation of solid deposits or precipitates. These solid deposits can block the pore spaces in the formation and limit the flow of hydrocarbons, ultimately reducing the well's productivity. The following categorization illustrates the types of precipitates commonly found: $FeOH_3$, K_2SiF_6, and SiO_2 in sandstone formations, and CaF_2 in carbonate formations. When mud acid (HCl-HF) is used in carbonate formations, the acid reacts with the carbonates in the formation, leading to the formation of solid salts such as calcium fluoride (CaF_2). In sandstone reservoirs containing chlorite minerals, when an acid job using HCl or HCl-HF is performed and an inadequate amount of iron chelating agent is utilized, a sudden decrease in the well's production rate can be

linked to the creation of $FeOH_3$ precipitate. This reaction occurs when the acid interacts with the chlorite minerals, leading to the release of iron ions. Without sufficient chelating agents, these iron ions can react with hydroxide ions in the formation water, leading to the precipitation of $FeOH_3$. Similarly, when an acid job is carried out using acid mud in sandstone reservoirs containing Illite or K-feldspar minerals and an inadequate overflush is used, a sudden decrease in the well's rate can be attributed to the formation of K_2SiF_6 precipitate. This occurs due to the reaction between the fluoride ions from the acid and the potassium and silicon ions released from the Illite or K-feldspar minerals. The inadequate overflush fails to adequately remove the reaction by-products, leading to the formation of K_2SiF_6 precipitates (Figure 8).

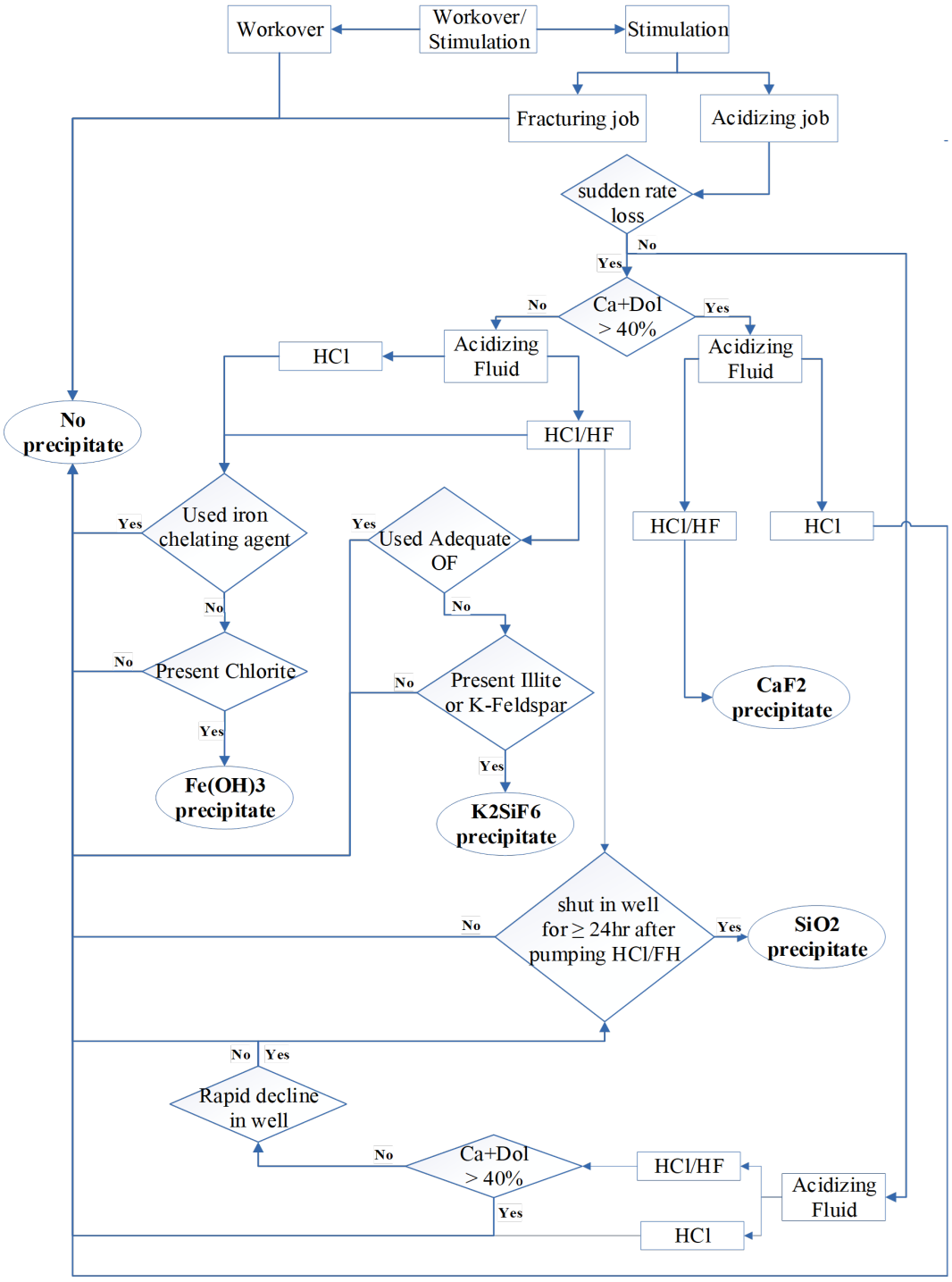

Figure 8. Diagnosis of Precipitate

2.2.8. Clay Swelling

Clay swelling in sandstone formations is primarily caused by the presence of minerals such as smectite or mixed-layers. Smectite, a type of clay mineral, tends to swell upon contact with water. Mixed-layers clays, composed of alternating layers of different clay minerals, can also contribute to swelling behavior in sandstone formations. The use of water-based drilling mud or completion fluids with lower salinity than the formation water in newly completed wells can increase the potential for clay swelling. This is due to the lower salinity creating an osmotic pressure difference between the fluids and the formation of water, leading to water absorption by the clay minerals in the sandstone formation. Clay swelling in wells utilizing oil-based fluids or water-based fluids with higher salinity than the formation water is typically the result of the interaction between the fluids and the clay minerals in the sandstone formation. For instance, the presence of water-sensitive clay minerals like Smectite in oil-based fluids can cause swelling upon contact with water infiltrated into the formation. Similarly, the use of water-based fluids with higher salinity than the formation water can lead to clay swelling due to osmotic pressure differences and subsequent water uptake by the clay minerals. During workover or stimulation operations, a sudden rate loss can indicate clay swelling. This occurs when the introduction of fluids into the wellbore causes the clay minerals to swell, reducing permeability and impeding fluid flow. Additionally, core analysis indicating water sensitivity can be a sign of potential clay swelling issues, suggesting that the clay minerals in the formation are prone to swelling upon contact with water (Figure 9).

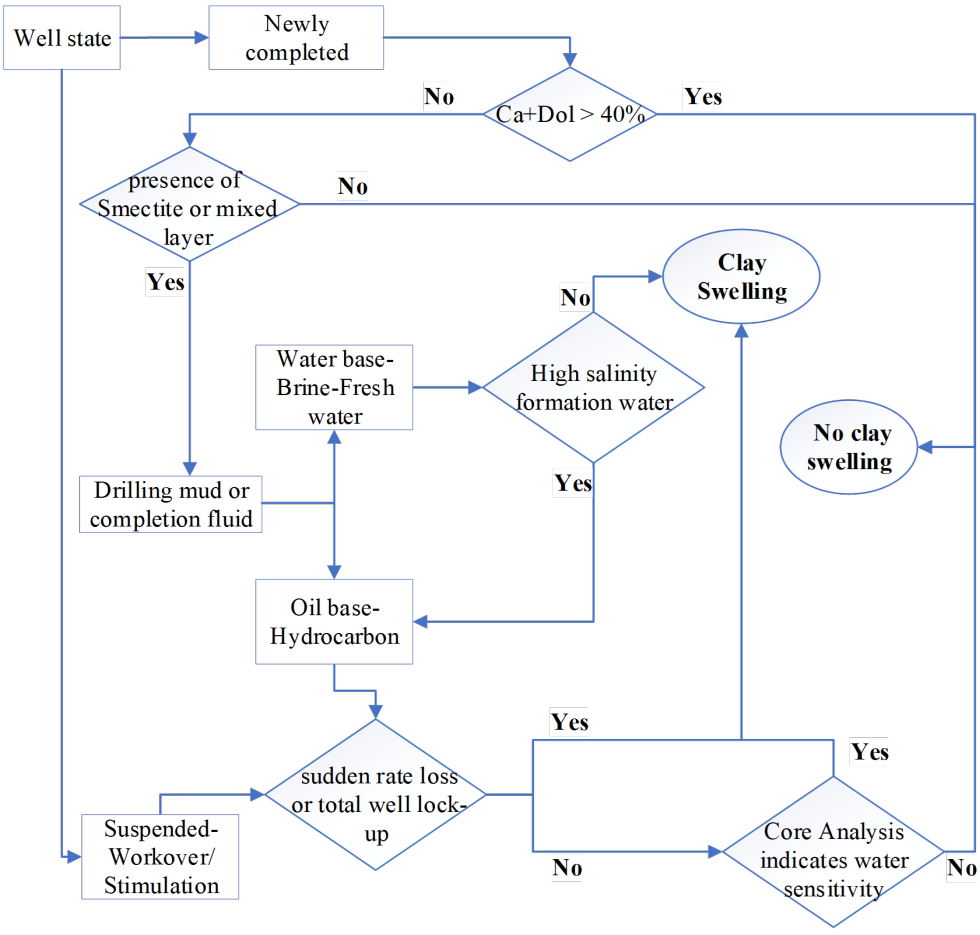

Figure 9. Diagnosis of Clay Swelling

2.2.9. Water Blocking

When a newly completed well utilizes water-based drilling mud with significant filtrate loss in low permeability reservoirs, it can result in water-blocking damage in oil and gas-producing wells. This occurs when the filtrate from the drilling mud infiltrates the formation, obstructing the flow of oil or gas through the reservoir rock. The significant filtrate loss can cause the formation to become plugged with the filtrate, reducing permeability and hindering the flow of hydrocarbons from the reservoir into the wellbore. In gas condensate and injection wells, water blocks can be identified by delayed cleanup over time, no rate increase during a pump-in test, or a positive response to methanol. These signs indicate that the well is experiencing water-blocking damage, which can lead to reduced production rates. During a well-stimulation operation on low permeability formations, failure to recover water in the acid job operation can indicate potential formation damage. This is attributed the acid's ability to create channels or pathways within the formation that are not effectually cleaned out, ultimately leading to reduced well productivity. Conversely, water-blocking damage can be inferred if the well fails to clean up over time, shows no rate increase during a pump-in test, or displays a positive response to methanol, even when mutual solvents are used. These observations are consistent with the presence of water blockage within the formation, which can hinder fluid flow and reduce production rates. In the case of high fluid loss during a water-based fluid kill job operation, the absence of a rate increase during a pump-in test, or a positive response to methanol indicates the possibility of water-blocking damage (Figure 10) (Shu and Yan 2008).

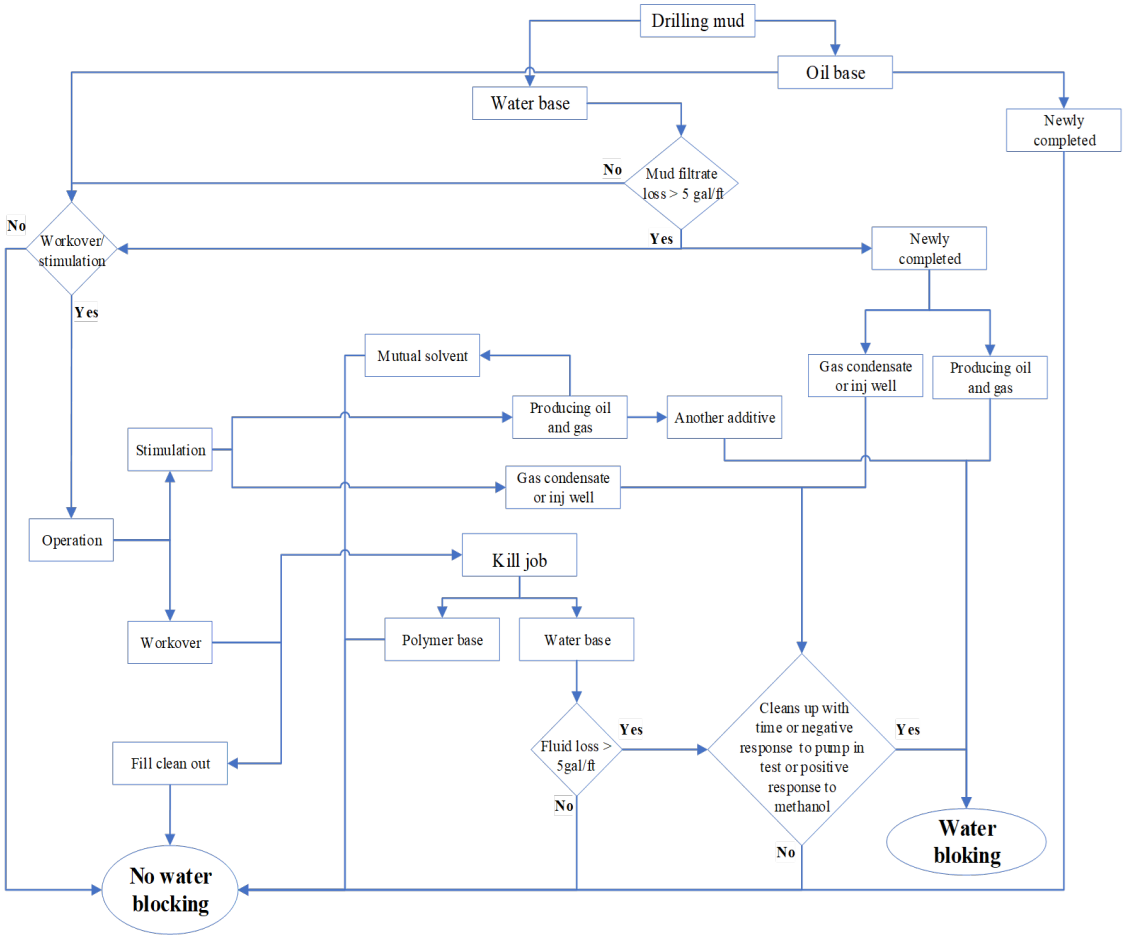

Figure 10. Diagnosis of Water Blocking

3. Results and Discussion

The operation of the expert system implemented for diagnosing formation damages in this research follows the rules obtained as illustrated in (Figures 2 to 10). The system considers all aspects, significantly reducing the number of possibilities through an elimination technique, thereby greatly enhancing the system's performance speed. For instance, clay swelling and fine migration are not common damages in carbonate formations. Therefore, if carbonate formation mineralogy is identified, these two types of damage are eliminated. The software begins by asking about the well state, initially considering only the damages likely to occur in that specific condition. It then further narrows down the number of damages by selecting the type of well (production or injection), the fluid used for production or injection in the well, and the type of drilling or completion fluid. After precisely identifying the well state, well type, type of injected or produced fluid, and the type of drilling mud or completion fluid, the system evaluates the well's history, test observations, surface equipment observations, well rate, past operations on the well, amount of lost drilling mud and its additives, and the types of these additives, among other factors, to identify potential damages. This step-by-step elimination technique reduces the number of possibilities, making the use of the expert system easier and faster, and enables the user to identify potential formation damages with minimal information and a lower error margin. The application of expert system criteria for selecting wells suitable for acid treatment was conducted on 10 wells chosen randomly. Among these, six wells are situated in a sandstone formation, while the remaining four are in a carbonate formation. Specifically, in the sandstone formation, there are four wells dedicated to oil production, one for gas production, and another for water injection purposes. As for the carbonate formation, it comprises two oil-producing wells, one well for gas production, and one utilized for water injection. As shown in (Table 1), skin can be determined using parameters such as geometry, flow rate, BHP, viscosity, net pay, permeability, K_v/K_h, and well length (for deviated wells). It is important to address mechanical issues that reduce well performance before calculating the skin factor. Out of the ten selected wells, six were found suitable for acidizing jobs, with three in the carbonate formation and three in the sandstone formation. Identifying the specific type of formation damage accurately is crucial before initiating an acid treatment operation. This crucial step informs the selection of the most suitable acid treatment fluid, which is key to the operation's success. The expert system, detailed in the appendix section with its figures, has successfully pinpointed the types of damage in both carbonate and sandstone formations. This diagnosis is based on a thorough analysis encompassing various factors: reservoir characteristics, well type, current state of the well, fluids used in past operations, well's operational history, observations from tests and ongoing operations, and production equipment assessments.

The outcomes of this analysis are meticulously documented in (Table 1), (Table 2), and (Table 3). These tables validate the expert system's effectiveness in accurately determining the formation damage.

Table 1. Results of an Expert System for Well Candidate

Well Candidate	1	2	3	4	5	6	7	8	9	10
Formation	Sandstone	Sandstone	Sandstone	Sandstone	Sandstone	Sandstone	Carbonate	Carbonate	Carbonate	Carbonate
Well Type	Oil	Oil	Oil	Oil	Gas	Water	Oil	Oil	Gas	Water
Well Geometry	Straight	Straight	Low Deviated	Horizontal	Straight	Straight	Heavy Deviated	Straight	Straight	Straight
Flow rate	300 STB/d	150 STB/d	70 STB/d	78 STB/d	7 MMscf/d	700STB/d	70 STB/d	61 STB/d	30MMscf/d	190STB/d
Pres (psi)	4710	2150	1460	2900	1430	2000	2950	2820	3500	2560
BHP (psi)	1200	1120	630	1050	560	1420	750	820	1700	1470
Viscosity (cp)	13	5	11	12	-	1.009	15	3	0.6	0.970
Net pay	20	35	30	15	40	70	30	47	51	12
Perm (md)	180	40	28	20	20	18	7	2	14	30
K_v/K_h	-	-	-	0.1	-	-	0.2	-	-	-
Lwell (ft)	-	-	-	27	-	-	100	-	-	-
Scalculated	15	6	-1	-3	3	0	-5	14	4	8
Qualification Candidate	Acceptable	Acceptable	Unacceptable	Unacceptable	Acceptable	Unacceptable	Unacceptable	Acceptable	Acceptable	Acceptable

Table 2. Results of Expert System for Formation Damage Detection in Sandstone Reservoirs

Well Candidate	1	2	5
Formation	Sand Stone	Sand stone	Sandstone
Well Type	Oil Producing	Oil producing	Gas Producing
Well State	Newly Completed	Suspended	Workover (Kill Job)
Produce Water	Yes	No	Yes - High CO_2 - PH<6 - NaCl > 50000 ppm
Completion Fluid & Salinity	Oil base - High salinity	-	Water Base - Low Salinity
Drilling Mud & Salinity	Water base - Low salinity	Oil Base - High salinity	-
Filtrate Lost- Mud Lost	High - High	High - High	*- High
Candidate Selection	Illite - Chlorite - Smectite - Calcite - Dolomite - Zeolite- K Feldspar - Quartz	Siderite - Mica - Calcite - Dolomite - Glauconite - Chlorite - Illite - Quartz - Mixed layer	Na Feldspar - Calcite - Dolomite - ZeoLite - Illite
Kill Fluid	-	-	Kill Water Not Filtered-Kill Tank Cleaned-Flushed Lines (Before Kill Job)
Completion Type	Cased Hole and Straight	-	Perforated Liner
Perforation	UBD-Perforated in Mud	-	
Reservoir Information	Not sour k=30md TVD = 180ft P = 2560 psi BHT=160 deg °F	-	Sour k=12md TVD = 2500ft P = 1500 psi BHT=150 deg °F
Flow Rates Observation	Unexpected Gradual Rate loss	Total well Lock-up	Unexpected Sudden Rate Loss
Well History	-	-	-
Pump-in Test	Yes	Yes	Yes
Able Pump Fluids in to the Damage zone	Yes	No	No
Increase Rate After Pump-in Test	No	Yes	No
Lost Circulation Pill Pumped	-	Yes	Yes
Lost Circulation Pill Solids Free	-	Yes	No
Lost Circulation Pill Polymer Base	-	Yes	Yes
Production Equipment Observation	Fill Tanks-Scale layered with Oil	Scale Deposits in Tubing - Fill in Tanks and Tubing -	Fill in Tubing-Evidence of Emulsion
Test Observation	Poor CBL&VDL	-	Oil has High acid Number- Poor CBL&VDL- Increase Gama Ray-
Operation Observation	-	-	WC Increase
Formation Damage Detected	1) Clay Swelling 2) Fines Migration 3) Mixed Deposits 4) Solid Completion Fluids 5) Water Blocking	1) Clay Swelling 2) Polymer	1) Emulsion 2) Fines Migration 3) Polymer 4) Solids Workover Fluids 5) Water Blocking 6) Scale ($CaCO_3$-Fe_2O_3-FeS-$MgCO_3$)

Table 3. Results of Expert System for Formation Damage Detection in Carbonate Reservoirs

Well Candidate	8	9	10
Formation	Carbonate	Carbonate	Carbonate
Well Type	Oil Producing	Gas Injection	Water Injection
Well State	Continuous Operation	Stimulations (Acidizing HCl)	Huff and Puff
Well Shut-in	-	30hr After Pumping Acid	-
Produce Water	Yes - High CO_2	-	-
Injection Well	-	Increase Pressure Used Produced Water	-
Completion Fluid & Salinity	-	Open Hole - Straight	Cased Hole - Straight
Drilling Mud & Salinity	-	Water Base - High Salinity	-
Filtrate Lost- Mud Lost	-	Low-High	-
Mineralogy	Calcite - Dolomite - Zeolites - Chlorite - Quartz	Calcite - Dolomite - Siderite - Smectite - Illite - Quartz	-
Kill Fluid	-	-	-
Completion Type	-	-	-
Perforation	-	-	
Reservoir Information	Not Sour k=40md TVD = 1200 ft P = 1700 psi BHT= 210 deg °F	-	-
Flow Rates Observation	Unexpected Gradual Rate Loss	Unexpected Sudden Rate Loss	-
Well History	Recent onset - Produced at High Drawdown - Sudden Drop PI	-	-
Pump-in Test	Yes	Yes	Yes
Able Pump Fluids in to the Damage Zone	Yes	Yes	No
Increase Rate After Pump-In Test	Yes	No	Yes
Lost Circulation Pill Pumped	-	Yes	Yes
Lost Circulation Pill Solids Free	-	Yes	Yes
Lost Circulation Pill Polymer Base	-	Yes	Yes
Production Equipment Observation	-	Fill in Tubing	-
Test Observation	Positive Response to Metha-Nol- Small Difference Viscosity oil-Water - High Acid Number	-	-
Operation Observation	WC Increase - WHP Changed - Fields on Pressure Maintenance	WC Increase - Field is on Water Flooding - WHP Changed	-
Formation Damage Detected	1) Scale ($CaCO_3$-Fe_2O_3-$MgCO_3$)	1) Injection Carryover (Emulsion-Formation Solids-Oil) 2) Polymer 3) Solid Stimulation Fluids 4) Water Blocking	1) Polymer

4. Conclusion

Determining whether a well is suitable for acidizing is a challenging process. This complexity continues even after several potential candidate wells have been identified, as the task then becomes identifying the best candidate well among those selected. In other words, selecting the best candidate from the identified wells requires a thorough assessment of the potential damage to each well. In this study, our goal was to develop an expert system capable of selecting appropriate wells for acidizing jobs and identifying formation damages. This system aids in determining which wells are suitable for acidizing and in detecting any formation damage. Given the varied conditions of hydrocarbon reservoirs and the multitude of operations on wells, identifying formation damage necessitates analyzing tens of millions of possibilities. This research introduces an expert system that, for the first time, is capable of rapidly assessing these scenarios through fundamental rules and an elimination technique. Tested on ten well samples, it detected damages with minimal error, showcasing its efficiency and the potential to significantly advance formation damage diagnosis in the industry. Moreover, in future research, we aim to further enhance these investigations by leveraging fuzzy logic and developing a system based on this logic for more accurate detection of formation damage and identification of wells susceptible to acidizing.

References

Abdulmalek, A. S., S. Elkatatny, A. Abdulraheem, M. Mahmoud, Z. A. Abdulwahab and I. Mohamed (2018). Pore pressure prediction while drilling using fuzzy logic. SPE Kingdom of Saudi Arabia Annual Technical Symposium and Exhibition, SPE.

Abobaker, E. E., A. Elsanoose, F. Khan, M. A. Rahman, A. Aborig, K. Noah and S. Butt (2022). "A new assessment of perforation skin factor for vertical perforated wells in near-wellbore region." Journal of Petroleum Exploration and Production Technology: 1-17.

Braswell, G (2013). "Artificial intelligence comes of age in oil and gas." Journal of Petroleum Technology 65(01): 50-57.

Chew, A. K., S. Jiang, W. Zhang, V. M. Zavala and R. C. Van Lehn (2020). "Fast predictions of liquid-phase acid-catalyzed reaction rates using molecular dynamics simulations and convolutional neural networks." Chemical science 11(46): 12464-12476.

Furui, K., D. Zhu and A. Hill (2005). "A comprehensive skin-factor model of horizontal-well completion performance." SPE Production & Facilities 20: 207-220.

Garrouch, A. A. and H. M. Labbabidi (2003). Using fuzzy logic for UBD candidate selection. SPE/IADC Managed Pressure Drilling and Underbalanced Operations Conference and Exhibition, SPE.

Khurshid, I., E. W. Al-Shalabi and W. Alameri (2020). "Influence of water composition on formation damage and related oil recovery in carbonates: A geochemical study." Journal of Petroleum Science and Engineering 195: 107715.

Liew, C. X., R. Gholami, M. Safari, A. Raza, M. Rabiei, N. Fakhari, V. Rasouli and J. V. Vettaparambil (2019). "A new mud design to reduce formation damage in sandstone reservoirs." Journal of Petroleum Science and Engineering 181: 106221.

Moghadasi, J., M. Jamialahmadi, H. Müller-Steinhagen and A. Sharif (2004). Formation damage due to scale formation in porous media resulting from water injection. SPE International Conference and Exhibition on Formation Damage Control, SPE.

Qazvini, S., A. Golkari, A. Azdarpour, R. M. Santos, M. S. Safavi and M. Norouzpour (2021). "Experimental and modelling approach to investigate the mechanisms of formation damage due to calcium carbonate precipitation in carbonate reservoirs." Journal of Petroleum Science and Engineering 205: 108801.

Radwan, A. E., D. A. Wood, A. Abudeif, M. Attia, M. Mahmoud, A. A. Kassem and M. Kania (2022). "Reservoir formation damage; reasons and mitigation: A case study of the Cambrian-Ordovician Nubian 'C'Sandstone Gas and Oil Reservoir from the Gulf of Suez Rift Basin." Arabian Journal for Science and Engineering 47(9): 11279-11296.

Shu, Y. and J. Yan (2008). "Characterization and prevention of formation damage for fractured carbonate reservoir formations with low permeability." Petroleum Science 5: 326-333.

Tan, Q., L. You, Y. Kang and C. Xu (2021). "Formation damage mechanisms in tight carbonate reservoirs: The typical illustrations in Qaidam Basin and Sichuan Basin, China." Journal of Natural Gas Science and Engineering 95: 104193.

Umoh, G. T. (2019). Candidate well selection for intervention and workover: an artificial intelligence approach, department of chemical and petroleum engineering, faculty of engineering ... . Department of chemical and petroleum engineering, faculty of engineering

Wang, Z., H. Li, X. Lan, K. Wang, Y. Yang and V. Lisitsa (2021). "Formation damage mechanism of a sandstone reservoir based on micro-computed tomography." Advances in Geo-Energy Research 5(1): 25-38.

Xiong, H., B. M. Robinson and S. Foh (2001). Using an expert system to diagnose formation damage mechanisms and design stimulation treatments for gas storage wells. SPE Eastern Regional Meeting, SPE.

Xu, C., Y. Kang, Z. You and M. Chen (2016). "Review on formation damage mechanisms and processes in shale gas reservoir: known and to be known." Journal of Natural Gas Science and Engineering 36.

Yildiz, T. (2006). "Assessment of total skin factor in perforated wells." SPE Reservoir Evaluation & Engineering 9(01): 61-76.

Zhang, Z., J. Guo, H. Liang and Y. Liu (2021). "Numerical simulation of skin factors for perforated wells with crushed zone and drilling-fluid damage in tight gas reservoirs." Journal of Natural Gas Science and Engineering 90: 103907.

Zoveidavianpoor, M., A. Samsuri and S. R. Shadizadeh (2012). Development of a fuzzy system model for candidate-well selection for hydraulic fracturing in a carbonate reservoir. SPE Oil and Gas India Conference and Exhibition, SPE.

JOURNAL OF GAS TECHNOLOGY

Volume 8 /Issue 2 / Winter 2023/ Pages 27-34

Journal Home page: http://jgt.irangi.org

Fabrication of a Polyetherimide/ZIF-8 Composite Membrane for Separating Carbon Dioxide from Methane

Shiva Falahati[1], Omid Alizadeh[2*], Masoud Mokhtary[3]

1. M.Sc. Student, Department of Chemistry and Chemical Engineering, Rasht branch, Islamic Azad University, Rasht, Iran
2. Assistant Professor, Department of Chemistry and Chemical Engineering, Rasht branch, Islamic Azad University, Rasht, Iran
3. Professor, Department of Chemistry and Chemical Engineering, Rasht branch, Islamic Azad University, Rasht, Iran

ARTICLE INFO

ORIGINAL RESEARCH ARTICLE

Article History:
Received: 07 November 2023
Revised: 10 December 2023
Accepted: 30 December 2023

Keywords:
Polyetherimide
Mixed matrix membrane
ZIF-8
Gas separation

DOR: 20.1001.1/JGT.2024.2022467.1034

ABSTRACT

In the present work, a polyetherimide/ZIF-8 composite membrane was fabricated by solution casting technique. The prepared membranes were Characterized using Scanning Electron Microscopy (SEM), Fourier transform infrared spectroscopy - attenuated total reflectance (FTIR-ATR), energy dispersive X-ray (EDAX) and X-ray diffraction (XRD). Furthermore, the membrane's performance in separating carbon dioxide and methane was analyzed through single gas permeability measurements. FTIR-ATR spectrum of the prepared membrane confirmed the functional groups of polyetherimide. XRD analysis showed that the additive was well dispersed in the polymer, resulted in a reduction in the membrane's crystallinity. EDAX analysis confirmed the existence and proper dispersion of Zn particles in the membrane. Finally. The results of permeability tests showed that adding ZIF-8 to the membrane significantly increased its permeability and selectivity. The permeability of the composite membrane for CO_2 gas was 5.91 GPU, more than twice that of the pure polyetherimide membrane. Additionally, the permeability for CH_4 gas was 0.31 GPU, representing a significant improvement over the pure membrane's permeability of 0.17 GPU. The carbon dioxide/methane selectivity also rose from 15.3 in the pure membrane to 19.1 in the composite membrane. In conclusion, the study demonstrated that adding ZIF-8 to a polyetherimide matrix can improve the effectiveness of the resulting composite membrane for separating CO_2 from CH_4. The improvement in selectivity was primarily due to the increased solubility coefficient of carbon dioxide compared to methane in the composite membrane.

How to cite this article
S. Falahati, O. Alizadeh, M. Mokhtary, Fabrication of a Polyetherimide/ZIF-8 Composite Membrane for Separating Carbon Dioxide from Methane. Journal of Gas Technology. 2023; 8(2): 27-34. (https://jgt.irangi.org/article_712978.html)

* Corresponding author.
E-mail address: alizadeh@iaurasht.ac.ir, (O. Alizadeh).

Available online 31 December 2023

1. Introduction

Among the different technologies to reduce CO_2, membrane technology is suggested because of its great performance and environmental friendliness. Typically, polymer and inorganic membranes have been utilized in gas separation, with a specific type of membrane known as mixed matrix membranes being created by incorporating inorganic particles as fillers in polymer membranes. In the fabrication of mixed matrix membranes, polymer materials are commonly used as the membrane network, and other materials such as mineral nanoparticles and ionic liquids are added to improve the polymer structure and its permeability and selectivity characteristics.

Zeolites, molecular sieve carbons and organic-metal frameworks (MOFs) are frequently employed materials in the development of composite network membranes (Setiawan et al., 2019). Since the discovery MOFs, scientists have attempted to utilize them in gas separation membranes. Zeolitic imidazolate frameworks (ZIFs) are a novel category of nanoporous materials that can be produced with various pore sizes and applied as nanofillers in mixed matrix membranes (MMM). Zn(2-methylimidazolate)2, also known as ZIF-8, has been extensively researched for membrane applications because of its uncomplicated synthesis, strong chemical and thermal stability, widespread availability in the market, and the size of its adsorbent pores (Xia et al., 2014).

Murali et al.(2010) synthesized a membrane based on Pebax 1657 and carbon nanotubes (MWNT) as a filler to investigate the permeability of H_2, N_2, O_2 and CO_2 gases. They used 2,4-toluylene diisocyanate to modify the polymer structure, which led to a reduction in the size of the holes in the polymer chains and amplified the screening properties of the membrane. In 2016, Dai et al.(2016) investigated the gas permeability of the composite matrix membrane based on Pebax polymer and graphene oxide nanoparticles. Their studies have shown that carbon dioxide shows greater permeability than H_2, CH_4 and N_2 gases due to its higher solubility in polymer matrix. In addition, carbon dioxide gas has a relatively good interaction with the imidazole group and its absorption in graphene increases the selectivity of this gas compared to other gases. Dorosti et al.(2014) investigated the mixed matrix membrane composed of Matrimid polymer and MIL-53 nanoparticles (from the composition of 0 to 20 percent by weight). They used this membrane to separate carbon dioxide from methane.

Azizi et al.(2017) studied composite mixed matrix membranes using Pebax 1074 polymer and ZnO nanoparticles with weight percentages of 2, 4, 6 and 8%. They noted that as the proportion of nanoparticles in the polymer matrix rose, the permeability of carbon dioxide gas increased significantly, whereas the increase for nitrogen and methane was much more modest. Perez et al.(2009) assessed the CO_2 and CH_4 permeability of 5-Matrimid/MOF composite matrix membrane. CO_2 permeability increased from 9 to 20.2 bar, while this permeability improvement in CH_4 was weaker. They also found that the CO_2/CH_4 selectivity decreased with the increase of 5-MOF weight percent. They clarified that in some cases, the aggregation of particles at higher concentrations can result in the formation of holes in the polymer and particle common phase, in order to interpret their findings.

Polyetherimide is a thermoplastic polymer known for its outstanding mechanical, thermal, and chemical resistance characteristics. It has high permeability to CO_2 and CH_4 gases due to its amorphous nature and presence of polar ether and imide groups. Polyetherimide also has moderate solubility selectivity for CO_2 over CH_4, which can be enhanced by incorporating porous ZIF-8 particles (Rahman et al., 2023). The dispersed ZIF-8 nanoparticles can facilitate gas

transport through the membrane by providing additional pathways for gas molecules to diffuse through the polymer matrix. Polyetherimide also has good compatibility with ZIF-8, allowing for uniform dispersion of ZIF-8 within the polymer. The high thermal stability of polyetherimide also permits high temperature processing to form mixed matrix membranes with ZIF-8 (Bergaoui et al., 2021). In the present work, a polyetherimide/ZIF-8 mixed matrix membrane was fabricated and its characteristics and potential for separation of CO_2/CH_4 separation was studied.

2. Materials and Methods

2.1. Materials and Reagents

Polyether imide as asymmetric membrane polymer phase and 2-methylimidazole and zinc nitrate ($Zn(NO_3)2.6H_2O$) as additive phase and 1-methyl-2-pyrrolidone as solvent were obtained from Merck.

2.2. Membrane Preparation

The PEI substrate with embedded ZIF-8 was created by synthesizing ZIF-8 particles within the casting solution of the PEI membrane. The complete dissolution of 2.2 g of PEI in 9.82 mL of NMP at 70 °C was followed by dissolving 0.1g of $Zn(NO_3)2.6H_2O$ in 9.82 mL of NMP and then adding it to the PEI mixture solution. The solution was agitated for 2 hours and then allowed to sit for 3 hours to facilitate the growth of ZIF-8 crystals. Following another 24 hours of stirring, the ZIF-8/PEI mixture solution was applied onto a glass sheet onto a glass sheet to form a uniform 0.5mm layer. The entire glass sheet was then submerged in DI water for 24 hours to undergo phase conversion and then dried at 30 °C for another 24 hours. The fabrication process of the pure PEI support was the same as that of the ZIF-8 in-situ embedded PEI substrate. The pure PEI support was fabricated using the same method, involving the dissolution of 2.2 g of PEI in 9.82 mL of NMP.

2.3. Characterization and Gas Permeance Test

FTIR analysis was performed using a Shimadzu 8900-model device. X-ray diffraction (XRD) pattern was conducted using a Philips PW1730 XRD device to identify the phases in the sample and the degree of crystallinity of the membranes. X-ray Energy Diffraction Spectroscopy (EDAX) analysis was performed to identify the constituent elements of the desired sample. Also, mapping images from electron microscope analysis (SEM) using FEI Quanta 200 SEM device were used to analyze the membrane's composition.

Permeability of pure carbon dioxide and methane gases along with selectivity of carbon dioxide/methane were measured and calculated. The flow of carbon dioxide or methane gas, passing through a pressure regulator set to 1 bar, enters the chamber with a known volume and hits the upper surface of the membrane. During the time it is recorded by the data logger, it passes through the mixed matrix membrane and gradually increases the pressure in the output area of the device, which is recorded by the pressure sensor. The raw data obtained from the permeability measurement setup is in the form of pressure changes with time, which will be calculated using the following relation of permeability values:

$$Permeability\ (GPU) = \frac{273.15 \times 10^6 \mathrm{v} \times \mathrm{t}}{760 \times \mathrm{ATP_0}} \quad (1)$$

In the given equation, P represents gas permeability, V stands for chamber volume (measured in cm^3), A denotes the membrane surface area (measured in cm^2), T represents the test temperature (measured in Kelvin), Po signifies the pressure of the gas feed to the system (measured in mmHg), and dp/dt indicates the rate of change in pressure of the permeable gas over time. The ideal selectivity is achieved by dividing the permeability of pure gases using the following formula:

$$\propto_{AB} = \frac{p_A}{p_B} \quad (2)$$

3. Results and Discussion

The FTIR-ATR graph of the fabricated composite membrane is depicted in (Figure 1). The peak at ~1715 cm^{-1} is related to the symmetric stretching vibration of carbonyl imide C=O and the peak at ~1775 cm^{-1} is related to the asymmetric stretching vibration of carbonyl imide C=O. The peaks at ~1475 cm^{-1} and ~1596 cm^{-1} are related to the stretching vibrations of the C=C vibration of the aromatic ring. The peak in the range of ~1232 cm^{-1} indicates the ethereal C-O bond. The peak at ~1442 cm^{-1} is caused by the stretching vibrations of the C-N bond, and the peak at ~2959 cm^{-1} is related to the stretching vibration of the aromatic C-H ring and the peak at ~740 cm^{-1} indicates the out-of-plane C-H vibration (Chen at al., 2006; Singh et al. 2011).

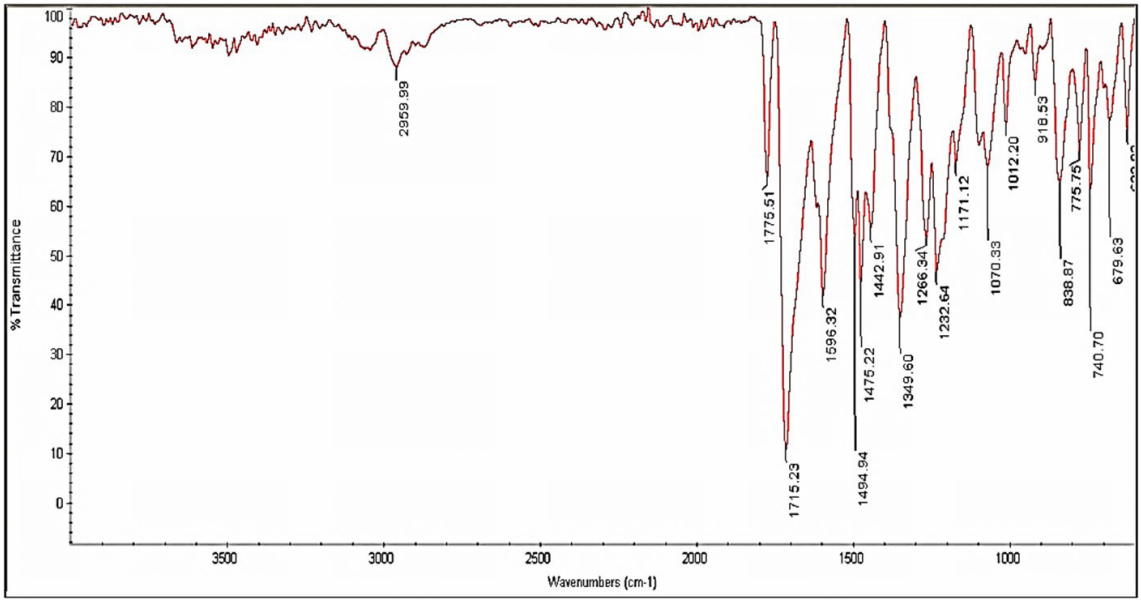

Figure 1. FTIR-ATR Spectra of PEI/ZIF-8 Membrane

The XRD patterns for both the pure polyetherimide membrane and the composite membrane are shown in (Figure 2). In the XRD pattern of the fabricated membranes, a broad diffraction peak is observed at 2θ of 14.24, consistent with references (Eiras et al., 2016).

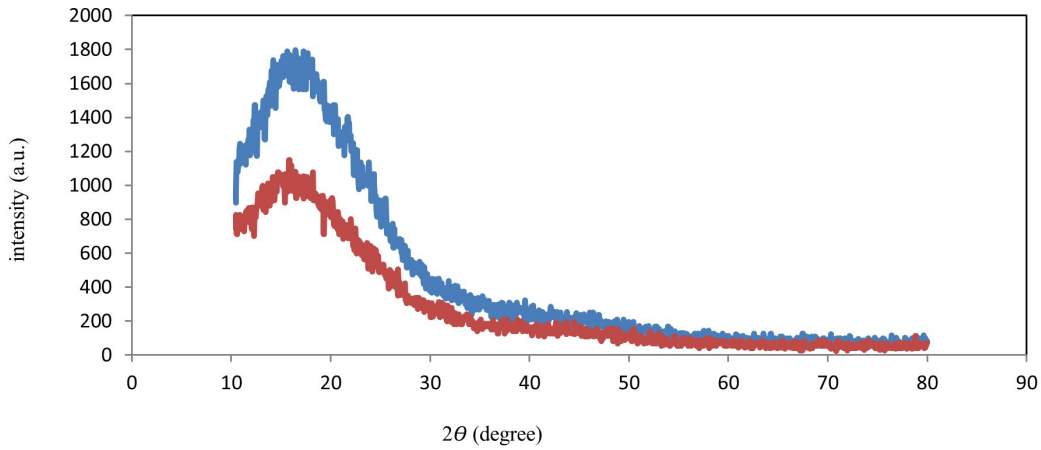

Figure 2. XRD Spectrum of Pure PEI (a) and PEI/ZIF-8 Membrane (b)

As depicted in the above figure, the intensity of the peak for pure polyetherimide has diminished by adding zinc nitrate, which means a decrease in crystallinity. Additives have reduced the crystallinity of the membrane and disrupted its structural unity. In fact, adding additives to the polymer body reduces the structural unity of the membrane due to the increase of amorphous parts. In amorphous materials, the rays weaken each other and the phenomenon of diffraction does not occur, but if the atoms are in the form of a crystalline material, i.e. they are placed next to each other with a certain order and distance, the difference in the path traveled is a multiple of the wavelength of the X-ray and so on. Which is seen in the pure polyether imide membrane, diffraction takes place. Typically, the addition of additives changes the degree of crystallinity of the membranes. The figure illustrates that the membrane's crystallinity decreased with the incorporation of additives. Adding additives to the structure of the polymer membrane causes more stimulation of the polymer chain, which is the reason for the reduction of inter-chain hydrogen bonds.

In order to identify the constituent elements of the desired sample and also to check the distribution of elements inside the membrane, X-ray Energy Diffraction Spectroscopy (EDAX) analysis and mapping images were used for the polymer composite membrane. The result of the EDAX test of the mixed matrix membrane confirms the existence of zinc (Zn) in the polymer matrix, which is shown in (Figure 3) with the Zn peak and it suggests that the ZIF-8 particles are evenly distributed across the membrane's cross-sectional area. The mixing of zeolite particles in the polyetherimide membrane has led to the accumulation of particles in the membrane, primarily because of the insufficient adhesion between the polyether imide membrane and additive particles. When a higher percentage of zeolite particles are included inside the membrane, the aggregation of particles that are in the form of aggregates becomes larger, which causes the formation of large pores, which leads to low performance in CO_2/CH_4 selectivity (Ma et al., 2018).

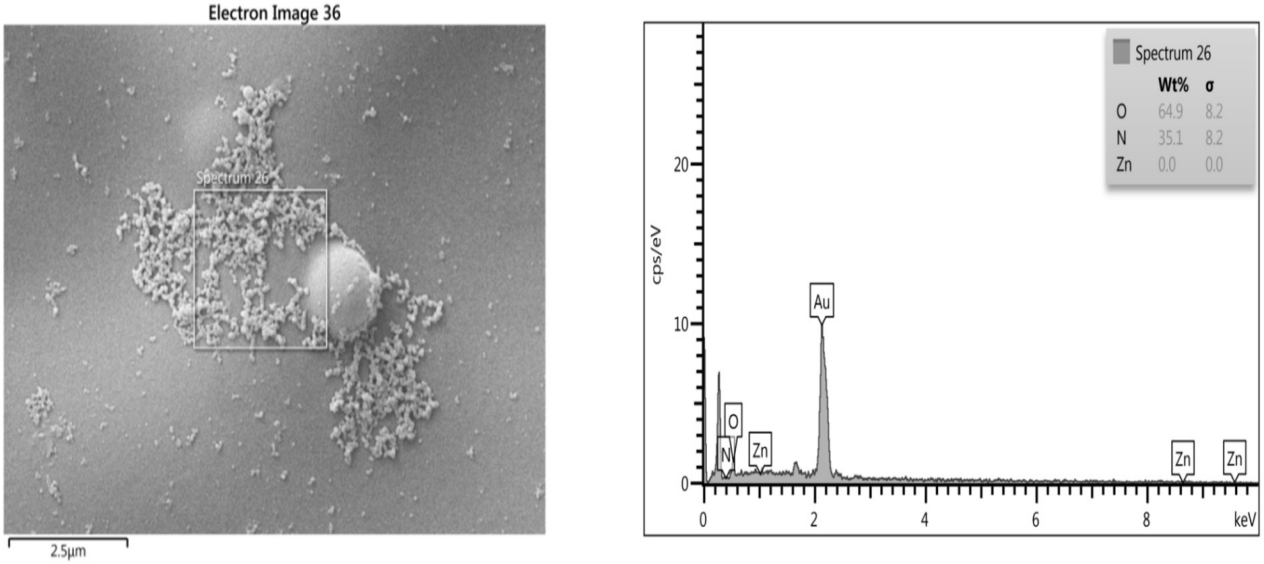

(a) **(b)**

Figure 3. SEM (a) Image and EDAX Analysis (b) of the PEI/ZIF-8 Membrane

The pressure changes over time for the constructed membranes are depicted in (Figure 4), while (Table 1) presents the calculated permeation values for both gases and the ideal carbon dioxide/methane selectivity for all constructed membranes, alongside similar investigations. It

was noted that the permeability of both gases rose with the introduction of additives to the pure polymer solution in the polymer matrix. This rise in permeability was more pronounced for carbon dioxide gas than for methane gas. One factor that contributed to the enhanced selectivity in the composite, as opposed to the pure membrane, was the selective absorption of CO_2 by the additive. This absorption facilitated and enhanced the passage of this gas, ultimately leading to an increase in selectivity. Moreover, the existence of additives enhanced the movement of the polymer chain, leading to chain breakage and increased free volume. Consequently, CO_2 exhibited higher permeability than CH_4 due to its greater solubility, thereby increasing the selectivity [20]. When comparing the obtained results with those of similar works, it's worth mentioning that the gas permeability and selectivity values varied due to differences in the thickness of the polymer films and the incorporation of additives with varying weight percentages, making direct comparisons challenging.

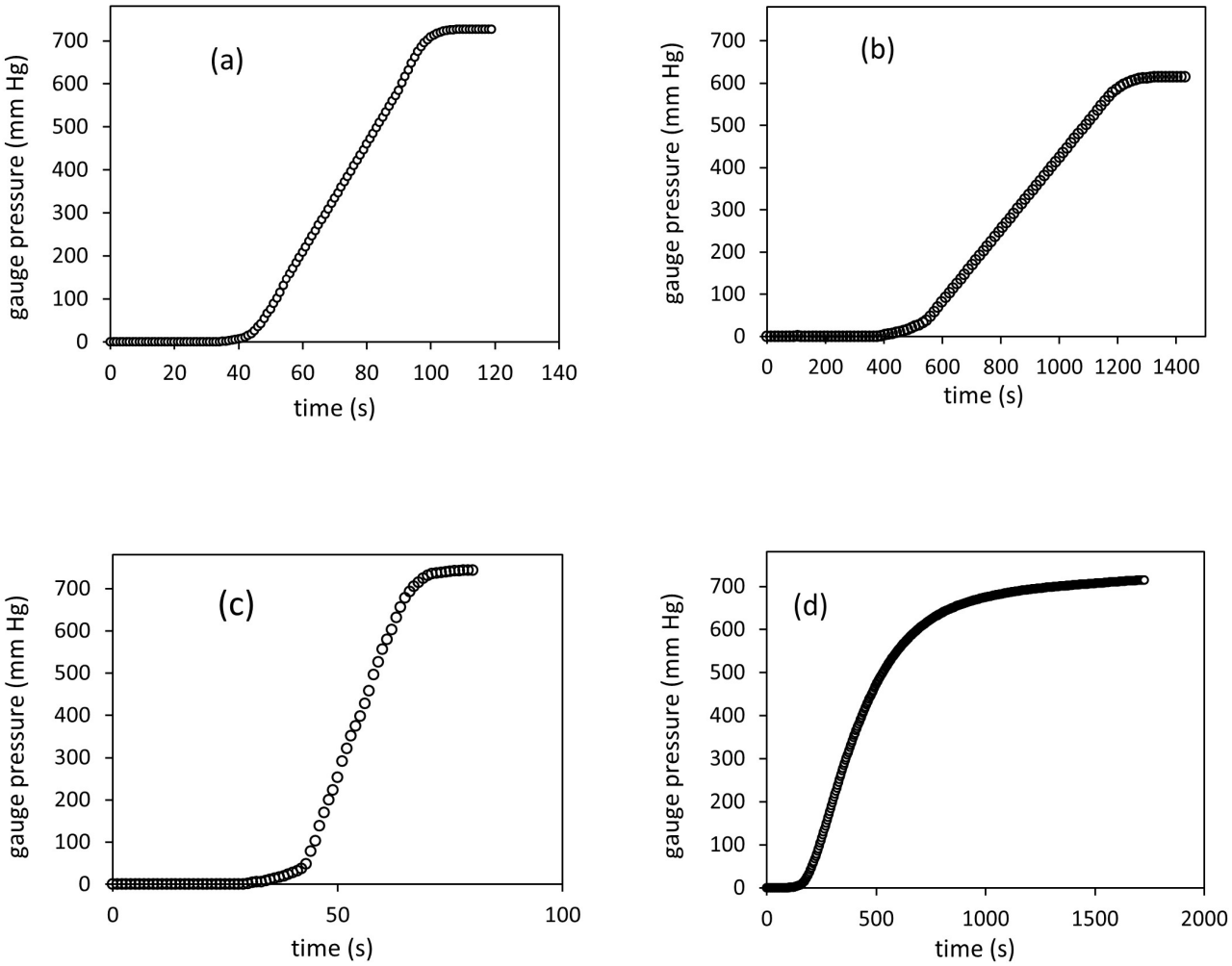

Figure 4. Diagram of Pressure Changes of Membranes:
a) Pure Polyetherimide Membrane for CO_2 Gas,
b) Pure Polyetherimide Membrane for CH_4 Gas,
c) Mixed Matrix Membrane for CO_2 Gas,
d) Mixed Matrix Membrane for CH_4 Gas

4. Conclusion

OIn this research, the effect of an additive such as zinc nitrate on the permeability properties of CO_2 and CH_4 gases of asymmetric composite membranes using polyetherimide by solution casting was evaluated. The prepared membranes were analyzed by Fourier transform infrared spectroscopic analysis (FTIR), X-ray diffraction analysis(XRD),energydispersiveX-rayspectroscopic analysis (EDAX) and scanning electron microscope image (SEM). Moreover, the effectiveness of the resulting membranes was checked by measuring the permeability of carbon dioxide and methane gases and also calculating the selectivity of carbon dioxide /methane. Fourier infrared spectroscopy analysis and X-ray diffraction showed the proper distribution of the additive or filler inside the polymer matrix, and the result of X-ray energy diffraction spectroscopy analysis confirmed the existence of zinc (Zn) in the membrane. The gas permeability test confirmed that the addition of additives to polymer membranes increases the permeability of gases (especially CO_2) and in addition to this, the Selectivity CO_2 / CH_4 has also had an upward trend in line with permeability.

Table 1. Comparison of Permeability and Selectivity of Pure Polymer and Mixed Matrix Membrane with other Reported Polymer Membrane

Membrane type	CO_2 permeability (GPU)	CH_4 Permeability (GPU)	CO_2/CH_4 selectivity	2005
Pure PEI	0.4333	0.0278	15.59	(Vega et al., 2019)
Mixed matrix membrane	0.5810	0.0458	12.68	
Pure PEI	1.535	0.0405	37.9	(Eiras et al., 2017)
Mixed matrix membrane	11.1	0.274	40.4	
Pure PEI	2.60	0.17	15.3	This Research
PEI/ZIF-8	5.91	0.31	19.1	

Acknowledgment

This manuscript is prepared based on the Master's thesis of the first author at Rasht Branch, Islamic Azad University, Rasht, Iran.

References

Azizi, N., Mohammadi, T. and Behbahani, R. M., 2017. Synthesis of a new nanocomposite membrane (PEBAX-1074/PEG-400/TiO_2) in order to separate CO_2 from CH_4. J. Nat. Gas. Sci. Eng., 37, 39. https://doi.org/10.1016/j.jngse.2016.11.038

Bergaoui, M., Khalfaoui, M., Awadallah, F. A. and Al-Muhtaseb, S., 2021. A review of the features and applications of ZIF-8 and its derivatives for separating CO_2 and isomers of C_3-and C_4-hydrocarbons. J. Nat. Gas Eng., 96, 104289. https://doi.org/10.1016/j.jngse.2021.104289

Chen, B. K., Su, C. T., Tseng, M. C. and Tsay, S. Y., 2006. Preparation of Polyetherimide Nanocomposites with Improved Thermal, Mechanical and Dielectric Properties. Polym. Bull., 57 (5), 671. http://dx.doi.org/10.1007/s00289-006-0630-3

Dorosti, F., Omidkhah, M. and Abedini, R., 2014. Fabrication and characterization of Matrimid/MIL-53 mixed matrix membrane for CO_2/CH_4 separation. Chem. Eng. Res. Des., 92 (11), 2439.

https://doi.org/10.1016/j.cherd.2014.02.018

Eiras, D., Labreche, Y. and Pessan, L. A., 2016. Ultem®/ZIF-8 Mixed Matrix Membranes for Gas Separation: Transport and Physical Properties. Mater. Res., 19 (1), 220. https://doi.org/10.1590/1980-5373-MR-2015-0621

Ma, Y., Sun. Y., Yin, J., Sun, H., Wu, H. and Wang, H., 2019. A MOF membrane with ultrathin ZIF-8 layer bonded on ZIF-8 in-situ embedded PSf substrate. J. Taiwan Inst. Chem. Eng., 104, 273. https://doi.org/10.1016/j.jtice.2019.08.012

Murali, R. S., Sridhar S., Sankarshana, T. and Ravikumar, Y. V. L., 2010. Gas Permeation Behavior of Pebax-1657 Nanocomposite Membrane Incorporated with Multiwalled Carbon Nanotubes. Ind. Eng. Chem. Res., 49 (14), 6530. http://dx.doi.org/10.1021/ie9016495

Perez, E. V., Balkus, K. J., Ferraris, J. P. and Musselman, I. H., 2009. Mixed-matrix membranes containing MOF-5 for gas separations. J. Membr. Sci., 328(1-2), 165. http://dx.doi.org/10.1016/j.memsci.2008.12.006

Rahman, S. N., Saleem, H. and Zaidi, S. J., 2023. Progress in membranes for pressure retarded osmosis application. Desalination., 549, 116347. http://dx.doi.org/10.1016/j.desal.2022.116347

Setiawan, W. K. and Chiang, K. Y., 2019. Silica applied as mixed matrix membrane inorganic filler for gas separation: a review, Sustain. Environ. Res., 29 (1), 1. https://doi.org/10.1186/s42834-019-0028-1

Singh, K., Devi, S., Bajaj, H. C., Ingole, P., Choudhari, J. and Bhrambhatt, H., 2014. Optical Resolution of Racemic Mixtures of Amino Acids through Nanofiltration Membrane Process, Sep. Sci. Technol., 49 (17), 2630. https://doi.org/10.1080/01496395.2014.911023

Vega, J., Andrio, A., Lemus, A. A., Díaz, J. A. I., del Castillo, L. F., Gavara, R. and Compañ, V., 2019. Modification of polyetherimide membranes with ZIFs fillers for CO_2 separation. Sep. Purif. Technol., 212, 474. https://doi.org/10.1016/j.seppur.2018.11.033

Xia, W., Zhu, J., Guo, W., An, L., Xia, D. and Zou, R., 2014. Well-defined carbon polyhedrons prepared from nano metal-organic frameworks for oxygen reduction. J. Mater. Chem. A., 2 (30), 11606. http://dx.doi.org/10.1039/C4TA01656D.

JOURNAL OF GAS TECHNOLOGY

Volume 8 /Issue 2 / Winter 2023 / Pages 35-55

Journal Home page: http://jgt.irangi.org

Simulation and Economic Evaluation of Flare Gas Recovery Using Nano Adsorbents

Meisam Bijanikhooy[1], Zohreh Saadati[2*], Afsaneh Maleki[2]

1. Ph.D. Student, Department of Chemistry, Omidiyeh Branch, Islamic Azad University, Omidiyeh, Iran
2. Associate Professor, Department of Chemistry, Omidiyeh Branch, Islamic Azad University, Omidiyeh, Iran

ARTICLE INFO

ORIGINAL RESEARCH ARTICLE

Article History:
Received: 15 October 2023
Revised: 16 November 2023
Accepted: 06 December 2023

Keywords:
Sorbent
Silica gel
Molecular sieve
Flare simulation
Natural gas

ABSTRACT

The oil and gas industry is facing a critical challenge with the growing emissions of flare gases, driven by the global expansion of the industry and increased fossil fuel consumption in refineries and petrochemical plants. The significant environmental impact of these flare gas emissions has created a pressing need to develop effective strategies to minimize the associated environmental risks. However, implementing technologies to reduce flare gas emissions presents both economic and environmental hurdles.

In this study, we investigated the application of nanoadsorbents in packed bed towers as a promising approach to recover and repurpose flare gases. Using MATLAB software, we conducted two case studies to evaluate the performance of different adsorbent materials, including Ws and H silica gels, as well as a 4 $\AA$ molecular sieve, for the recovery and conversion of sour flare gas into sweet, moist gas. The analysis revealed that the Langmuir isotherm model provided the most suitable simulation results, demonstrating the technical feasibility and effectiveness of this approach.

DOR: 20.1001.1/jgt.2024.2025628.1037

How to cite this article
M. Bijanikhooy, Z. Saadati, A. Maleki, Simulation and Economic Evaluation of Flare Gas Recovery Using Nano Adsorbents. Journal of Gas Technology. 2023; 8(2): 35-55. (https://jgt.irangi.org/article_714871.html)

* Corresponding author.
E-mail address: zo.saadati@iau.ac.ir, (Z. Saadati).

Available online 31 December 2023

1. Introduction

Petrochemical and oil & gas industries commonly use flaring stacks to burn flammable gas components, which is an unavoidable process for pressure control and safety management. However, gas flaring has become one of the most critical energy and environmental issues worldwide, resulting in environmental consequences and intense health issues for local populations (Mirrezaei and Orkomi, 2020). Flare gas production is particularly high in countries such as Russia, Nigeria, and Iran, which account for a significant portion of the total volume of gasses burned globally. Additionally, gas flaring causes energy loss and economic costs in countries. While waste hydrocarbon gasses contain valuable compounds such as methane, natural gas, and ethylene that have significant economic value, the proper disposal of these gasses is still one of the most pressing environmental problems in the oil, gas, and petrochemical industries (Soltanieh 2016, Bank 2004, Anejionu 2015). (Table 1) shows the amount of flare gas production from 2007 to 2011 in different countries, highlighting the increase in flare gas production in the United States from 2.2 billion m^3 in 2007 to 7.1 billion m^3 in 2011(Davoudi 2013).

Table 1. The Amount of Flare Gas Production from 2007 to 2011 in the Different Countries

Year	2007	2008	2009	2010	2011	Changes from 2010 to 2011
Russia	52.3	42	46.6	35.6	37.4	1.8
Nigeria	16.3	15.5	14.9	15	14.6	-0.3
Iran	10.7	10.8	10.9	11.3	11.4	0.1
Iraq	6.7	7.1	8.1	9	9.4	0.3
America	2.2	2.4	3.3	4.6	7.1	2.5
Algeria	5.6	6.2	4.9	5.3	5	-0.3
Kazakhstan	5.5	5.4	5	3.8	4.7	0.9
Angola	3.5	3.5	3.4	4.1	4.1	0
Saudi Arabia	3.9	93	3.6	3.6	3.7	0.1
Venezuela	2.2	2.7	2.8	2.8	3.5	0.7
All the first 20 countries	132	124	127	118	121	3.1
Other parts of the world	22	22	20	20	19	-1.1
The whole world	154	146	147	138	140	1.9

Flare gas burning has negative consequences on the ecosystem as well. Economic loss is another outcomes. According to estimates, the value of the gases flared globally in 2019 was $30.6 billion,or 30% of the gas consumed by EU (Tofigh and Abedian, 2016). To address this issue, the World Bank initiative "Zero routine flaring by 2030" aims to eliminate routine gas flaring and reduce the environmental impact of flare gasses. There are numerous approaches to decrease gas flaring, but they will probably call for fresh ways to gas monetization, incentives and business plans. A growing number of businesses have pledged to do away with flaring by 2030 (Mansoor and Tahir, 2021). By 2030, all non-emergency and wasteful flaring must be stopped in order to reach the net-zero flaring plan by 2050, this will allow for

the reduction or elimination of 90% of flare gasses by that time. One alternative to reduce flaring is the use of flare gas recovery (FGR) systems, which recover flammable gas for reuse as fuel for process heaters. The FGR system is a new technique applicable to refining waste that reduces the continuous flare operation, decreasing thermal radiation, associated smoke, noise, and pollutant emissions related to flaring (Bank 2004). Numerous researches indicate that this process and its usage are promising economically (Heydari, 2016, Hajizadeh 2018 Barekat-Rezaei 2018, Romsom and McPhail, 2021, Jafari 2021, Sabaghian 2022). However, the collection and exploitation of flare gasses have limitations that oil and gas-producing countries are facing, making performance optimization and modification of this part of the oil and gas industry crucial (Ahsan 2019). In this case, unfortunately, because of the high cost of recovery infrastructures, technical challenges, and a lack of suitable policies and regulatory frameworks prior to such commericial endeavors, flare gas recovery in Iran is still in its infancy (Barati 2019).

In a study in 2012, Rahimpour and Jokar discussed the technical feasibility of flare gas conversion and its use in the Farashband gas refinery using a simulation model. They concluded that electricity generation from Aghar and Dalan gas fields is economical (Rahimpour 2012).

In 2015, Wallace investigated the Bacon Formation as the world's largest shale reservoir. Its studies led him to the conclusion that flare gases can be applied to fuel drilling rigs during drilling operations (Wallace 2015).

In another work conducted in 2015, three approaches to flare gas reduction were suggested. These included injection gas into; South Pars reservoir, the feed stream of South Pars gas refineries, and Aghajari oil field. From an operational perspective, gas compression and injection into the fifth national pipeline was the best course of action. The outcomes showed that flare gas could be recovered at a high ratio and that gas transmission capacity could be increased (Hashemi Fard and Shafiee, 2019).

In 2016, Adekomaya et al, in a conducted resaearch stated that 42.6% of the extracted gas in Nigeria is flared daily, which can be used in thermal power plants, and the failure to supply electricity is the result of the lack of gas for power plants. They stated that by using flare gas, they will reach a sustainable level in the production and distribution of electricity (Adekomaya 2016).

In a different study conducted in 2016, Khanipour investigated the recovery of gas from flare gas and its subsequent reintroduction to the methanol synthesis reactor. According to the modelling data, there was an increase in methanol production with the returned gas. Furthermore, the analysis and simulation of important gas separation parameters revealed the ultrahigh ratio separation of recovered gases (khanipour 2016).

In 2019, Ojiagwo et al in a work examined the use of gas technology as an option to minimize gas degassing in Nigeria and minimize its environmental impact. The results of this study showed that electricity production through the use of part of the annual 18.27 BCM of gas in Nigeria will improve from its current daily production of 4358 MW to about 12000 MW. This serves as fuel for 50 gas turbine units with an output power of 150 MW each, with a potential increase in daily power generation of 7,500 MW.20 (Ojiagwo 2019).

Recent studies have focused on the recovery of valuable compounds from gas sent to the flare using a membrane or simulation model. For instance, In 2017, the economic investigation and technical characterization of FGR in different gas processing plants were examined in a research by Zolfaghari. Aspen HYSYS has been used to simulate three different process: GTL, gas turbines generation (GTG), and gas to ethylene (GTE). The outcomes demonstrated

how profitable these techniques are very year and how economical they are (Zolfaghari 2017).

In 2018, the integrated flare gas to gasoline (FGTG) process was studied by Jafari through technical analysis and simulation. In this work the Aspen HYSYS software was used to simulate integrated FGTG process for turning flare gas to gasoline. The simulation findings showed that gasoline may be raised by an average of 55% and 10% respectively, by recycling all gas emissions back into the process, including off gas from the methanol and MTG units (Jafari 2018).

in 2019 in a study, Saeedi et al estimated the use of catalytic membrane reactor as a new approach for gas recovery. In this research a comprehensive two-dimensional non-isothermal model was developed to evaluate the performance of gas recovery process with flame in membrane reactor. The environmental investigation showed that by using the catalytic membrane reactor to recover the greenhouse gases of Assalouye gas processing plant (Iran), the equivalent volume of greenhouse gas emission was reduced considereably (Saidi 2019).

Another study by Zhao et al. in 2021 proposed a novel approach to recover natural gas liquids (NGLs) from flare gas using a membrane separation process. The study demonstrated that the proposed membrane-based NGL recovery process can achieve high NGL recovery rates with low energy consumption (Zhao 2021).

In 2021 in a similar work by Jafari, design, simulation and economic investigation the process of DME (turning flare gas to dimethyl ether) in order to the production of gasoline, LPG (Liquefied petroleum gas) and hydrogen were conducted by Aspen HYSYS v.11 software, which the results were very promising (Jafari 2021).

In 2022, in a project by Sabaghian, the perspective use of the separated CO_2 from the flare gas in Parsian refinery for injection into a gas condensate reservoir was studied, which the results were very desirable (Sabaghian 2022).

To sum up, gas flaring contributes significantly to greenhouse gas emissions that contaminate the environment (Deljoo 2023). Nevertheles, there are precious compunds whith substantial economic worth found in the waste hydrocarbon gases from industrial units and complexes. Therefore, it is crucial to recognize alternatives for decreasing the flaring of these components by reusing and recovering this resource (Ng 2023). One option for reducing flaring is the use of FGR systems, and optimizing the oil and gas industry is essential in this regard. Several Studies have investigated the recovery of valuable compounds from the gas sent to the flare using a membrane or simulation models (Deljoo 2023).

The current project investigates the recovery of flare gases using nanoadsorbents to remove harmful compounds and assesses the technical and economic aspects of flare gas recovery from natural gas resources. The use of silica gel Ws, silica gel H, and molecular sieve 4 $\mathring{A}$ for dehumidification and sweetening of flare gas is explored to recover these valuable gases for different purposes contributing to increased national income. MATLAB software is used to model and simulate adsorption systems with nano-adsorbers, optimize the flaring system of two refineries as case studies, and evaluate the economic benefits of adsorption towers filled with nano-adsorbents as an alternative to flaring. The Parsian gas refinery, which is the third largest refinery in Iran and a significant supplier of the country's energy, was chosen as the first case study. The characteristics of the input and output gasses of the adsorption towers are presented, indicating the potential for recovery. The twelfth phase of South Pars with the most input gas flow and the highest volume of gas sent to flare is chosen as the second case study, highlighting the importance of recovering these gasses for economic gain and preventing environmental damage. The project findings provide valuable insights into reducing flare gas emissions and utilizing these valuable resources, indicating the novelty and importance of this work in contributing to Iran's

economic growth and sustainability.

2. Methodology

In this study, we investigated the use of MATLAB software to model and simulate adsorption systems with nanoadsorbers. We also conducted case studies to optimize the flaring systems of two refineries. For the first case study we conducted simulations and modeling using the isotherms of Langmuir and LAST. We then compared and evaluated the simulation outcomes with experimental results. For the second case study we used an appropriate isotherm model with modified modeling and examined the results of the simulation under different operating conditions. We also evaluated the economic feasibility of using adsorption towers filled with nanoadsorbents as an alternative to flare. The simulations were performed using the powerful MATLAB software, and the project was evaluated based on the simulation results.

As the first case study, we examined the Parsian gas refinery, as the third largest refinery in Iran which has a daily production capacity of 82 Mm^3 of natural gas and supplies 10% of the country's energy. In this complex, after separation processes in floodgates and separator containers, natural gas is dehumidified and the dew point is adjusted before being injected into the fourth nationwide line. The temperature of the gas entering the adsorption tower is 35-45 ℃ in summer and 25-30 ℃ in winter, and the dry gas comes out from the bottom of the tower after passing through a filter. The refinery has four towers that are used to adjust the dew point, with two towers for adsorption and the others for cooling and heating. The adsorption towers are placed in a specific order in the circuit, and the maximum pressure drop along the length of the tower is 0.7 according to the tower design. (Table 2) presents the input and output gas characteristics of the towers.

As our project focused on the recovery of flare gas, we chose the ninth refinery or the twelfth phase of South Pars for investigation. This was due to the fact this refinery currently has the highest input gas flow, which this means it sends the highest gas volume to the flare. Recovering these gases can have a positive impact on the economy and prevent irreparable damage to the environment. (Tables 3, 4, & 5) provide the characteristics of the sent gas to the flare during normal operating mode.

During the full operation mode, this refinery injects 3 Mft^3 of sour gas (equivalent to 75 Mm^3 of sweet gas) into the national network daily. Additionally, this phase produces 120 thousand barrels of gas condensate and 750 tons of sulfur for export. With the inclusion of this phase in the production circuit as well as the increase in Iran's gas contribution from the world's largest gas field, the country's gross national product is expected to increase by three percent, leading to a fundamental change in the national economy. This underscores the importance of the twelfth phase of South Pars (Keshavarz 1394).

Table 2. The Characterization of the Input and Output gases of Towers are Presented

No	Characteristic	Unit	Input amounts	Output amounts
1	Gas temperature	℃	34.3	37
2	Ws packed-tower height	m	0.64	0.64
3	H packed-tower height	m	6.36	6.36
4	Gas pressure	Bar	90	≈89.3
5	Water molar fraction in gas (Y_A)	--	0.00084	0.00080
6	C_5^+ molar fraction in gas (Y_C)	--	0.00498	0.0030

Table 3. Specifications of the Gas Components Sent to the Flare

No	Components	Molar percentage
1	H_2O	1.746
2	Nitrogen	0.607
3	Carbon Dioxide	10.549
4	H_2S	5.699
5	Methane	41.867
6	Ethane	8.346
7	Propane	5.983
8	i-Butane	1.812
9	n-Butane	3.544
10	i-Pentane	3.500
11	n-Pentane	3.428
12	C6	3.011
13	C7	3.089
14	C8	3.540
15	C9	3.377
	Total	100

Table 4. Specifications of the Gas Flow Rate Sent to the Flare

Parameter	Unit	Value
Flow	$Kg.h^{-1}$	76880
Temperature	°C	50
Pressure	Barg	7.0
Molecular weight	g/mol	40.08

Table 5. Characteristics of the Gas Entering the Circuit

Item	Unit	Value
Water molar fraction	%	0.19
CO_2 molar fraction	%	0.01019
Heavy hydrocarbon molar fraction	%	0.089
Temperature	°C	65
Pressure	Barg	5

3. Results and Discussion

3.1. Modelling of Moisture Adsorbent Tower with Silica Gel

In this study, we developed a model for the adsorption of water and heavy hydrocarbons in Ws and H silica gel, respectively. Due to the low concentrations of these two components in the inlet gas, only the adsorption of these components was considered. A mass transfer equation was written for the adsorbed component in the bed, and Langmuir and IAST models were used to communicate gas-solid equilibrium data. To account for the exothermic process, energy balance equations were used for non-isothermal substrate. Heat transfer in the radial direction was neglected due to the insulation of the walls of the adsorption tower. The system was not isothermal along the length of the tower, so the equations were solved element to element for the calculation of the equilibrium concentration. Mass transfer inside particles was diffusion and outside the bed medium was convection. Langmuir and IAST models were used to compare the results obtained in modeling and the most suitable model was selected. Surface adsorption was applied as a single layer on an ideal surface (Hajizadeh 2019). For the modeling of the adsorbent bed, several assumptions were made, including the same size of adsorbent grains, constant transfer coefficients, constant velocity along the tower, constant overall mass transfer coefficients independent of pressure changes, and a plug flow pattern with axial dispersion. Additionally, only heavy hydrocarbon particles were adsorbed in the H silica gel bed, and only water molecules were adsorbed in the Ws silica gel bed (Gholami 2010). (Figure 1) shows the selective element of silica hemadsorption substrate.

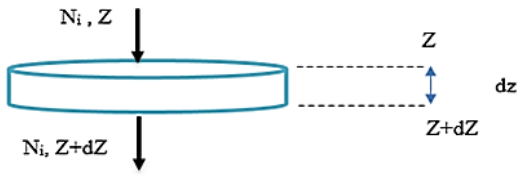

Figure 1. Selective Element of Silica Gel Adsorption Substrate

The considered assumptions for the modeling of the adsorbent bed:

- The same size is assumed for adsorbent grains.
- The transfer coefficients are considered constant.
- Velocity along the tower is considered constant.
- The overall mass transfer coefficients are considered constant and independent of pressure changes.
- The plug flow pattern with axial dispersion is considered.
- In the H silica gel bed, only heavy hydrocarbon particles are adsorbed.
- Only water molecules are adsorbed in the Ws silica gel bed.

The overall mass balance equation is as follows:

$$Input+Output+Generation - Consumption=Accumulation \quad (1)$$

The balance of water component (first part) mass transfer on the surface of Ws silica gel is presented by Eqs. (2) & (3).

$$-Dl\frac{\partial^2 C_1}{\partial z^2}+u\frac{\partial C_1}{\partial z}+\frac{\partial C_1}{\partial z}+\frac{nVp}{\varepsilon\Delta z}\left[\frac{\partial q_1}{\partial t}\right]=0 \quad (2)$$

The volume of adsorbent particles/the void volume of bed:

$$\frac{nVp}{\varepsilon\Delta z}=\frac{Vt-\varepsilon Vt}{\varepsilon Vt}=\frac{1-\varepsilon}{\varepsilon} \quad (3)$$

Integrating Eqs. (2) & (3) will have the following:

$$-Dl\frac{\partial^2 C_1}{\partial z^2}+u\frac{\partial C_1}{\partial z}+\frac{\partial C_1}{\partial z}+\frac{1-\varepsilon}{\varepsilon}\left[\frac{\partial q_1}{\partial t}\right]=0 \quad (4)$$

Eq.(4) shows the concentration change along the bed and time.

The basic conditions for mass balance in Eq.(4) are:

The water vapor concentration in the solid phase is zero Eq. (5). The initial concentration of water vapor in the gas phase is presented in Eq.(6).

Also, the boundary condition for mass balance in Eq. (4) is in accordance with Eqs. (7) & (8).

$$(q_A)_{t=0}=0 \quad (5)$$

$$(C_A)_{t=0}=C_{A0} \quad (6)$$

$$Z=0,\ C_A=C_{A0} \quad (7)$$

$$\mathrm{Z=L},\ (\frac{\partial C_A}{\partial Z})=0 \quad (8)$$

The mass transfer rate for the adsorbed components was calculated by the linear driving force model. In Eq. (8), concentration alteration in the adsorbed phase is proportional to the rate of mass transfer into the particles. Also, only one component (water vapor) is adsorbed by the adsorbent.

$$\frac{\partial q_A}{\partial t}=K_A(q_A^*-q_A) \quad (9)$$

Where K_A is the mass transfer coefficient and q_A^* is the equilibrium concentration in solid and gas phase interface.

The equation of Langmuir and Freundlich isotherm is as follows (Freundlich 1926):

$$\frac{q_A}{q_A^*}=\frac{B_0\exp(\Delta H)P_A}{1+B_0\exp(\Delta H)P_A},\ P_A=P_t\times V_A \quad (10)$$

The adsorption equation of ISTA is shown in Eq. (11).

$$\frac{q_A}{q_A^*}=a\times PA_n^1,\ P_A=P_t\times V_A \quad (11)$$

3.2. Heat Transfer Balance for Water Component (the First Component) in Silica Gel Bed

By simplifying Eq. (1) for energy transfer in the gas phase and simplifying it, the following equation is obtained:

(12)

$$\lambda_L.\frac{\partial^2 T}{\partial x^2}+\rho_g.C_{pg}.u\frac{dT}{dZ}+\rho_s.\frac{(1-\varepsilon)}{\varepsilon}C_{ps}.\frac{dT_s}{dt}+\rho_s.C_{pg}.\frac{dT}{dt}$$

$$=\rho_s.\frac{(1-\varepsilon)}{\varepsilon}\sum_{k=0}^{n}(-\Delta H).\frac{dq1}{dt}+\frac{4h_w}{\varepsilon d}.(T_f-T_w)$$

The energy balance for the solid phase is:

$$\rho_s C_{ps} \frac{dTs}{dt} + \rho(1-\varepsilon_p)\sum_{i=0}^{n=c}(-\Delta H).\frac{dq_1}{dt} = \frac{2h_p}{R_p}(T_f - T_s) \quad (13)$$

The initial conditions were as follows:

$t = 0,\ T(z,0) = T_{0,1}$

$t = 0,\ T_s(z,0) = T_{0,s}$

$t = 0,\ T_f(z,0) = T_{0,f}$

Also, the boundary conditions for energy balance are as Eqs. (14) & (15):

$$Z = L, T_{(L,t)} = T_{Out\ in\ layer\ 1} \quad (14)$$

$$Z = L,\ \frac{dT}{dz}(Z = L) = 0 \quad (15)$$

3.3. Momentum Balance for the Water Component (the First component) in the Silica Gel bed *Ws*

Due to the small pressure drop along the length of the tower, the momentum balance and Organ's equation were ignored.

3.4. The Modeling of Heavy Hydrocarbon Absorber Tower with Silica Gel *H*

Since the system of adsorption of humidity and heavy hydrocarbons is the same, the modeling of the heavy hydrocarbon adsorbent tower is completely similar to that of water vapor removal. However, values such as adsorption coefficients, and mass transfer, related to heavy hydrocarbons replace water vapor in modeling.

3.5. Describing the Numerical Solution of the Above Equations in MATLAB Software

According to the conditions and assumptions included in each section (gas phase and the solid phase in the adsorbent bed), after driving the model for the process in the both sections, differential equations were obtained for each component. In order to obtain the numerical solution of differential equations obtained from modeling in MATLAB software, the explicit finite difference method is used.

3.6. Explaining the Numerical Solution of Different Parts in MATLAB Software Side of Gas Phase

The differential equation obtained for each component is a PDE. To solve the PDE of each component, a finite difference numerical method of pure explicit type was used. The implementation process was as follows: along the length and in middle points in the center with second-order error, in the center of the bed as forward with first-order error, and at the end of the bed as backward with first-order error. To determine the number of steps along the length of the bed, PDE was opened numerically, and the concentration coefficient was obtained in the desired step. Then, considering the number of 100 steps toward the length and observing the condition of stability in such a way that the concentration coefficient becomes positive, the number of steps toward the length of the tower was determined.

3.7. The Contact Surface with the Adsorbent

Since the Langmuir and Freundlich isotherm was chosen for the model, the concentration amount in the first step was obtained in the radius direction and in all steps obtained along the length using the Langmuir-Freundlich equations. In the following, in each specific longitudinal step considering the molar flux from the gas phase side, the concentrations in the longitudinal direction were obtained according to the relationship of the isotherms.

3.8. Modelling

As in the input data, two case studies were investigated. In the modeling must be each two case studies investigated separately. In the first case study, two Langmuir and IAST isotherm models were simulated, which will be discussed.

3.9. The Simulation of the First Part (the First Case Study)

Considering that the case study data is based on the mole fraction of water vapor and

heavy hydrocarbons as well as the inlet and outlet gas temperature, for better comparison and evaluation, the graphs extracted from the simulation are provided based on the mole fraction and gas temperature. On the other hand, since the adsorption system is unstable, for better evaluation and optimization of the process, simulation has also been reported in 4 different periods (15, 30, 45 and 60 min).

First, the outcomes of the simulation by the Langmuir isotherm model are explained. On the other hand, according to the selected explicit finite difference method in the numerical solution of the obtained equations from the modeling the results of the simulation in the MATLAB software are as follows.

3.10. Simulation Based on Langmuir Isotherm

(Figure 2) shows the molar fraction of water vapor along the length of the bed filled with silica gel Ws in the period of 30 min after the beginning of the process. Water vapor molecules are adsorbed by silica gel Ws along the bed and their concentration decreases. As can be seen in (Figure 2), the mole fraction of water vapor output is very close to the actual data from the refinery.

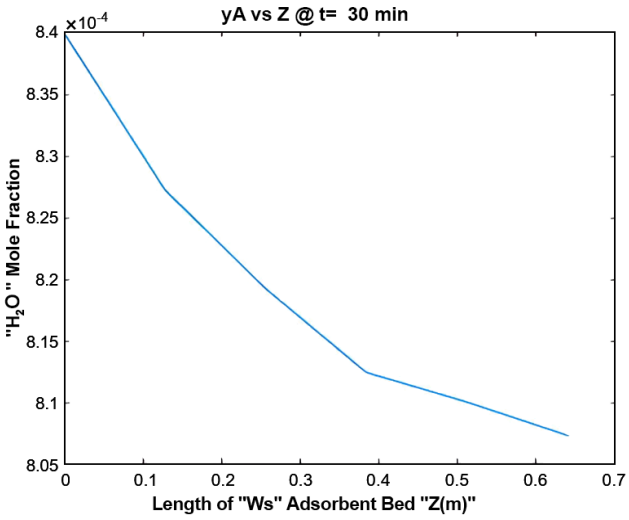

Figure 2. The Mole Fraction of Water Vapor along the Silica Gel bed Ws in Langmuir Model

(Figure 3) shows the molar fraction of C_5^+ along the length of the bed filled with silica gel H in the period of 30 min after the start of the process. C_5^+ molecules are adsorbed by silica gel H along the substrate and their concentration decreases. As can be seen from the (Figure 3), the molar fraction of C_5^+ output is very close to the actual data from the refinery.

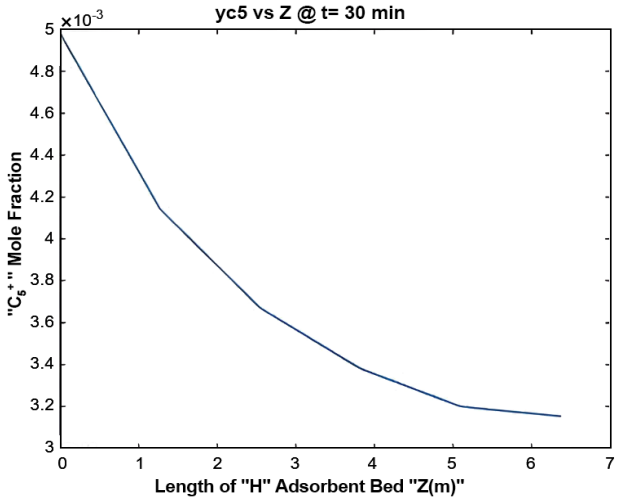

Figure 3. C_5^+ Mole Fraction along the Silica Gel Substrate H in Langmuir Model

According to (Figures 4 & 5), and this fact that the surface adsorption process is exothermic and as well as considering the insulation of the outer surface of the filled bed, the temperature of the gas will be increased along the bed. The temperature increasing trend is more intense in the early stages of the bed length due to more surface adsorption resulted from the large concentration difference in the gas and solid phases. By passing through the final stages of the substrate, the temperature increase is reduced.

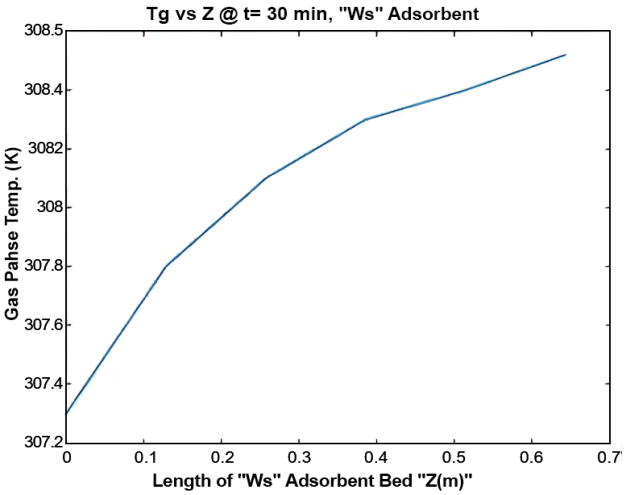

Figure 4. Gas-phase Temperature along the Silica Gel bed Ws in Langmuir Model

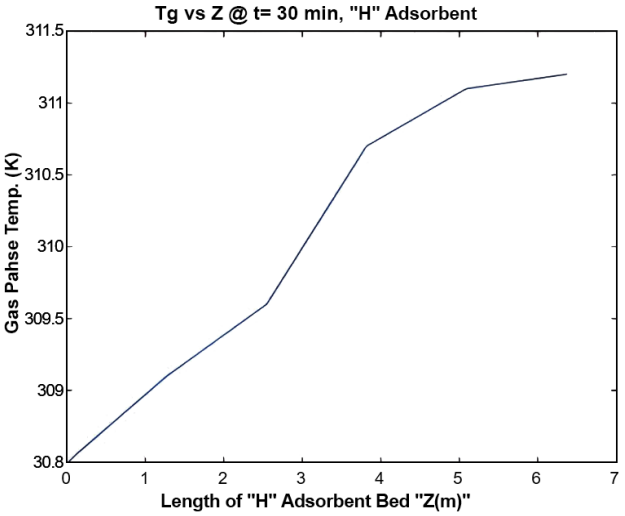

Figure 5. Gas-phase Temperature along the Silica Gel bed H in Langmuir Model

Owing to the instability of adsorption process, the amount of water molecule adsorption was checked in four periods for better evaluation. The outcomes can be seen as shown in the (Figure 5). As can be understood from (Figure 6), due to the concentration polarization difference in the solid and gas phase, the adsorption process in the early times is more, (do not saturation of silica gel with absorbable molecules). Then, over time, based on the saturation of the solid phase, the adsorption process progresses slowly and the filled tower must be entered the reviving stage. As can be seen from the above graphs, the best time to move to reviving stage is between 30 and 60 min.

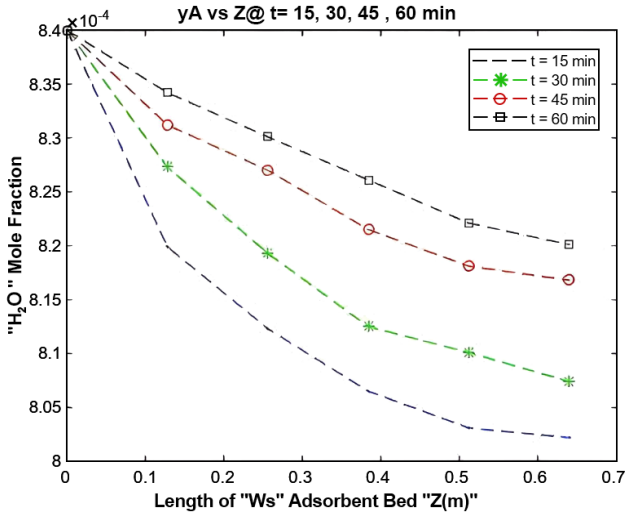

Figure 6. Water Vapor Molar Fraction along the Length of Silica Gel bed Ws in the Langmuir Model in Four Periods

Due to the instability of the adsorption process, the amount of adsorption of C_5^+ molecules was checked in four time periods for better evaluation, and the results can be seen as shown in (Figure 7).

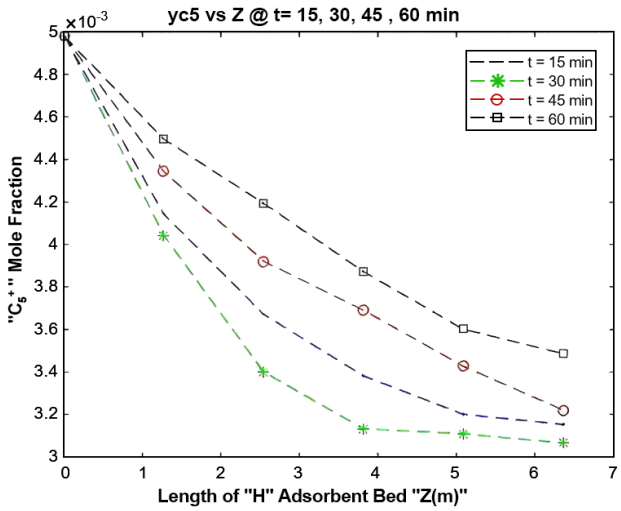

Figure 7. The Mole Fraction (C_5^+) along the Length of Silica Gel bed H in Langmuir Model in Four Time Intervals

As can be understood from the (Figure 7), the adsorption process is higher in the early times due to the concentration potential difference in the solid and gas phase (unsaturation of silica gel from absorbable molecules). Then, over time, based on the saturation of the solid phase, the adsorption process progresses slowly and the filled tower must be entered the regeneration stage. As can be seen from the above charts, the best time to move to the resuscitation stage is between 30 and 60 min.

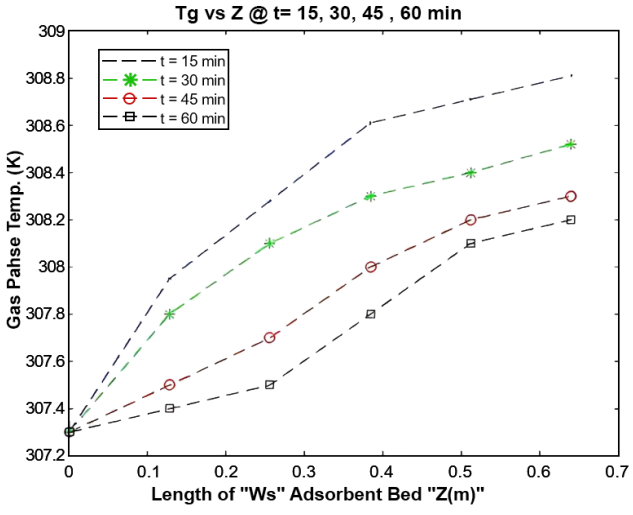

Figure 8. The Temperature of the Gas Phase along the Length of the Silica Gel bed Ws in Langmuir Model in Four Time Intervals

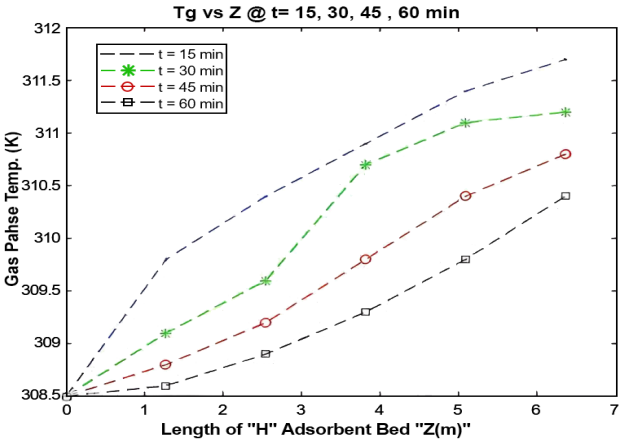

Figure 9. The Temperature of the Gas Phase along the Length of the Silica Gel bed H in the Langmuir Model at Four Time Intervals

According to (Figures 8 & 9), the temperature of the gas fluid experiences a lower temperature increasing over time along the bed, which the reason for this happening is the high concentration potential difference in the early times as explained earlier. Moreover, the saturation of the adsorbent bed with desired molecules over the time is another reason for this.

3.11. The Simulation Based on the IAST Isotherm Model

The above graph (Figure 10) shows the mole fraction of water vapor along the length of the bed filled with silica gel Ws for 30 minutes after the start of the process. Water vapor molecules are adsorbed by silica gel Ws along the bed and their concentration are decreased. As can be seen from the (Figure 9), the mole fraction of water vapor output is far from the actual data from the refinery, which this indicates the inadequacy of this isotherm in this system.

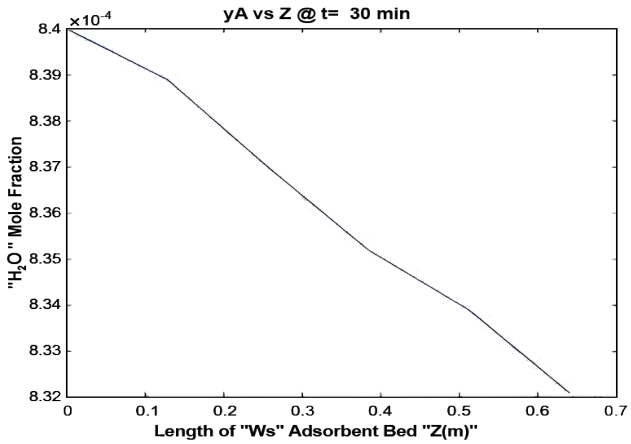

Figure 10. The Molar Fraction of Water Vapor along the Length of the Silica Gel bed Ws in the LAST Model

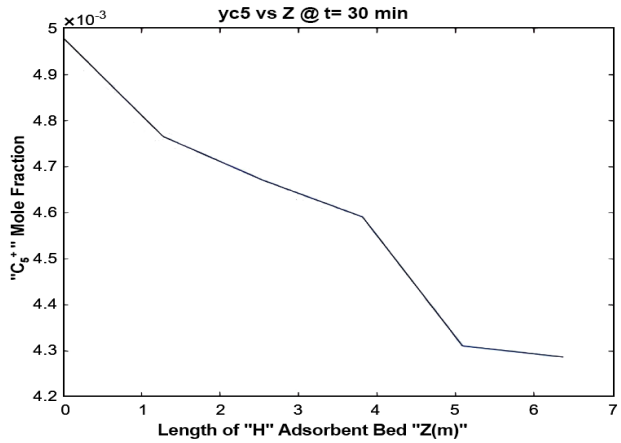

Figure 11. C_5^+ Mole Fraction along the Length of Silica Gel bed H in IAST Model

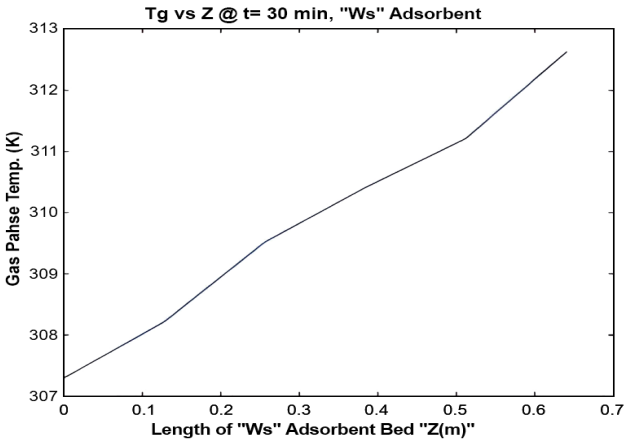

Figure 12. The Temperature of the Gas Phase along the Length of the Silica Gel bed Ws in the IAST Model

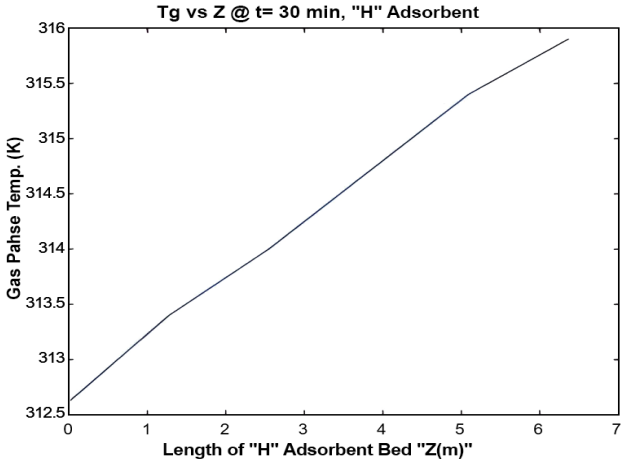

Figure 13. Gas-phase Temperature along the Length of the Silica Gel bed H in the IAST Model

5along the length of the bed filled with silica gel H within 30 min after the start of the

process. C_5^+ molecules are adsorbed by H silica gel during the bed and their concentration decreases. The output mole fraction of C_5^+ molecules is far from the actual data from the refinery, and this indicates the inadequacy of this isotherm in this system.

According to the above graphs (Figures 12 & 13) and the fact that the surface adsorption process is exothermic and also considering the outer surface of the filled bed as insulation, the gas temperature will be increased along the bed. This temperature increasing process is more intense in the early stages of the bed length due to more surface adsorption, due to the large concentration difference in the gas and solid phases. Therefore, by passing through the final stages of the substrate, the temperature increase is reduced. Based on the outputs of the IAST isotherm model, there is a big difference between the data obtained from the model and the actual data of the refinery, which indicates that the IAST isotherm is not suitable for the above system.

Due to the instability of adsorption process, the amount of adsorption of water and C_5^+ molecules were checked in four time periods for better evaluation and the results can be seen in the (Figures. 14 & 15). According to the results of the figures, the adsorption process is more in the early times due to the concentration potential difference in the solid and gas phase (unsaturation of silica gel from absorbable molecules). Over time, based on the saturation of solid phase, the adsorption process progresses slowly and the filled tower must enter the regeneration stage. According to the diagrams, the IAST isotherm has a high error in accurate and appropriate evaluation in the above system, and the output results differ greatly from the real data.

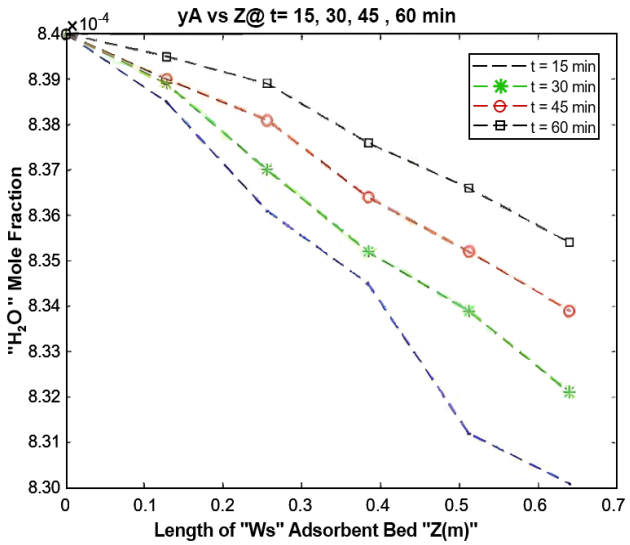

Figure 14. The Molar Fraction of Water Vapor along the Length of Silica Gel bed Ws in the IAST Model in Four Time Periods

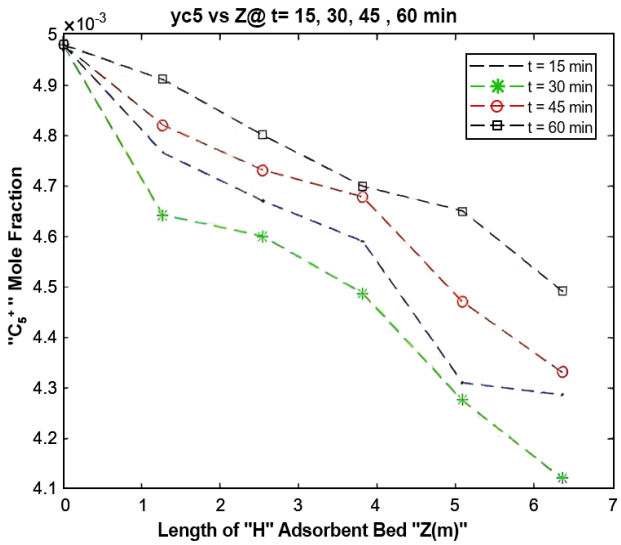

Figure 15. C_5^+ Mole Fraction along the Length of Silica Gel bed H in IAST Model in Four-time Intervals

According to the results in (Figures 16 & 17), the temperature of the gas fluid experiences a lower temperature increase over time along the bed, and the reason is based on what was explained earlier, the high concentration potential difference in the initial times and also, over time, the adsorbent bed becomes saturated with the desired molecule. As can be seen from the (Figure 16), the IAST isotherm has a high error in accurate and appropriate evaluation in the above system, and the output results differ greatly from the real data.

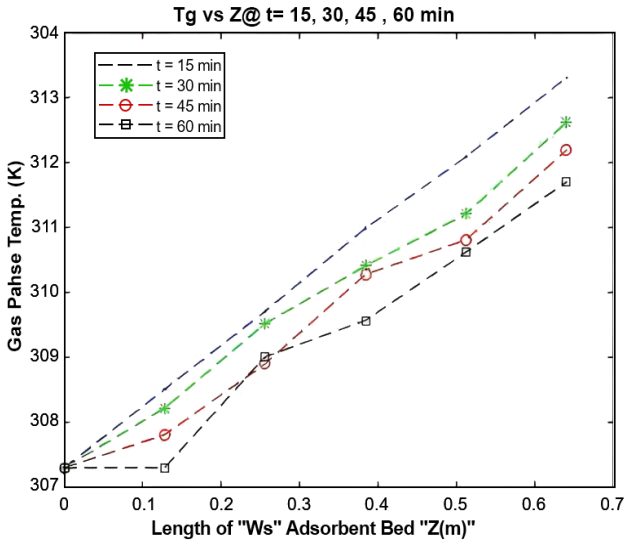

Figure 16. The Temperature of the Gas Phase along the Length of the Silica Gel bed *Ws* in the IAST Model at Four Time Intervals

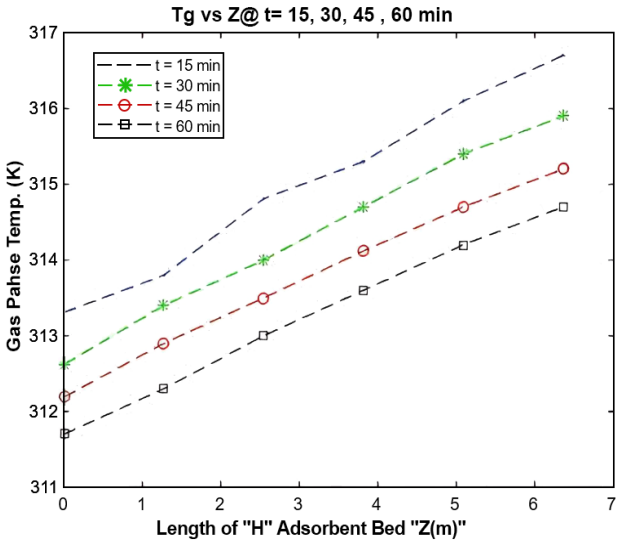

Figure 17. Gas-phase Temperature along the Length of the Silica Gel bed *H* in the IAST Model at Four Time Intervals

3.12. Comparing the Simulation Results of Langmuir Isotherm Model and IAST

According to the carried out simulations in the initial study case, for a better comparison of the results of using two Langmuir and IAST isotherm models in modeling the entire system of the adsorption process, the results of the output data from the adsorption towers and their difference with the real data, concretely, are given in the (Tables 7 & 8). According to the tables, the error rate of the IAST adsorption isotherm model for modeling the surface adsorption process in silica gel adsorbent is very high. Therefore, this is not suitable for the gas flare recovery system, sweetening and dehumidification using Nano adsorbents. In contrast, Langmuir isotherm model showed just an little error (less than 5%) in the three investigated parameters. This shows that for modeling and simulating the recovery process of gas flare by Nano adsorbents the Langmuir model is more suitable for adsorption on the surface of the adsorbent.

Table 7. The Comparison of Simulation Results of Two Isotherm Models Used

Row	Characteristic	The amount of input to the adsorp-tion unit	The amount of output from the adsorption unit (real data)	The amount of output from the adsorption unit (Simulation results) "Langmuir model"	The amount of output from the adsorption unit (Simulation results) "IAST Model"
1	Gas temperature	34.3 ℃	37 ℃	38.2 ℃	42.9 ℃
2	The mole fraction of water in the gas phase (Y_A)	0.00084	0.0008	0.0008074	0.0008321
3	C_5^+ molar fraction in the gas phase (Y_C)	0.00498	0.0030	0.003154	0.004287

Table 8. The Comparison of Simulation Results of Two Isotherm Models Used

Row	Characteristic	Some errors from the simulation "Langmuir model"	Some errors from the simulation "IAST Model"
1	Gas temperature	3.24%	15.94%
2	The mole fraction of water in the gas phase (Y_A)	0.92%	4.01%
3	C_5^+ molar fraction in the gas phase (Y_C)	5.13%	42.9%

3.13. The Simulation of the Second Part (Secondary Study Case)

In this section, the study case of the South Pars Phase 12 Gas Refinery is used. According to the investigations in the previous section, Langmuir isotherm was chosen as the most appropriate isotherm model for adsorption systems. Considering that the goal of this project is to recover gas flare by sweetening and its returning to the consumption line, three beds filled with nonadsorbent were selected to remove water vapor, heavy hydrocarbons and carbon dioxide. The dehumidifica-tion bed with *Ws* silica gel, heavy hydrocarbon removal bed with H-type silica gel, and carbon di-oxide removal bed with 4 *Å* molecular sieve adsorbent were considered. The used modeling in all three platforms was similar to the presented modeling in the previous sections, with the same boundary conditions and assumptions. In the simulation, the initial length of each bed was consid-ered to be 12 meters. According to the simulation in 4 time periods (similar to the simulation in the previous section), it is possible to obtain the optimal length for the bed in the best adsorption state for the South Pars Phase 12 refinery. On the other hand, due to the selection of 4 time periods in the simulated results, it is possible to obtain the appropriate and optimal time to start the regenera-tion process of each of the towers filled with adsorbent. In the following, the results of the simula-tion in the Matlab software environment are presented.

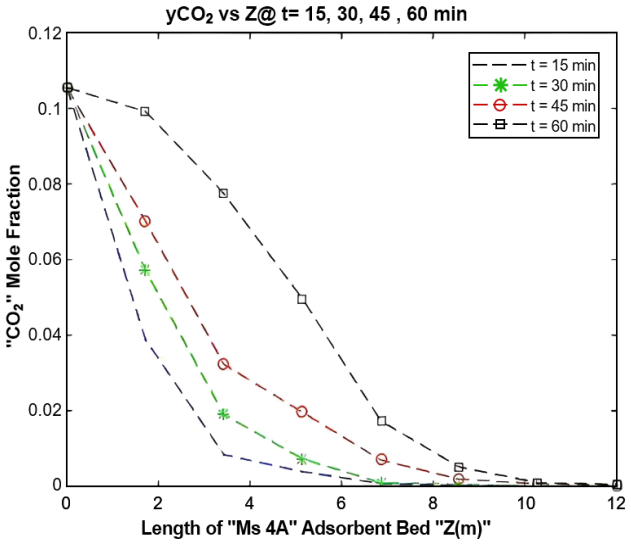

Figure 18. CO_2 Molar Fraction along the Length of the Ms-4A Silica Gel bed in the Langmuir Model for Four Time Periods

Due to the instability of the adsorption process, the amount of carbon dioxide adsorption was checked in four time periods for better evaluation and the results can be seen as shown in (Figure 18). According to the (Figure 18), the adsorption process is higher in the early times due to the concentration potential difference in solid and gas phase (unsaturation of silica gel from absorbable molecules). Over time, with the saturation of solid phase, the adsorption process progresses slowly and the filled tower must enter the regeneration stage. As it is clear from the graphs, the best time to move to the resuscitation stage is between 30 and 45 min. According to (Figure 19), in order to achieve an acceptable outlet concentration and in accordance with the experimental data of South Pars Refinery, the height of 11.1 meters

from the filled bed is the most optimal height to obtain the desired result in adsorption.

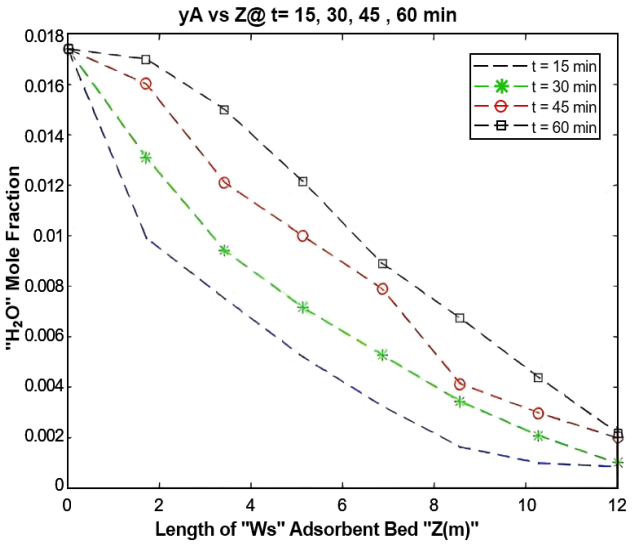

Figure 19. The Molar Fraction of Water Vapor along the Length of Silica Gel bed Ws in Langmuir Model in Four Time Intervals

Due to the instability of the adsorption process, the amount of water vapor adsorption was checked in four time periods for better evaluation and the results can be seen as shown in the (Figure 19). As can be understood from the (Figure 19), the adsorption process is higher in the early times due to the concentration potential difference in solid and gas phase (unsaturation of silica gel from absorbable molecules). Over time, based on the saturation of solid phase, the adsorption process progresses slowly and the filled tower must enter the regeneration stage. As can be seen from the above diagrams, the best time to move to the resuscitation stage is between 45 and 60 min. According to the above graphs, to achieve an acceptable outlet concentration and in accordance with the experimental data of the South Pars Refinery, the height of 10.5 meters from the filled bed is the most optimal height to obtain the desired result in adsorption. Due to the instability of the adsorption process, the amount of adsorption of heavy hydrocarbons was checked in four time periods for better evaluation, and the results can be seen as shown in the (Figure 20). According to (Figure 20), the adsorption process is higher in the early times due to the concentration potential difference in the solid and gas phases (unsaturation of silica gel from absorbable molecules). Over time, with the saturation of solid phase, the adsorption process decreases and the filled tower must enter the regeneration stage. As it is clear from the graphs, the best time to move to the resuscitation stage is between 45 and 60 min. According to the diagrams, in order to achieve an acceptable output concentration and in accordance with the experimental data of South Pars Refinery, a height of 10 meters from the filled bed is the most optimal height to obtain the desired result in adsorption.

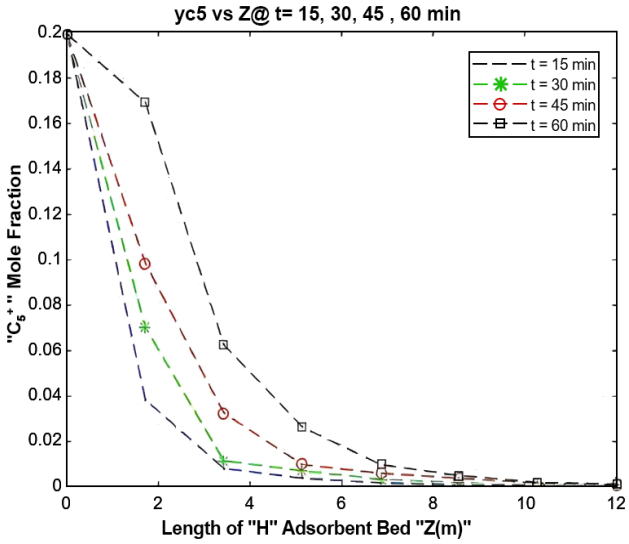

Figure 20. The Molar Fraction of Heavy Hydrocarbons along the Length of the Silica Gel bed H in the Langmuir Model in Four Time Periods

According to (Figure 20 & 21), as what was explained earlier, over the time, due to the high concentration potential difference in the early times and the saturation of the adsorbent bed over time of the desired molecule, the temperature of the gas fluid along the bed experiences a lower temperature rise. The temperature graphs for the other two substrates repeated a similar trend to the above trend. Therefore, we limited ourselves to only the above diagram for the substrate filled with a molecular sieve.

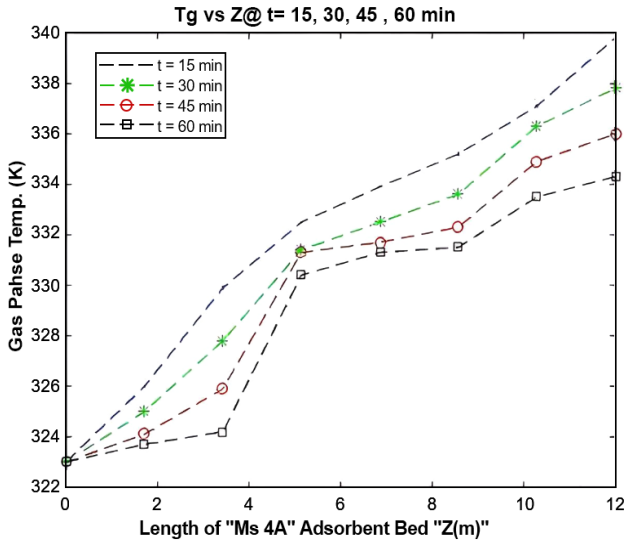

Figure 21. The Temperature of the Gas Phase along the Length of the Ms-4A Silica Gel bed in the Langmuir Model for Four Time Periods

3.14. Approximate Economic Evaluation

According to the carried out technical investigations in the previous sections, an economic evaluation is needed for a better analysis. In this way, by comparing the value of the gas flare price that is burned with the investment value in the construction and design of the adsorption unit to recover the gas flare, an approximate economic estimate is made. In this section, first, in the second study case (Phase 12 of South Pars), based on the amount of gas flow sent to the flare for burning, we estimate the dollar price of this flow. Also, the number of produced pollutants from this amount of flaring is calculated and reported. Then, based on the considered diagram for the adsorption unit, we calculate an approximate estimate of the fixed cost of the equipment, maintenance cost and etc.

3.15. Estimating the Price of Gas Flare and the Pollutants Caused by burning it

According to the reports of reliable authorities (Natural Gas Trading Economics), the current price of natural gas is 4.69 dollars per MMBtu. Every 1000 cubic meters of natural gas contains 36 MMBtu.

$$\frac{4.69\$}{1mmBtu}\times\frac{36mmBtu}{1000m^3}\times\frac{1m^3}{4.421Kg}\times\frac{76880Kg}{hr}=2936.02\,{}^{\$}/_{hr}=25.7\,{}^{m\$}/_{year}$$

According to the official and international rates of natural gas, the burning of natural gas sent to Flaring is 2936.02 dollars per hour and 25.7 million dollars per year, respectively.

3.16. The Amount of CO, NO_x Gas Emissions

In the desired gas refinery, steam-assistance flares are used, which in it steam employed to create smokeless combustion. Regarding to the high calorific value of the burned gases, the emission coefficients of the pollutants were selected and further with the help of the emission coefficients, the amount of emission of the pollutants can be calculated. The emission coefficients of NO_x and CO pollutants are presented in the (Table 9).

Table 9. Emission Coefficients of NOx and CO Pollutants in the Flaring System

Metal type	The calorific value of waste gas	NO_x (bm. $MMBtu^{-1}$)	CO (bm. $MMBtu^{-1}$)
(bm. MMBTU-1)	Top. >1000 BTU/Ft^3	0.0485	0.3503
Steam assist	Down. <1000 BTU/Ft^3	0.068	0.3465

3.17. Calculation of the Amount of Produced NO_x Pollutant

According to the calculation, the number of NO_x pollutants released from gas flaring is about 3000 tons per year.

$$(\frac{0.0485lb_{NO_x}}{MMBTU})\times(\frac{1270.77BTU}{SCF})\times(\frac{1MMBTU}{10^6BTU})\times(\frac{26.76\times10^6SCF}{1day})=1649.4\,{}^{lb_{NO_x}}/_{day}$$

$$(\frac{0.0485lb_{NO_x}}{MMBTU})\times(\frac{1270.77BTU}{SCF})\times(\frac{1MMBTU}{10^6BTU})\times(\frac{26.76\times10^6SCF}{1day})\times(\frac{1ton}{2000lb})\times(\frac{1000Kg}{1ton})=824.6\,{}^{Kg_{NO_x}}/_{day}$$

3.18. Calculation of CO Production Pollutant Amount

According to the calculation, the emission rate of carbon monoxide pollutants from gas flaring is about 2142 tons per year.

$$\left(\frac{0.35lb_{CO}}{MMBTU}\right)\times\left(\frac{1270.77BTU}{SCF}\right)\times\left(\frac{1MMBTU}{10^{6}BTU}\right)\times\left(\frac{26.76\times10^{6}SCF}{1day}\right)=11912.2\,{}^{lb_{CO}}\!/_{day}$$

$$\left(\frac{0.35lb_{CO}}{MMBTU}\right)\times\left(\frac{1270.77BTU}{SCF}\right)\times\left(\frac{1MMBTU}{10^{6}BTU}\right)\times\left(\frac{26.76\times10^{6}SCF}{1day}\right)\times\left(\frac{1ton}{2000lb}\right)\times\left(\frac{1000Kg}{1ton}\right)=5951\,{}^{Kg_{CO}}\!/_{day}$$

3.19. Approximate Economic Estimate of Setting Up an Adsorption Unit

According to the technical review and analysis of the flare gas recovery process using adsorbent towers, the economic estimation of this method helps to improve deciding for the faster use of flare gas recovery technology. In the economic evaluation of this study, some fixed costs (such as land, obtaining permits, etc.) and current costs (facility and utility costs, etc.) were considered for an approximate evaluation of 10% of the total fixed costs. First, in order to correct estimation of the adsorption process, an initial process map of the intended system is needed, which was designed by Microsoft Visio software (Figure 22).

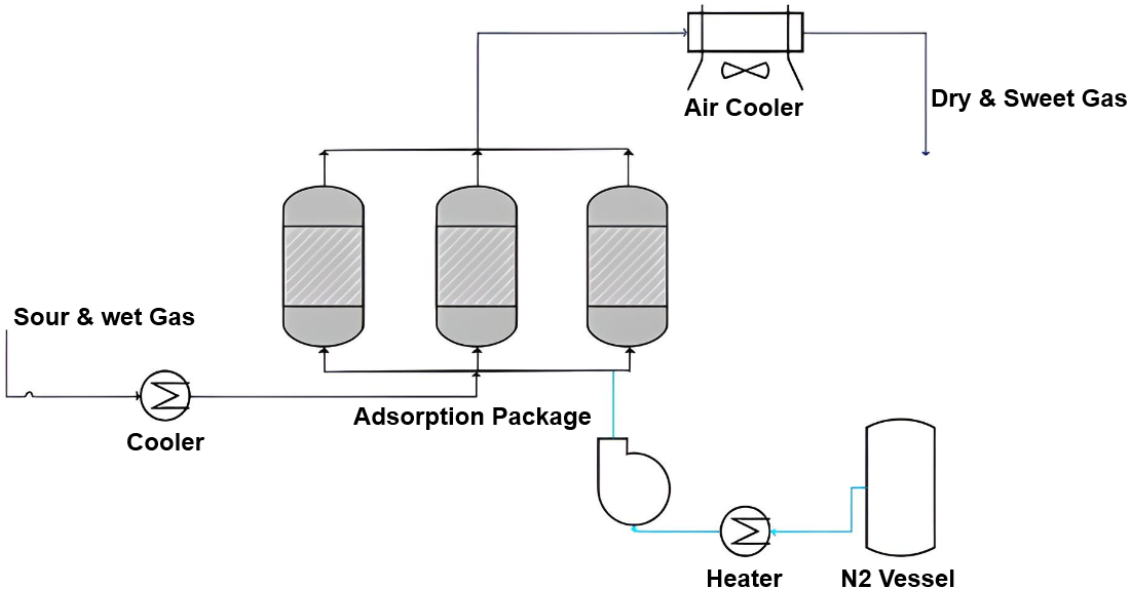

Figure 22. Schematic of the Adsorption Process in the Recovery of Gas Flares in South Pars Refinery

Due to the performed desired approximate comparison in the evaluation, the mentioned numbers in different references were employed. Thus, in some references, the cost of construction and maintenance of some equipment was in the form of curves with variable flow rates, which were extracted based on the mentioned gas flow rate in the previous sections (Voutchkov 2013). Some rotating equipment such as pumps, compressors, heat exchangers and air coolers were extracted from Aspen Hysys simulation software. Considering the above cases and assumptions, all the costs of equipment and maintenance and the method of using the absorber in the recovery of gas flare are given as follows.

Table 10. Estimated Costs of the Method of Using an Adsorbent to Recover Gas Flares in the South Pars Study Case

Row	Equipment	Fix Cost	Maintenance Cost
1	Inlet Cooler	458,000	68.700
2	Adsorbent Package	3*1650,000 4950,000	495,000
3	Air Cooler	300,000	45,000
4	N_2 Gas Vessel	510,000	76,500
5	N_2 Heater	210,000	21,000
6	N_2 Compressor	330,000	33,000
	Total Costs	6,300,000	739,200
	Total Fixed Costs of Equipment and Maintenance	7,039,200	
	Additional Costs (Such as Instruments, Permits, Piping)	703,920	
	The Total Approximate Cost of Project Implementation (the Dollar)	7,743,120	

To reach the decision point in the first phase of the study, simple payback period and simple rate of return (ROR) methods are usually used:

- Simple payback analysis
- Net present value
- A simple rate of return (Internal Rate of Return)

3.20. Simple Payback Analysis

This method is based on profitability criteria, and it is shown as a period of time that the total income related to the operation and installation of the facility after deducting all expenses, including taxes, is equivalent to the amount of investment required for consultation, purchase, and construction of the facility. This amount is equal to the ratio of the initial investment to the cash flow of annual earnings in the capital recovery period. In other words, it means:

$$\frac{\text{initial investment}}{\text{Annual savings}}$$

3.21. Net Present Value

In this method, all future incomes and expenses are converted to present value and added together. The interest rate is used to value money at this time:

$$NPV = \sum_{i=1}^{n} \left(\frac{R_i - C_i}{(1+r)^n} - C_0\right)$$

3.22. Internal Rate of Return

This method considers both the expected magnitude and timing of the cash flows in each period of the project's life. The internal rate of return for any investment proposal is the discount rate that equates the present value of the cash flow of expected costs to the present value of the cash flow of expected income.

$$NPV = 0 = \sum_{i=1}^{i} \left(\frac{R_j - C_j}{(1+r)^n} + 10\right)$$

In other words, the internal rate of return is the rate that makes the net present value of the project equal to zero. Now, according to the interpolation method, the amount of IRR can be calculated. The following diagram shows how to draw this process:

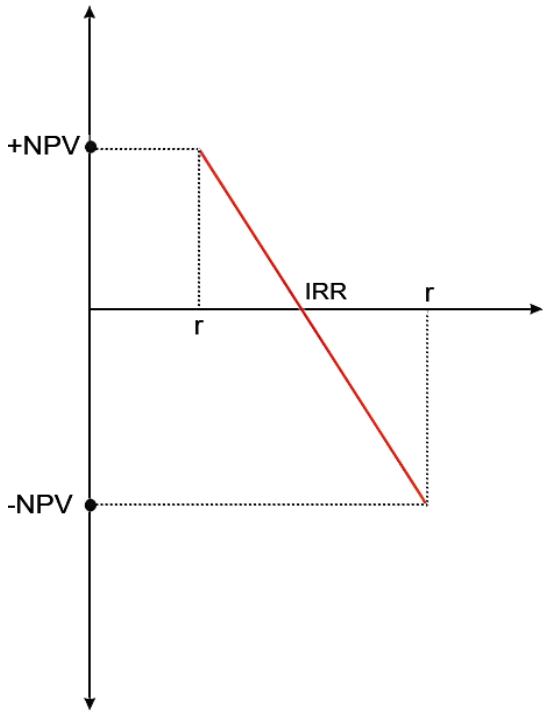

Figure 23. The Method for Drawing and Finding the IRR in the Graph

According to the chart, its formula is as follows, which can easily obtain the IRR amount.

$$IRR = [r_{low} + (r_{high} - r_{low})(\frac{NPV^{+}}{-NPV^{-} + NPV^{+}})] \times 100$$

In order to check this matter, it is always possible to achieve this by obtaining the investment cost, production rate, current cost, lifetime of the units, and annual profit of the project. The annual discount norm includes three factors:

- Inflation
- Interest rate
- Risk rate

This is not considered in these risk rate calculations. The (Table 11) shows the items calculated in the mentioned cases:

Table 11. Economic Evaluation of Gas Flare Recovery Methods

Unit Investment Cost	The Current Cost of the Unit	Unit Production Rate	The Amount of Profit Obtained from the Unit.	Return on Investment Period	NPV^{+}	IRR
The (Dollar)	The (Dollar)	M^3/hr	(Dollars/year)	(Year)	The (Dollar)	%
6.300.000	739.200	17389.7	25.700.000	3	459.750	13.141

4. Conclusion

One of the most important ways to prevent energy wastage is its management. According to the performed simulations related to the recovery method of gas flares, the output of each of the simulations, result in increase production and consequently decrease of environmental pollution. But the important point in this part is the economic evaluation and comparison of the flare gas recovery method with adsorbent towers filled with silica gel Ws, silica gel H and 4 $\mathring{A}$ molecular adsorbers, with considering the amount of pollution and the waste of capital in burning gas flare, which is very important in terms of an economic priority compared to the burning of gas sent to the flare. According to the performed economic evaluation, with the implementation of the flare gas recovery unit by absorber towers filled with nanoadsorbents, with an investment of approximately 25% of the cost of burned flare gas per year, within three years the entire cost returned and can to make the unit profitable. This is a reason for the recovery of the flare gas, on the other hand, it prevents much environmental pollution. In order to validation of derived results from modeling and simulation, actual operation data were used also.

Legend Caption

C_1	Water vapor concentration in gas phase
q_1	Vapor concentration in solid phase
Vp	The volume of the adsorbent beads in bed
Z	Length of bed
t	Time
K_A	Mass transfer coefficient
q_A^*	Equilibrium concentration in solid and gas phase interface.
d	Diameter of bed
P_A	Partial pressure of gas
P_t	Total pressure of gas
C_{pg}	Average heat capacity of gas balk
h_w	Convection heat transfer coefficient between gas balk and internal surface of bed side
C_{ps}	Average heat capacity of solid phase
h_p	Convection heat transfer coefficient between gas balk and adsorbent particles
ΔH	Exchanged heat in adsorbent process
ε	Porosity of bed
T_0	Base temperature
T_w	Temperature of side bed
T_f	Temperature of fluid phase
T_s	Temperature of solid particles
ρ_g	Density of gas phase
ρ_s	Density of solid phase
λ_L	Axial heat transfer coefficient

References

A. Ahsan, H. Ahsan, J. S. Olfert, L. W. Kostiuk. Experimental Thermal and Fluid Science 2019, 103, 133-142.

A. A. Tofigh, M. Abedian. Renewable and Sustainable Energy Reviews 2016, 57, 1296-1306.

M. Jafari, S. Ashtab, A. Behroozsarand, K. Ghasemzadeh, D. A. Wood. Gas Processing Journal 2018, 6, 1-20.

A. A. Keshavarz, the fourth national process engineering conference, refinement and petrochemical, 2015.

M. Jafari, A. Vatani, M. S. Deljoo, A. Khalili-Garakani. Journal of Gas Technology 2021, 6, 28-44.

A. Hajizadeh, M. Mohamadi-Baghmolaei, R. Azin, S. Osfouri, I. Heydari. Chemical Engineering Research and Design 2018, 131, 506-519.

H. Freundlich, H. Hatfield. Ltd., London 1926, 110-114

E. Barekat-Rezaei, M. Farzaneh-Gord, A. Arjomand, M. Jannatabadi, M. H. Ahmadi, W.-M. Yan.

K. Fard, M. Shafiee. Adv. J. Chem. A 2019, 3, 49-57.

A. Hajizadeh, M. Mohamadi-Baghmolaei, R. Azin, S. Osfouri, I. Heydari. Chemical Engineering Research and Design 2018, 131, 506-519.

M. Heidari, A. Ataei, M. H. Rahdar. Applied Thermal Engineering 2016, 104, 687-696.

E. L. Ng, J. Honeysett, Y. Scorgie. Sustainable Production and Consumption 2023, 35, 116-128.

F. G. U. Strategy. The International Bank for Reconstruction and Development. The World Bank 2004, 113.

M. Khanipour, A. Mirvakili, A. Bakhtyari, M. Farniaei, M. R. Rahimpour. Fuel Processing Technology 2017, 166, 186-201.

M. Zolfaghari, V. Pirouzfar, H. Sakhaeinia. Energy 2017, 124, 481-491.

M. Davoudi, M. Rahimpour, S. Jokar, F. Nikbakht, H. Abbasfard. Journal of Natural Gas Science and Engineering 2013, 13, 7-19.

M. Gholami, M. Talaie. Industrial & engineering chemistry research 2010, 49, 838-846.

M. Saidi. International Journal of Hydrogen Energy 2018, 43, 14834-14847.

M. R. Rahimpour, S. M. Jokar. Journal of hazardous materials 2012, 209, 204-217.

1. E. N. Ojijiagwo, C. F. Oduoza, N. Emekwuru. Procedia Manufacturing 2018, 17, 444-451.

M. Xue, X. Li, X. Cui, X. Cheng, S. Liu, W. Xu, Y. Wang. SPE Prod. Oper 2023, 49, 504-512.

M. Jafari, A.Vatani, MS. Deljoo, A. Khalili-Garakani, Journal of Gas Technology. 2021, 6, 28-44.

M. M. Sabaghian, M. Hajipour. Journal of Gas Technology. 2022, 7, 4-15.

JOURNAL OF GAS TECHNOLOGY

Volume 8 /Issue 2/ Winter 2023 / Pages 56-73

Journal Home page: http://jgt.irangi.org

Design and Simulation of Hydrogen Production from Diesel Reforming for Fuel Cell Applications

Mostafa Jafari[1], Majid Khorshidian[2*], Mazaher Rahimi Esboee[3], Vahid Kord Firouzjaei[2], Ali Vatani[4]

1. Researcher, Institute of Liquefied Natural Gas (I-LNG), School of Chemical Engineering, College of Engineering, University of Tehran, Tehran, Iran
2. Researcher, Malek Ashtar University of Technology, Northern Research Center for Science and Technology, Feridonkenar, Iran
3. Associate Professor, Malek Ashtar University of Technology, Northern Research Center for Science and Technology, Feridonkenar, Iran
4. Full Professor, Institute of Liquefied Natural Gas (I-LNG), School of Chemical Engineering, College of Engineering, University of Tehran, Tehran, Iran

ARTICLE INFO

ORIGINAL RESEARCH ARTICLE

Article History:
Received: 09 October 2023
Revised: 12 November 2023
Accepted: 07 December 2023

Keywords:
Diesel
Reforming
Hydrogen
Fuel Cell
Electricity
Aspen HYSYS

DOR: 20.1001.1/jgt.2024.2030854.1040

ABSTRACT

Hydrogen production encounters significant challenges in transportation and storage, such as leakage, transit safety, and the need for efficient storage conditions. On-site production through diesel fuel reforming presents a promising solution due to diesel's affordability, availability, and ease of transport. However, sulfur and carbon monoxide in diesel must be removed to protect the catalysts involved in the process. This study designs a conceptual process for reforming sulfur-containing diesel to generate 300 kW of electricity in a fuel cell system using the Douglas method, which structures chemical process design into a decision hierarchy. It starts with the Input-Output Structure, summarizing the process by detailing input and output streams based on designated design variables. The Recycle Stream Structure further divides the process into reactor and separation sections, each incorporating defined recycling flows. Finally, the Overall Separation Section Structure integrates gas and liquid recycling systems, providing a comprehensive strategy for separation unit design. The process flow diagram (PFD) was initially developed and subsequently analyzed in detail through simulation using Aspen HYSYS software. The results indicate that producing 300 kW of electricity requires 17 kg/h of pure hydrogen, which necessitates 47 kg/h of sulfur-free diesel. Overall, 60 kg/h of diesel is needed. Future research should focus on optimizing sulfur removal, reducing carbon monoxide levels, enhancing the water-gas shift reaction, maximizing energy efficiency, and assessing economic viability, including ROI and payback period.

How to cite this article
M. Jafari, M. Khorshidian, M. Rahimi Esboee, V. Kord Firouzjaei, A. Vatani, Design and Simulation of Hydrogen Production from Diesel Reforming for Fuel Cell Applications. Journal of Gas Technology. 2023; 8(2): 56-73. (https://jgt.irangi.org/article_714881.html)

* Corresponding author.
E-mail address: khorshidian@mut.ac.ir, (M. Khorshidian).

Available online 31 December 2023

1. Introduction

Producing and exporting hydrogen on-site is a significant challenge(Jafari, Deljoo, et al., 2020). Using liquid fuels in fuel cell systems expands the potential for deploying this technology in regions lacking readily available infrastructure for hydrogen production or facing difficulties in hydrogen due to volume constraints or transportation challenges (Le et al., 2023). Consequently, reforming liquid fuels emerges as a viable solution for global hydrogen production, considering the greater convenience and cost-effectiveness of exporting liquid products (Jafari, Vatani, et al., 2021; Lindström et al., 2009). Numerous researchers view hydrogen production from liquid fuels (such as diesel, kerosene, biodiesel, methanol, ethanol, etc.) as a promising midterm option (Dawood et al., 2020; Ghasemzadeh et al., 2017). Considering the complexities associated with the composition of diesel fuel and the challenges posed by numerical simulations in modeling various components and chemical reactions involved in diesel fuel reforming, it becomes necessary to employ rational and simplifying approximations. In this regard, (Table 1) presents a compilation of essential compounds utilized in simulations or models as surrogates for diesel fuel. Sulfur compounds in diesel act as a poison for fuel cell catalysts (platinum) and steam reforming catalysts (nickel) (Hoguet et al., 2009). (Table 2) shows the common sulfur compounds in diesel fuel and their weight percentages. Sulfur compounds are deemed the most significant impurities in diesel fuel.

Table 1. List of Compounds Used in Diesel Reforming Process

Chemical formula	Reference	Chemical formula	Reference
$C_{13.88}H_{24.053}$	(Lindström et al., 2009)	$C_{14}H_{26}$	(Creaser et al., 2011)
$C_{17}H_{36}$ - $C_{19}H_{38}$	(Samsun et al., 2020)	$C_{11.6}H_{19.6}$	(M. Bae et al., 2021)
$C_{12}H_{20}$	(Fauteux-Lefebvre et al., 2011)	$C_{13.4}H_{24.7}$	(Samsun et al., 2015)
$C_{14.342}H_{24.75}O_{0.0495}$	(Sahin, 2008)	$C_{12}H_{23}$	(Wang et al., 2021)
$C_{13.75}H_{27.14}$	(Brown, 2001)	$C_{12}H_{26}$	(J. Bae et al., 2016)
$C_{16.2}H_{30.6}$	(Lindermeir et al., 2007)	$C_{14}H_{26}$	(Dolanc et al., 2016)
$C_{13.3}H_{24.7}$	(Martin et al., 2015)	$C_{16}H_{34}$	(Liu et al., 2004)

Table 2. Common Sulfur Compounds and Mass Fraction in Diesel Fuel

Chemical formula	Mass Fraction	Reference
Dibenzothiophene (DBT)	0.012	(Jafari & Garakani, 2021; Permatasari et al., 2016)
Dibenzothiophene (DBT)	0.015	(Jafari & Khalili-Garakani, 2021; Pereira et al., 2000)
4,6-Dimethyldibenzothiophene (4,6-DMDBT)	-	(Kaila et al., 2008)
Dibenzothiophene (DBT)	0.014	(Gonzalez et al., 2018)

(Amphlett et al., 1998) simulated a 250-kW diesel fuel processor/PEM fuel cell system. They developed a process simulation model incorporating a higher temperature model for liquid hydrocarbon fuels and a steady-state electrochemical fuel cell model. Their investigation assessed the system's performance under various conditions and conducted a

preliminary assessment of thermal integration issues. (Ersoz et al., 2006) Three reforming technologies (steam reforming, partial oxidation, and autothermal reforming) were compared for hydrogen production from fossil fuels for PEM fuel cells. They studied 100-kW PEM fuel cell systems using natural gas, gasoline, and diesel, aiming to assess their overall efficiency. The study highlighted steam reforming as the most efficient fuel preparation option, with natural gas and steam reforming showing the highest fuel cell system efficiency. (Samsun et al., 2015), Investigated reforming diesel and jet fuel for fuel cells at a systems level. They focused on steady-state and transient operations of a 28-kWh fuel processor, addressing complexities and stability issues. Their results demonstrated high conversion efficiencies and effective CO management, enhancing the application of fuel cell technology in auxiliary power units and remote power systems. (Wang et al., 2021) studied a new SOFC-CCHP system fueled by diesel reforming with chemical looping hydrogen generation. Using Aspen software and a FORTRAN program, they analyzed system performance, achieving a power efficiency of 54.1% and identifying peak values for critical parameters. These findings lay the groundwork for future diesel-based energy systems, offering energy-saving and carbon recovery optimization insights. (Ješić et al., 2022), Conducted a computational investigation into diesel's auto-thermal reforming (ATR) process for hydrogen production, aiming to support PEM fuel cell applications. The study validated product composition through Gibbs minimization and investigated various parameters, including heat input, pressure potential, feed ratios, and kinetic parameters from the literature. Their findings facilitate the successful design and operation of ATR processes by enhancing the understanding of thermodynamic equilibria, transport phenomena, and mechanistic chemical rates.

(Geng et al., 2023) investigated the co-reforming of diesel and methanol into hydrogen-enriched gases for solid oxide fuel cell applications. They used Ru/γ-Al_2O_3 and Ni/γ-Al_2O_3 catalysts for steam reforming of diesel, achieving 100% diesel conversion and high hydrogen selectivity at temperatures above 600 °C. While the Ni/γ-Al_2O_3 catalyst showed poor carbon tolerance, adding methanol to the steam-diesel mixture extended the process life from 120 to 600 hours at 750 °C. The reformed diesel gas (RDG) fed into a solid oxide fuel cell (SOFC) achieved a peak power density of 1.34 W/cm^2 at 750 °C, with stable cell voltage and no carbon deposition on the Ni-YSZ anode, demonstrating RDG's suitability as a fuel for SOFC applications.

The production of hydrogen from diesel reforming for fuel cell applications is feasible and can be optimized using various reforming techniques and simulation tools. Proper control of operating parameters and efficient thermal integration are crucial for maximizing hydrogen yield and system efficiency. This study identifies research gaps in diesel fuel reforming for electricity generation in fuel cell systems, particularly at low capacities. Despite existing advancements, crucial areas have yet to be thoroughly explored. One significant gap is the effective removal of sulfur from diesel fuel, which is essential for preventing fuel cell catalyst poisoning. Additionally, there is a need for an integrated approach that combines both design and simulation to optimize the efficient conversion of sulfur-containing diesel into electricity. Our research aims to address these gaps by developing a comprehensive Process Flow Diagram (PFD) for steam-reforming diesel to produce hydrogen, which will be used to power a 300-kW fuel cell system. The novelty of our study lies in its detailed focus on sulfur removal and the subsequent integration of design and simulation processes. After synthesizing the PFD, we will thoroughly examine and simulate the process using Aspen HYSYS software to ensure optimal performance and efficiency.

2. Conceptual Design

Conceptual design in diesel steam reforming is crucial for creating an efficient blueprint for hydrogen production. It establishes optimal process flow diagrams and refines operating conditions, paving the way for effective implementation and resource utilization. The Douglas method's decision-making hierarchy guides this process through four key steps: evaluating process continuity, defining input and output streams, structuring recycled streams, and outlining separation section strategies (Douglas, 1988).

2.1. Input Information

The initial data emphasizes the conditions required for diesel steam reforming reactions. Key processes include hydrodesulfurization (HDS) and the pre-reforming reaction (PREF). (Tables 3 & 4) outline the design parameters, process inputs, and diesel composition. Estimating hydrogen consumption is critical for producing 300 kW of electricity.

Table 3. Design Conditions and Input Information

Parameters	Value
Power Generation (kW)	300
Operating Pressure (bar)	30
HDS Reactor Outlet H_2S Concentration (ppm)	<5
Requirements for Purified Hydrogen Stream	
Water (µmol/mol)	5
Total Hydrocarbons (µmol/mol)	2
Oxygen (µmol/mol)	5
CO_2 (µmol/mol)	2
CO (µmol/mol)	0.2
Total Sulfur (µmol/mol)	0.004

Table 4. Condition and Composition of Sour-Diesel
(Permatasari et al., 2016)

Properties	Value
Stream Name	Sour-Diesel
Temperature (°C)	25
Pressure (bar)	1.013
Component	Mass Fraction
(DBT)	0.0150
Naphthalene	0.0080
n-$C_{16}H_{34}$	0.9050

The HDS reaction operates at 200-300 °C temperatures 1-18 MPa pressures using NiMo/Al_2O_3 or CoMo/Al_2O_3 catalysts in a packed-bed reactor (Jejurkar et al., 2020). The PREF reaction occurs at 500-550 °C and 2-5 MPa, using Ni/Al_2O_3 catalysts in an adiabatic fixed-bed reactor (Ramantani et al., 2022). Steam methane reforming (SMR) reactions are crucial for hydrogen production, operating at 700-850 °C and 2-5 MPa (Cherif et al., 2021). The output of the SMR reactor enters the water-gas-shift (WGS) reactor to enhance hydrogen production. Typically, WGS processes encompass high-temperature (300-450 °C) and low-temperature (200-250 °C) stages, employing Fe-Cr and Cu-Zn-Al catalysts, respectively (Lee et al., 2023).

Given CO's detrimental effect on precious metal catalysts in fuel cells, Preferential Oxidation (PROX) reactions (120-160 °C) are implemented to eliminate CO, utilizing catalysts like platinum or copper supported by high-surface-area metal oxides such as alumina (Al_2O_3) or cerium (CeO_2) (Davǫ-Quiǫonero et al., 2020). The reforming furnace generates heat for steam production and heating the PREF reactor's outlet stream to attain the SMR reactor's reaction temperature. Its primary products include water, carbon dioxide, and heat, with reactions R9, R10, and R11 assumed to achieve complete conversion. (Table 5) details stoichiometry, reaction rates, and kinetics for the involved reactions.

Table 5. Stoichiometry and Reaction Rates of Synthetic Reactions in Diesel Reforming Processes

Parameters	Specification
HDS (R1) Stoichiometry	$C_{12}H_8S + H_2 \rightarrow C_{12}H_{10} + H_2S$
HDS (R1) Kinetic Data	$r_i = A_i.\exp\left(\frac{-E_i}{RT}\right).C^1_{C_{12}H_8S}$
	$r_i = \frac{kmol}{m^3.S}$, $A_i = 2.9 \times 10^7 \frac{1}{s}$, $E_i = 8.7 \times 10^4\ kJ/k\,mole$
PREF (R2) Stoichiometry	$C_{16}H_{34} + 16H_2O \rightarrow 33H_2 + 16CO$
PREF (R2) Kinetic Data	$r_i = A_i.\exp\left(\frac{-E_i}{RT}\right).C^1_{C_{16}H_{34}}.C^1_{H_2O}$
	$r_i = \frac{kmol}{m^3.S}$, $A_i = 2.01 \times 10^9 \frac{m^3}{kmole.s}$, $E_i = 116.9\ kJ/m\,ole$
PREF (R3) Stoichiometry	$C_{10}H_8 + 10H_2O \rightarrow 10CO + 14H_2$
PREF (R3) Kinetic Data	$r_i = A_i.\exp\left(\frac{-E_i}{RT}\right).C^1_{C_{10}H_8}\,C^1_{H2O}$
	$r_i = \frac{kmol}{m^3.S}$, $A_i = 10000\ \frac{m^3}{kmole.s}$, $E_i = 118\ kJ/m\,ole$
PREF (R4) Stoichiometry	$CO + 3H_2 \rightarrow CH_4 + H_2O$
PREF (R4) Kinetic Data	$r_i = A_i.\exp\left(\frac{-E_i}{RT}\right).C^1_{CO}$
	$r_i = \frac{kmol}{m^3.S}$, $A_i = 1 \times 10^9 \frac{1}{s}$, $E_i = 100\ kJ/m\,ole$
PREF (R5) Stoichiometry	$C_{12}H_{10} + 12H_2O \rightarrow 12CO + 17H_2$
PREF (R5) Kinetic Data	$r_i = A_i.\exp\left(\frac{-E_i}{RT}\right).C^1_{C_{12}H_{10}}\,C^1_{H2O}$
	$r_i = \frac{kmol}{m^3.S}$, $A_i = 11500\ \frac{m^3}{kmole.s}$, $E_i = 135\ kJ/m\,ole$
SMR (R6) Stoichiometry	$CH_4 + H_2O \rightarrow CO + 3H_2$
SMR (R6) Kinetic Data	$r_i = A_i.exp\left(\frac{-E_i}{RT}\right).C^1_{CH_4}\,C^1_{H_2O}$
	$r_i = \frac{kmol}{m^3.S}$, $A_i = 2.9 \times 10^7 \frac{1}{s}$, $E_i = 8.7 \times 10^4\ kJ/k\,mole$
WGS (R7) Stoichiometry	$CO + H_2O \rightarrow CO_2 + H_2$
WGS (R7) Kinetic Data	$r_i = A_i.exp\left(\frac{-E_i}{RT}\right).C^1_{CO}\,C^1_{H_2O}$
	$r_i = \frac{kmol}{m^3.S}$, $A_i = 1.4 \times 10^5 \frac{m^3}{kmole.s}$, $E_i = 54\ kJ/m\,ole$
PROX (R8) Stoichiometry	$2CO + O_2 \rightarrow 2CO_2$
PROX (R8) Kinetic Data	$r_i = A_i.\exp\left(\frac{-E_i}{RT}\right).C^1_{CO}$
	$r_i = \frac{kmol}{m^3.S}$, $A_i = 8 \times 10^7 \frac{1}{s}$, $E_i = 80\ kJ/m\,ole$
R9 Stoichiometry	$2C_{16}H_{34} + 49O_2 \rightarrow 34H_2O + 32CO_2$
R10 Stoichiometry	$C_{10}H_8 + 12O_2 \rightarrow 4H_2O + 10CO_2$
R11 Stoichiometry	$2C_{12}H_{10} + 29O_2 \rightarrow 10H_2O + 24CO_2$

2.2. Input-Output Structure

The input-output structure flowchart needs to be determined in the second stage of the conceptual process design for diesel steam reforming (Figure 1). A process box is drawn, focusing on inputs and outputs without considering other details. To define this box, it is necessary to answer questions about inputs, main and by-products, and other relevant details. Six fundamental questions must be addressed in the next stage to complete the inputs and outputs based on design variables. One of these questions examines the need for feed purification and the presence of recyclable by-products. For instance, sulfur compounds in diesel must be removed to ensure system stability and optimal performance.

Additionally, recyclable by-products are usually not recycled in steam reforming hydrogen production processes due to price differences and the return stream's importance, improving process efficiency and costs. In the HDS unit, there is no purge flow due to two factors. First, for a return and purge flow, at least one reaction product must be light invalid in HDS. Second, the required hydrogen is supplied from the downstream process, and since it is free of hydrogen sulfide, the condition for a purge is not met. Therefore, there is no purge flow in the reforming process, and hydrogen goes to the recycling process. According to (Table 6), there will be four output streams and one recycle stream.

Table 6. Determining Output Flows, Recycle, and Purge

Component	NBP (°C)	Stream
H_2	-252.8	Primary Product and Recycle
H_2	-252.8	Recycle
CO_2	-78.55	Waste
H_2S	-56.65	Waste
H_2O	100	Waste

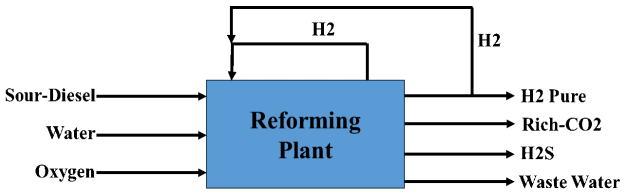

Figure 1. The Input-Output Structure of the Diesel Reforming Process

2.3. Recycle Structure

In the third step of the conceptual design of diesel reforming, critical decisions are made regarding the structure of return streams in the flowchart. This includes determining the number of reactor systems based on assessing reaction conversion levels, reaction types, and intensities, among other factors. The number of recycle streams is also determined by calculating the required stoichiometry. If the stoichiometry exceeds the required amount, additional input to the reactor may be necessary to maintain environmental equilibrium. Furthermore, if gas compression is needed for recycling streams or other purposes, a gas compressor may be required, with its costs typically estimated based on energy consumption requirements.

In the process, only the reactant recycled after purification is in the HDS reactor, which requires a compressor. This compressor increases the hydrogen pressure from 28.5 bar (Pressure of the hydrogen recovery unit by amine method) to 32.5 bar (input to the HDS reactor). Then, the stream enters the cooler for temperature adjustment. The produced hydrogen also supplies part of the required hydrogen. Two compressors are needed in this process, with the second compressor operating at a lower capacity than the first. The amine unit recovers most of the hydrogen needed for the HDS reactor. The type of reactor operation may necessitate adiabatic or non-adiabatic operation, depending on the need for precise temperature control in the reactor. (Figure 2) shows the recycle stream structure in the diesel reforming process.

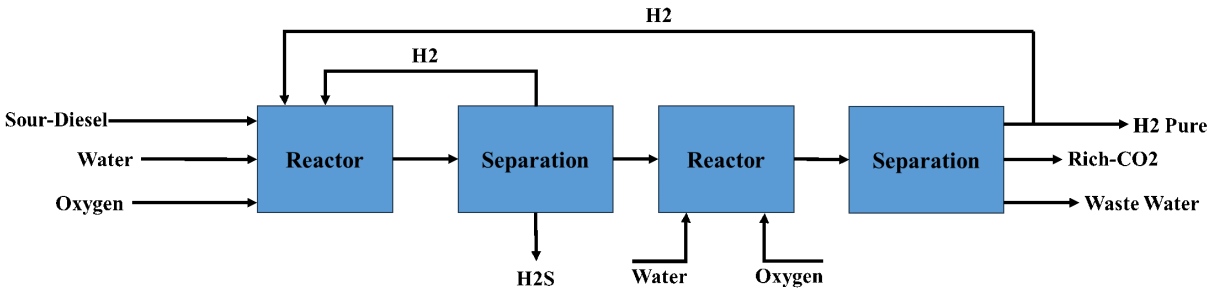

Figure 2. Recycle Stream Structure in the Diesel Reforming Process

The most important design variables in the diesel reforming process include the conversion percentage of the limiting reactant in the HDS, PREF, SMR, WGS, and PROX reactors, as well as the furnace; the molar ratio of the reactants; and the temperature and Pressure of the reactors. The hydrogen-to-oil ratio is considered to be 150 m^3/m^3 (Awad et al., 2020), calculated using Aspen HYSYS software (the molar ratio of hydrogen to diesel is 1.5 to 2.5). The oxygen-to-CO molar ratios in the PROX reactor are between 0.5 and 1 (Castaldi, 2009).

Reaction R1 occurs in the HDS reactor, reactions R2 to R5 in the PREF reactor, reaction R6 in the SMR reactor, the high-temperature WGS in an HTS reactor, the low-temperature WGS in an LTS reactor, and reaction R8 in a PROX reactor. Reactions R9 to R11 occur in the furnace, totaling seven reactors. (Figure 3) illustrates the number of reactors involved in the diesel reforming process.

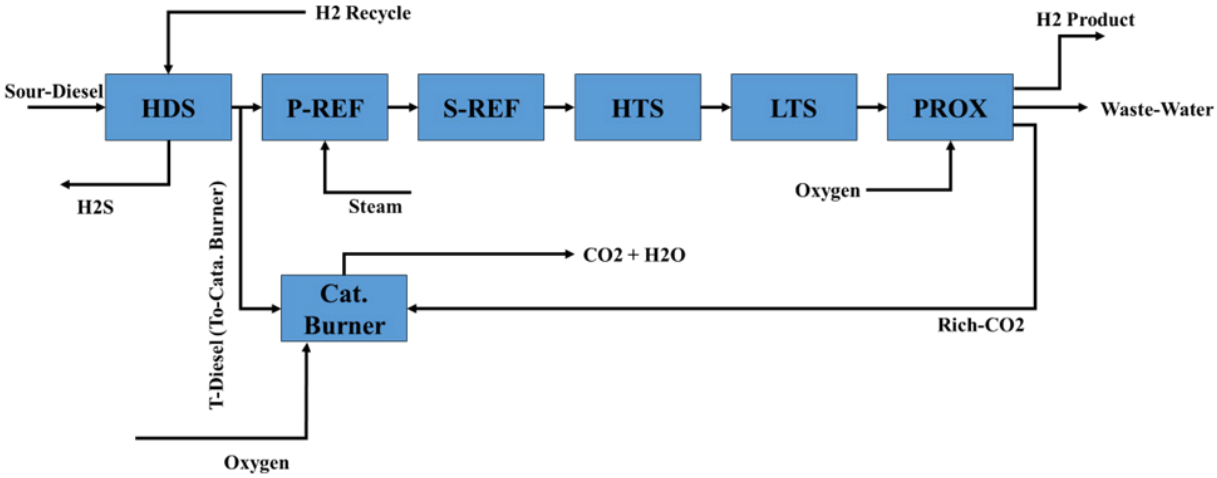

Figure 3. The Number of Reactors in the Diesel Reforming Process

4.1. Static Simulation

The fourth step in conceptual diesel reforming design, known as separation design, involves three main components: general structure, gas separation, and liquid separation. It establishes an overall separation framework based on the diverse states of the reactor output stream (liquid, vapor, or liquid-vapor mixture). Decisions on system configuration are guided by the phase of the reactor output, specifying methods for gas and liquid separation and detailing necessary tools and processes. Gas separation aims to isolate the gas phase, requiring the identification of appropriate tools such as two-phase separators, solid separators, or distillation towers. The HDS reactor output turns into a two-phase mixture after cooling

to 65 ℃, initially processed in a flash vessel or separator. At 120 ℃ and 24 bars, the PROX reactor output is released as a two-phase flow, then separated in a two-phase separator. Hydrogen gas and carbon dioxide are separated from the water-containing liquid stream.

The vapor separation system is designed using post-flash calculations to identify the vapor phase and then devise the vapor recovery system. The optimal placement and cost-effective type of vapor recovery system are determined by evaluating four potential scenarios: 1) in the Purge stream, 2) in the Recycle stream, 3) in the output vapor stream from the Flash, or 4) not needed. The steam exiting the first two-phase separator after the PROX reactor typically contains valuable hydrogen compounds and hydrogen sulfide, which must be separated. Since there is no Purge system, the gas recovery system is placed in the Recycle stream. Hydrogen recovery for return to the HDS reactor is done using the amine purification method with MDEA solvent, where hydrogen gas containing hydrogen sulfide is chemically absorbed in a tower with MDEA solution.

The liquid separation system design involves decisions on removing light components to maintain product quality, determining their destination, exploring azeotrope recycling, solvent use for breaking azeotropic points, assessing distillation feasibilities and column sequences, and exploring alternative methods if distillation is not viable. (Table 7) shows molar percentages of light components, indicating heavier diesel components causing light products to dissolve, prompting separation to remove hydrogen and hydrogen sulfide. While a two-phase separator can separate light components from liquids, vaporization of valuable components suggests that separating light components from liquids is preferable. After complete feedstock consumption and 100% conversion in the reactor, the light gas stream contains H_2 and H_2S. Distillation towers separate these compounds, with hydrogen extracted at the tower top due to its lighter nature. This purified hydrogen is crucial for fuel cell systems. Palladium membranes, known for their high selectivity in separating hydrogen from impurities like CO_2, are employed for this purpose. These membranes allow unhindered hydrogen passage while blocking other gases, ensuring cost-effective and efficient single-stage purification, which is essential for high-purity hydrogen processes. (Table 9) provides specifications of palladium membranes.

Table 8. Mole Fraction of Liquid Stream Post-HDS Reactor Two-phase Separator

Component	NBP	Mole Fraction
Hydrogen	-252.6	0.0151
H_2S	-59.7	0.0052
H_2O	100	0.0007
Naphthalene	218.0	0.1299
BiPhenyl	255.0	0.0169
n-C16	286.8	0.8332
DiBZThiphene	331.5	0.0000

Table 9. Palladium Membrane Specifications (Jafari, Deljoo, et al., 2020)

Specification	Value	unit
CH_4 permeance	1.00E-19	mol/m^2.s.pa
H_2 permeance	2.80E-04	mol/m^2.s.pa
O_2 permeance	5.50E-18	mol/m^2.s.pa
N_2 permeance	3.00E-17	mol/m^2.s.pa
CO_2 permeance	1.00E17-	mol/m^2.s.pa
H_2O permeance	5.00E21-	mol/m^2.s.pa

3. Simulation Strategy

The simulation process was conducted using Aspen HYSYS v.12, considering various kinetic models for the primary components of the studied operating system. Additional software, such as PRO/II, had to be employed to simulate the membrane purification section, and its results were integrated into the Aspen simulation. An important step in the simulation is the selection of units (Ghasemzadeh et al., 2017), in which the Euro SI unit has been used. The fluid package employed in this simulation is the Acid Gas equation (Jafari, Sarrafzadeh, et al., 2021); however, certain units require the definition of a separate fluid package for the simulation to be performed with very high accuracy (Jafari, Sarrafzadeh, et al., 2021). In the steam reforming section and fuel cell unit, the PRSV fluid package has been utilized (Jafari, Sarrafzadeh, et al., 2020). The simulation assumptions are as follows:

- Diesel Composition: Simplified to a single hydrocarbon, aromatic, naphthenic, and sulfur compound to reduce computational complexity.
- HDS Reactor Side Reactions: Side reactions are neglected to focus on the primary hydrogenation reaction, simplifying the model.
- HDS Reactor Modeling: Assumed to be a single tubular reactor with catalyst, instead of multi-stage catalytic beds, for reduced complexity.
- Reforming Furnace: Complete combustion reactions are assumed in a conversion reactor to achieve precise results.
- Reforming and Pre-Reforming: Both reactions occur in a single tubular reactor, simplifying the process and reducing computational complexity.
- Membrane Purification Unit: Simulated using Component Splitter in Aspen HYSYS, with membrane performance calculated in ProII and data imported to HYSYS.
- Hydrogen Stream for Fuel Cell: Pure hydrogen stream at 7.88 kmol/hr with required air enters the fuel cell system, with 80% hydrogen conversion and adjusted oxygen consumption for optimal performance.

4. Results and Discussion

With hydrogen's Lower Heating Value (LHV) at 120,000 kJ/kg (33.33 kWh/kg) and fuel cell efficiencies ranging from 40% to 60%, approximately 9 to 14.5 kg/h of pure hydrogen is required. Purifying hydrogen using a membrane process, with a recovery rate of 85% to 90%, is vital. Producing 17 kg/h of hydrogen necessitates approximately 42.5 kg/h of diesel. Moreover, purified diesel will be used for heat in the furnace, totaling over 45 kg/h. Precise calculations in Aspen HYSYS, assuming an additional 50-55% diesel consumption for the furnace, estimate a total input of 65-70 kg/h of diesel with sulfur compounds. In the HDS reactor, the hydrogen recycle stream is crucial, mostly recovered from the HDS unit, with some supplemented by in-process hydrogen. A compressor is necessary to return hydrogen due to pressure and temperature adjustments. Two compressors are needed, with the second operating at a lower capacity. Compressor costs include installation, operation, maintenance, energy consumption, and performance-related expenses. For the HDS reactor, hydrogen availability is 0.55 kilomoles per hour at 2.4 bar and 0.8 kW power. The second compressor receives 0.0172 kilomoles per hour at 1 bar pressure, with a flow of 0.97 cubic meters per hour, increasing to 27.90 bar with 0.96 kW power.

Since the pre-reforming reactor's outlet temperature is lower than the SMR reactor, the pre-reforming reactor's outlet temperature

needs to increase before entering the SR reactor. Hence, a heat transfer device is needed between the pre-reforming and reforming methane reactors for heating. This heat will be provided by passing the pre-reforming reactor's outlet stream through the reforming furnace. The output stream from the reforming reactor enters the HTS and LTS reactors. These reactors also operate adiabatically, with the HTS reactor's inlet temperature at 300 °C and the LTS reactor at 200 °C. Finally, the PROX reactor also operates adiabatically, with an inlet temperature of 120 °C. With these interpretations, after the steam-methane reformer, the outlet streams must be cooled before entering the HTS, LTS, and PROX reactors. Cooling water will be used in heat exchangers for cooling these streams (Figure 4).

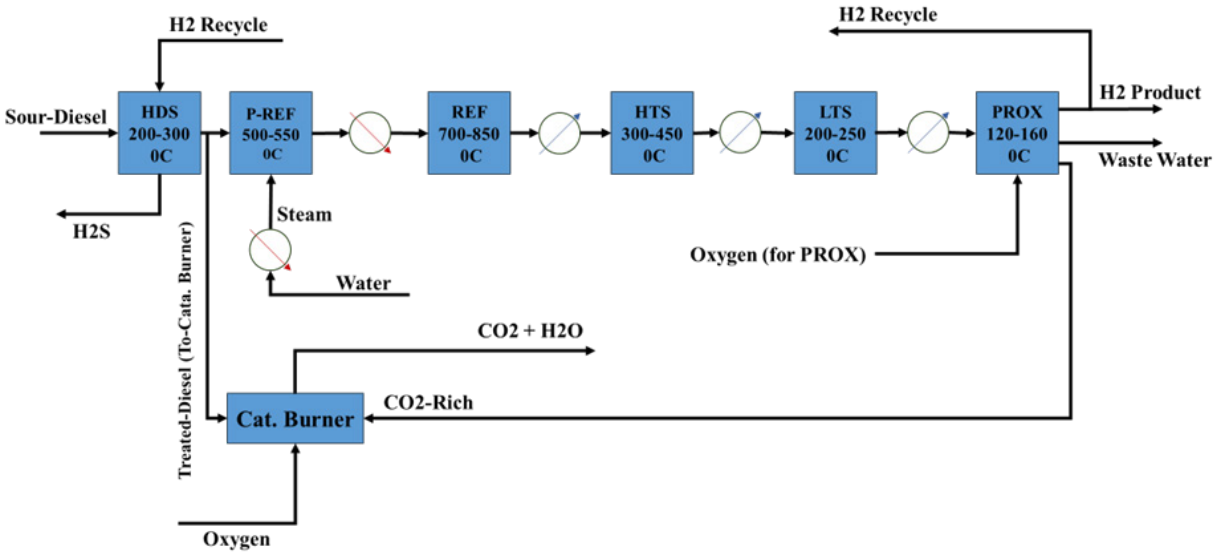

Figure 4. Reactor Sections and Temperature Ranges

A distillation column is used to separate H_2S from diesel fuel. In fuel cell systems, it is crucial to extract pure, impurity-free hydrogen from the reformer gas streams to ensure the longevity of the fuel cell. The quality of hydrogen must be guaranteed according to the international standards ISO 14687-2:2012 and ISO/DIS 19880-8 (Bacquart et al., 2019). Using palladium membranes to purify hydrogen from CO_2-rich streams is valued for its cost-effectiveness, efficiency, and single-step process. This method is essential for industries needing high-purity hydrogen, improving process quality and efficiency. This section analyzes heat transfer equipment and temperature adjustment requirements, including the placement of heat exchangers. In the HDS reactor, the output cools to 65 °C, becoming biphasic, and enters a flash vessel. Cooling is achieved with water at 26 °C inlet and 31 °C outlet temperatures. Using Aspen software, the coolant flow rate is calculated. This coolant then cools the condensers in the hydrogen recovery and separation towers. Each tower has reboilers heated by LP and HP steam. The treated diesel flows into the pre-reforming reactor, with some entering a catalytic furnace to produce steam. The furnace generates LP, MP, and HP steam, which heat the prereformer's endothermic reaction. Methane reforming reactor input is at 850 °C and output at 550 °C, needing cooling to 450 °C for the WGS reactor, using 26 °C coolant water exiting at 31 °C. LTS reactors at 200 °C and PROX reactors at 160 °C also require heat exchangers. Finally, the PROX reactor output is cooled to 50 °C for water separation before membrane processing. (Figure 4) illustrates the process flow diagram for steam diesel reforming.

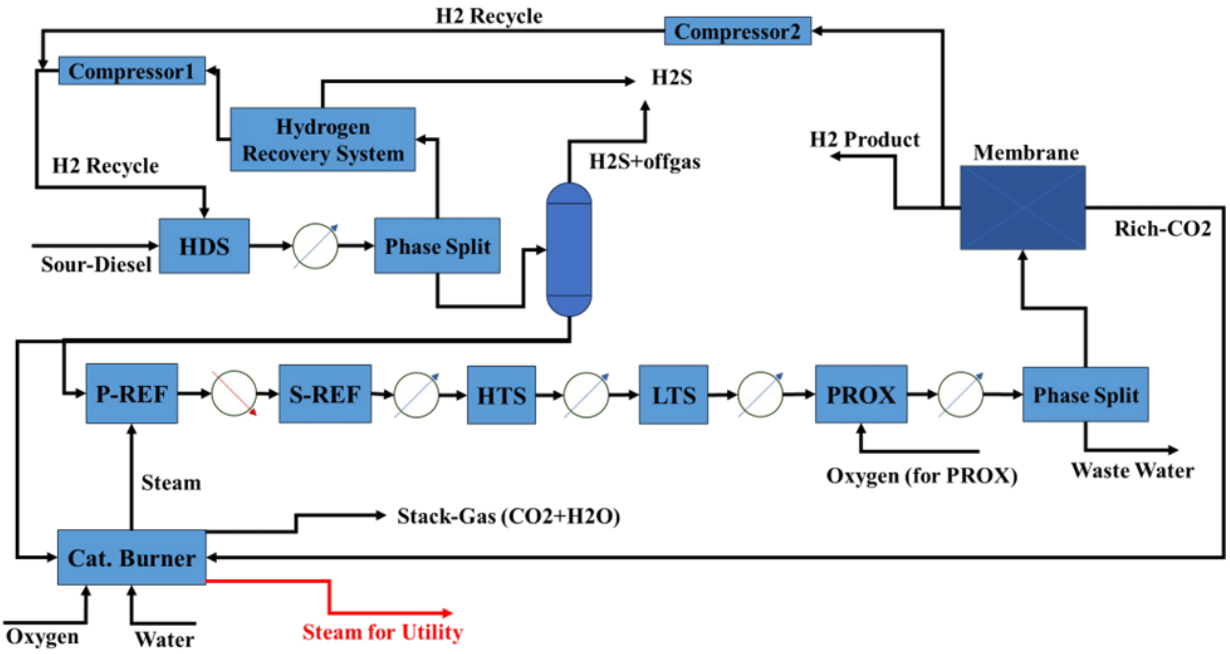

Figure 5. Process Flow Diagram of Diesel Steam Reforming

The simulation schematics of the final HDS unit and the hydrogen recovery unit in the amine solvent-based hydrogen sweetening unit are shown in (Figures 6, 7 and 8). In this simulation, the diesel stream undergoes hydrodesulfurization in the HDS reactor. Then, the hydrogen used in this process is introduced into the sweetening process via an amine solvent for recovery and reuse. The desulfurized diesel, primarily free of sulfur compounds like dibenzothiophene, enters the steam reformer reactor.

Both high-temperature and low-temperature shift reactions are conducted to enhance the quality of the syngas. Increasing the H_2/CO ratio directs the gas to the PROX reactor, converting CO to CO_2. The output stream from the PROX reactor subsequently enters the membrane process to produce pure hydrogen. The pure hydrogen is fed into the fuel cell system to generate electricity. (Table 10) summarizes the input and output streams for converting sulfur-containing diesel fuel into pure hydrogen and then converting hydrogen into electricity in the fuel cell system. (Table 11) shows the utility consumption and net electricity produced.

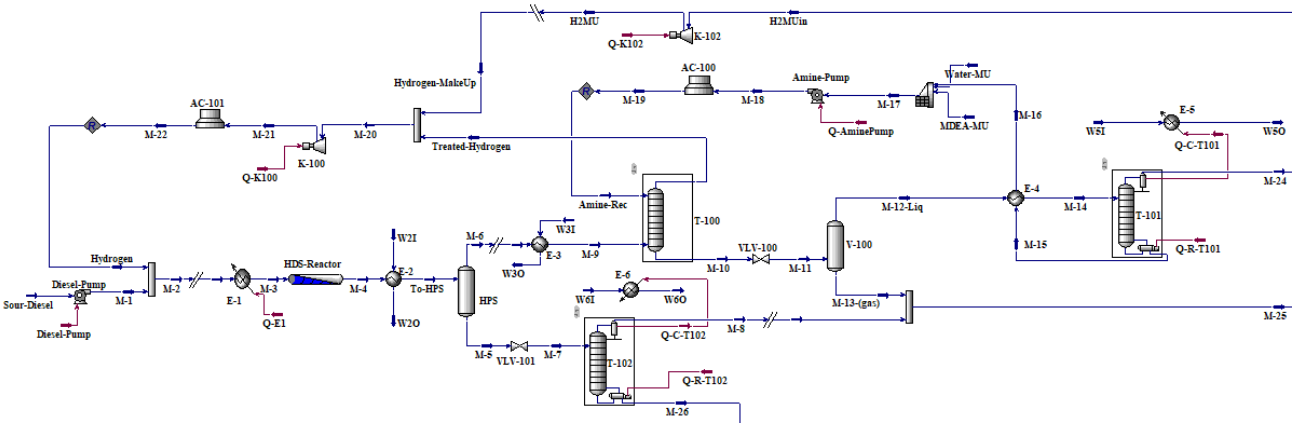

Figure 6. Schematic Simulation of the HDS Process with Hydrogen Gas Recovery

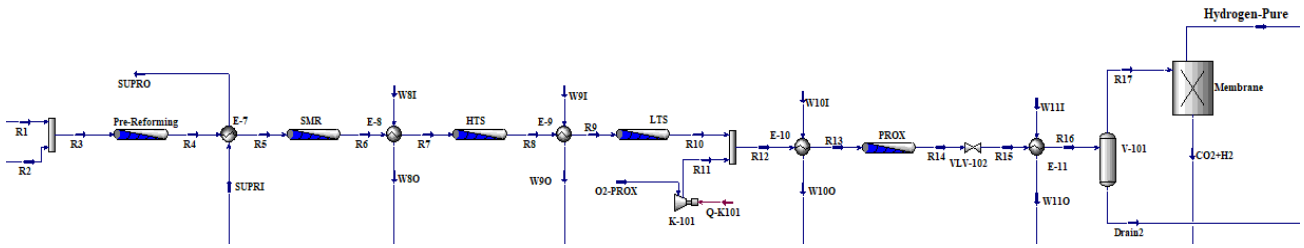

Figure 7. Schematic Simulation of the Diesel Reforming Process with Hydrogen Purification

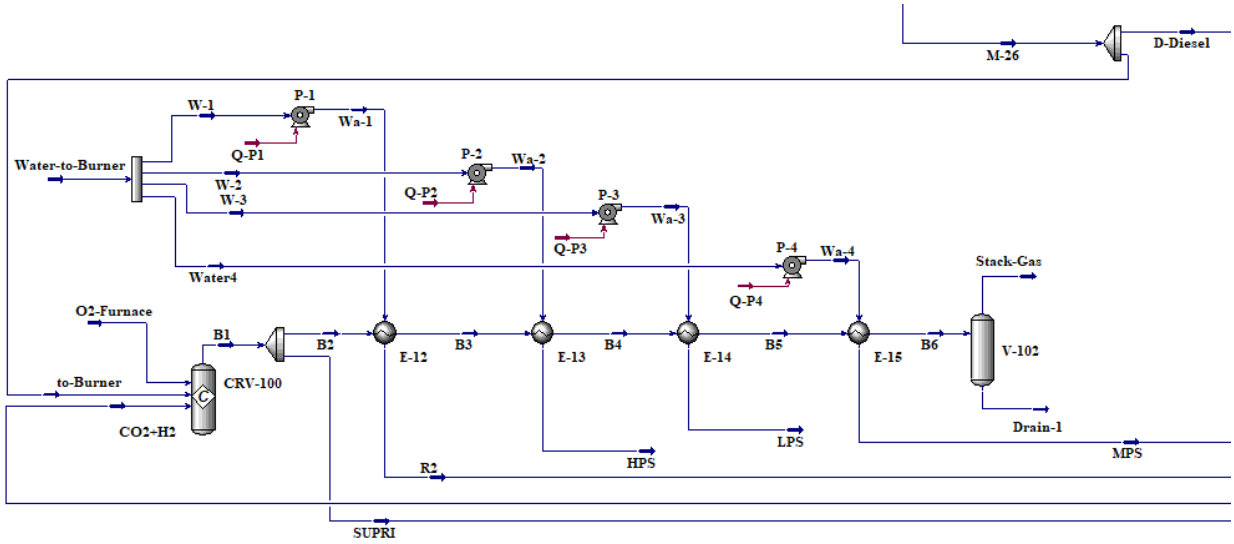

Figure 8. Schematic Simulation of the Reforming Furnace Section

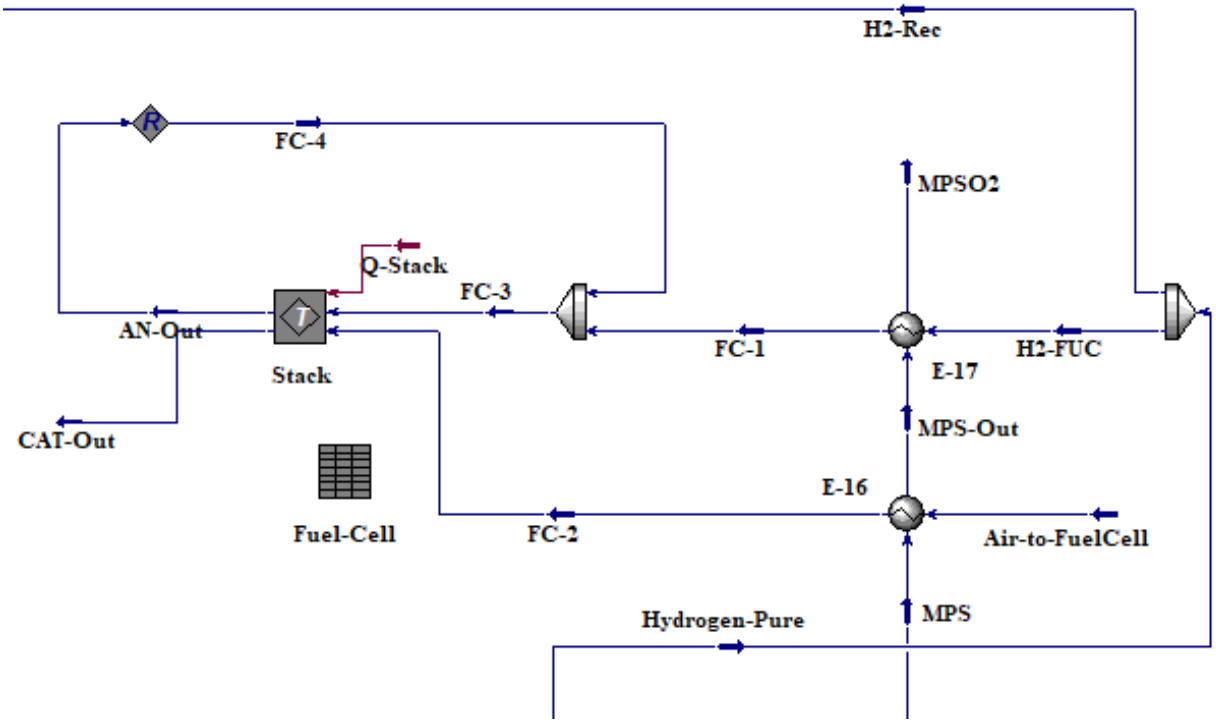

Figure 9. Schematic Simulation of the Fuel-Cell Section

Table 10. Summary of the Input and Output streams of Sour-Diesel Fuel to Power process

	Sour-Diesel	Hydrogen	M-4	Amine-Rec	Treated-Hydrogen	M-24	M-26	D-Diesel	to-Burner
Vapor Fraction	0	1	1	0	1	1	0	0	0
Temperature (°C)	25	25	251	45	45	87	266	266	266
Pressure (bar)	1.0	32.0	30.5	29.4	28.9	1.2	1.1	1.1	1.1
Molar flow (kgmole/h)	0.30	0.50	0.79	1.00	0.48	0.01	0.30	0.22	0.07
Mass Flow (kg/h)	63.00	1.04	64.03	29.17	1.00	0.21	62.71	47.00	15.71
Comp Mole Frac (Naphthalene)	0.13	0.00	0.05	0.00	0.00	0.00	0.13	0.13	0.13
Comp Mole Frac (n-C16)	0.85	0.00	0.32	0.00	0.00	0.00	0.85	0.85	0.85
Comp Mole Frac (DBT)	0.02	0.00	0.00	0.00	0.00	0.00	0.00	0.00	0.00
Comp Mole Frac (Hydrogen)	0.00	1.00	0.62	0.00	1.00	0.01	0.00	0.00	0.00
Comp Mole Frac (H_2S)	0.00	0.00	0.01	0.00	0.00	0.46	0.00	0.00	0.00
Comp Mole Frac (H_2O)	0.00	0.00	0.00	0.89	0.00	0.53	0.00	0.00	0.00
Comp Mole Frac (MDEA)	0.00	0.00	0.00	0.11	0.00	0.00	0.00	0.00	0.00
Comp Mole Frac (BiPhenyl)	0.00	0.00	0.01	0.00	0.00	0.00	0.02	0.02	0.02
	R1	**R2**	**R10**	**O_2-PROX**	**R16**	**Hydro-gen-Pure**	**CO_2+H_2**	**Air-to-FuelCell**	**CAT-Out**
Vapor Fraction	0	1	1	1	1	1	1	1	1
Temperature (°C)	268	750	202	25	50	50	65	50	190
Pressure (bar)	30.0	30.0	28.4	1.0	10.9	1.0	11.0	1.0	1.0
Molar flow (kgmole/h)	0.22	7.83	14.37	0.16	14.37	8.33	4.53	28.09	33.92
Mass Flow (kg/h)	47.00	141.00	188.01	5.03	193.03	16.79	147.86	810.66	834.15
Comp Mole Frac (Naphthalene)	0.13	0.00	0.00	0.00	0.00	0.00	0.00	0.00	0.00
Comp Mole Frac (n-C16)	0.85	0.00	0.00	0.00	0.00	0.00	0.00	0.00	0.00
Comp Mole Frac (Hydrogen)	0.00	0.00	0.66	0.00	0.66	1.00	0.25	0.00	0.00
Comp Mole Frac (Oxygen)	0.00	0.00	0.00	1.00	0.00	0.00	0.00	0.21	0.00
Comp Mole Frac (Nitrogen)	0.00	0.00	0.00	0.00	0.00	0.00	0.00	0.77	0.64
Comp Mole Frac (Argon)	0.00	0.00	0.00	0.00	0.00	0.00	0.00	0.01	0.01
Comp Mole Frac (H_2O)	0.00	1.00	0.12	0.00	0.12	0.00	0.03	0.01	0.35
Comp Mole Frac (CO)	0.00	0.00	0.02	0.00	0.00	0.00	0.00	0.00	0.00
Comp Mole Frac (CO_2)	0.00	0.00	0.20	0.00	0.23	0.00	0.71	0.00	0.00
Comp Mole Frac (Ethane)	0.00	0.00	0.00	0.00	0.00	0.00	0.00	0.00	0.00
Comp Mole Frac (BiPhenyl)	0.02	0.00	0.00	0.00	0.00	0.00	0.00	0.00	0.00

Table 11. Utility Consumption and Net Total Power Generation of the Process

Utility	Value	Unit
Cooling Water	32367.7	kg/h
LP Steam	4.1	kg/h
MP Steam	60.3	kg/h
HP Steam	41.5	kg/h
Net Power Generation	300	kW

(Table 12) compares the requirements for a purified hydrogen stream with the simulation results, highlighting the relative error for each component.

- Water: The simulation shows a 4% relative error, indicating a very close match to the requirement.
- Total Hydrocarbons: With a 5% relative error, the hydrocarbons are also very close to the required amount.
- Oxygen: The oxygen level in the simulation has a minimal deviation, with a 2% relative error.
- CO_2: The CO_2 level in the simulation shows a 10% relative error, which is slightly higher but still within an acceptable range.
- CO: The simulation matches the requirement exactly, resulting in a 0% relative error.
- Total Sulfur: The sulfur content has a relative error of 12.5%, indicating the need for some adjustment.

The average relative error across all components is 7.62%. This indicates that the simulation results are generally close to the required specifications for the purified hydrogen stream, with only minor deviations. The process appears to be well-calibrated, with the sulfur content being the only area requiring more attention.

Table 12. Comparison of Simulation Results with Purified Hydrogen Stream Requirements

	Requirements for Purified Hydrogen Stream (µmol/mol)	Simulation (µmol/mol)	Relative Error, %
Water	5	4.8	4
Total Hydrocarbons	2	1.9	5
Oxygen	5	4.9	2
CO_2	2	1.8	10
CO	0.2	0.2	0
Total Sulfur	0.004	0.0035	12.5
	Average Error		7.62

4.1. Environmental Impacts

Generating hydrogen, especially when CO_2 is emitted as a by-product, has notable environmental consequences. Evaluating the sustainability of hydrogen as an energy source depends heavily on this process. Hydrogen production via steam reforming of gas or liquid hydrocarbons releases significant CO_2, substantially contributing to global warming (Nowotny & Veziroglu, 2011). The retentate stream exiting the hydrogen purification unit (CO_2+H_2) enters the diesel reforming process. When combined with the diesel burned in the furnace, it generates a stack-gas, which acts as the conduit for all the CO_2 produced in the process. All the CO_2 is released through the stack-gas stream. (Table 13) provides the detailed specifications of the stack-gas stream, including its composition, temperature, pressure, and flow rate. This information is essential for understanding the environmental impact and efficiency of the process.

Table 13. Stack-Gas Stream Specifications

Properties	Stack-Gas
Vapor Fraction	1
Temperature (°C)	50
Pressure (bar)	1
Molar flow (kgmole/h)	4.63
Mass Flow (kg/h)	180.48
Comp Mole Frac (CO_2)	0.75
Comp Mole Frac (H_2O)	0.2
Comp Mole Frac (O_2)	0.05

In contrast, green hydrogen, produced using renewable energy sources, has a significantly lower environmental impact compared to hydrogen generated from fossil fuels (Amin et al., 2022). The environmental impact of hydrogen generation depends heavily on the production method. Fossil fuel-based methods, such as steam methane reforming, produce significant CO_2 emissions contributing to global warming. In contrast, green hydrogen production using renewable energy sources, coupled with CO_2 capture and storage technologies, can substantially reduce these emissions, making hydrogen a more sustainable energy source.

5. Conclusions

Hydrogen production faces significant challenges in transportation, making liquid fuel reforming an attractive solution. The ability to export liquid products efficiently and cost-effectively enhances the global accessibility of hydrogen. Utilizing process design software like Aspen HYSYS and PRO/II allows for efficient simulation and design of sour diesel fuel conversion processes, including membrane units. Liquid fuels, particularly diesel, offer promise for mid-term hydrogen production. However, developing a satisfactory hydrogen supply system remains critical for commercial viability. Diesel's attributes, including low cost, high hydrogen carrier potential, availability, ease of transportation, and high energy density, position it as an attractive option. Sulfur compounds in diesel must be removed before reforming to avoid catalyst poisoning. Steam reforming of liquid fuel offers a high hydrogen-to-carbon monoxide ratio, but carbon monoxide levels must be minimized, as they are toxic to catalysts and fuel cells. Fuel cells, with their high efficiency in converting chemical energy to electricity, provide a clean and efficient energy source. In a scenario where 63 kg/h of diesel is introduced into the process to produce 300 kW of net power from the fuel cell, the power consumption is 2.50 kW, with cooling water consumption at 32367 kg/h, LP steam consumption at 4.1 kg/h, MP steam consumption at 60.3 kg/h, and HP steam consumption at 41.5 kg/h. For future investigations, it is imperative to delve into advanced catalyst materials to optimize sulfur removal and reforming processes and explore innovative approaches for reducing carbon monoxide levels and enhancing the water-gas shift reaction. Developing integrated systems to maximize energy efficiency and minimize utility consumption should also be a priority. Furthermore, rigorous assessments of the scalability and economic viability of large-scale liquid fuel reforming processes, including ROI and Payback Period considerations, are essential. Lastly, there is a critical need to explore emerging technologies, such as hydrogen storage and distribution systems, to overcome existing hydrogen transportation and utilization challenges, ensuring a sustainable and economically viable energy future. Additionally, a more detailed comparison of hydrogen production from renewable sources and methods that do not produce secondary emissions (such as electrolysis) would be beneficial.

References

Amin, M., Shah, H. H., Fareed, A. G., Khan, W. U., Chung, E., Zia, A., Farooqi, Z. U. R., & Lee, C. (2022). Hydrogen production through renewable and non-renewable energy processes and their impact on climate change. International Journal of Hydrogen Energy, 47(77), 33112-33134.

Amphlett, J. C., Mann, R. F., Peppley, B. A., Roberge, P. R., Rodrigues, A., & Salvador, J. P. (1998). Simulation of a 250 kW diesel fuel processor/PEM fuel cell system. Journal of Power Sources, 71(1-2), 179-184.

Awad, S. A., Gheni, S. A., Abdullah, G. H., & Ahmed, S. M. R. (2020). Design and evaluation of a Co-Mo-supported nano alumina ultradeep hydrodesulfurization catalyst for production of environmentally friendly diesel fuel in a trickle bed reactor. ACS Omega, 5(21), 12081-12089.

Bacquart, T., Arrhenius, K., Persijn, S., Rojo, A., Auprêtre, F., Gozlan, B., Moore, N., Morris, A., Fischer, A., & Murugan, A. (2019). Hydrogen fuel quality from two main production processes: Steam methane reforming and proton exchange membrane water electrolysis. Journal of Power Sources, 444, 227170.

Bae, J., Lee, S., Kim, S., Oh, J., Choi, S., Bae, M., Kang, I., & Katikaneni, S. P. (2016). Liquid fuel processing for hydrogen production: A review. International Journal of Hydrogen Energy, 41(44), 19990-20022.

Bae, M., Cheon, H., Oh, J., Kim, D., Bae, J., & Katikaneni, S. P. (2021). Rapid start-up strategy of 1 kWe diesel reformer by solid oxide fuel cell integration. International Journal of Hydrogen Energy, 46(52), 26575-26581.

Brown, L. F. (2001). A comparative study of fuels for on-board hydrogen production for fuel-cell-powered automobiles. International Journal of Hydrogen Energy, 26(4), 381-397.

Castaldi, M. J. (2009). Removal of trace contaminants from fuel processing reformate: preferential oxidation (Prox). Hydrogen and Syngas Production and Purification Technologies; Liu, K., Song, C., Subramani, V., Eds, 329-356.

Cherif, A., Nebbali, R., Sheffield, J. W., Doner, N., & Sen, F. (2021). Numerical investigation of hydrogen production via autothermal reforming of steam and methane over Ni/Al_2O_3 and Pt/Al_2O_3 patterned catalytic layers. International Journal of Hydrogen Energy, 46(75), 37521-37532.

Creaser, D., Karatzas, X., Lundberg, B., Pettersson, L. J., & Dawody, J. (2011). Modeling study of 5 kWe-scale autothermal diesel fuel reformer. Applied Catalysis A: General, 404(1-2), 129-140.

Davó-Quiṇonero, A., Bailon-Garcia, E., Lopez-Rodriguez, S., Juan-Juan, J., Lozano-Castello, D., García-Melchor, M., Herrera, F. C., Pellegrin, E., Escudero, C., & Bueno-Lopez, A. (2020). Insights into the oxygen vacancy filling mechanism in CuO/CeO_2 catalysts: a key step toward high selectivity in preferential CO oxidation. ACS Catalysis, 10(11), 6532-6545.

Dawood, F., Anda, M., & Shafiullah, G. M. (2020). Hydrogen production for energy: An overview. International Journal of Hydrogen Energy, 45(7), 3847-3869.

Dolanc, G., Pregelj, B., Petrovčič, J., Pasel, J., & Kolb, G. (2016). Control of autothermal reforming reactor of diesel fuel. Journal of Power Sources, 313, 223-232.

Douglas, J. M. (1988). Conceptual design of chemical processes. (No Title).

Ersoz, A., Olgun, H., & Ozdogan, S. (2006). Reforming options for hydrogen production from fossil fuels for PEM fuel cells. Journal of Power Sources, 154(1), 67-73.

Fauteux-Lefebvre, C., Abatzoglou, N., Braidy, N., & Achouri, I. E. (2011). Diesel steam reforming with a nickel-alumina spinel catalyst for solid

oxide fuel cell application. Journal of Power Sources, 196(18), 7673-7680.

Geng, J., Guo, Q., Pan, J., Chi, B., & Pu, J. (2023). Enhanced stability of co-reforming diesel and methanol into hydrogen-enriched gases for solid oxide fuel cell application. Journal of Power Sources, 564, 232830.

Ghasemzadeh, K., Jafari, M., & Basile, A. (2017). Theoretical Study of Various Configurations of Membrane Processes for Olefins Separation. International Journal of Membrane Science and Technology, 4, 1-7.

Gonzalez, A. M., Lora, E. E. S., Palacio, J. C. E., & del Olmo, O. A. A. (2018). Hydrogen production from oil sludge gasification/biomass mixtures and potential use in hydrotreatment processes. International Journal of Hydrogen Energy, 43(16), 7808-7822.

Hoguet, J.-C., Karagiannakis, G. P., Valla, J. A., Agrafiotis, C. C., & Konstandopoulos, A. G. (2009). Gas and liquid phase fuels desulphurization for hydrogen production via reforming processes. International Journal of Hydrogen Energy, 34(11), 4953-4962.

Jafari, M., Deljoo, M. S., & Vatani, A. (2020). Simulation and Economic Evaluation of Polygeneration System for Coproduction of Power, Steam, CH_3OH, H_2, and CO_2 from Flare Gas. Iranian Journal of Oil and Gas Science and Technology, 9(4), 93-114. https://doi.org//10.22050/ijogst.2020.227023.1547

Jafari, M., & Garakani, A. K. (2021). Simulation and techno-economic analysis of hydrotreating process of mazut. Journal of Applied Research of Chemical-Polymer Engineering, 5(1), 17-30.

Jafari, M., & Khalili-Garakani, A. (2021). Techno-Economic Analysis of Heavy Fuel Oil Hydrodesulfurization Process for Application in Power Plants. Iranian Journal of Oil and Gas Science and Technology, 10(1), 40-65.

Jafari, M., Sarrafzadeh, M. H., & Deljoo, M. S. (2021). Economic Evaluation of Water Desalination and Power Generation Using Flare Gases of Assaluyeh. Iranian Journal of Gas Engineering, 8(1), 7-17. https://www.ijge.irangi.org/article_251915.html

Jafari, M., Sarrafzadeh, M.-H., & Ghasemzadeh, K. (2020). Simulation and economic evaluation of heat and power generation from flare gases in a combined cycle power plant. Energy Equipment and Systems, 8(4), 307-322.

Jafari, M., Vatani, A., Deljoo, M. S., & Khalili-Garakani, A. (2021). Techno-Economic Analysis of Flare Gas to Gasoline (FGTG) Process through Dimethyl Ether Production. Journal of Gas Technology, 6(2), 28-44. https://doi.org//jgt.irangi.org/article_251676.html

Jejurkar, S. Y., Khanna, A., & Verma, N. (2020). Maldistribution effects in an industrial-scale trickle bed reactor. Industrial & Engineering Chemistry Research, 59(16), 7405-7415.

Ješić, D., Erklavec Zajec, V., Bajec, D., Dolanc, G., Berčič, G., & Likozar, B. (2022). Computational investigation of auto-thermal reforming process of diesel for production of hydrogen for PEM fuel cell applications. International Journal of Energy Research, 46(12), 17068-17083.

Kaila, R. K., Gutiérrez, A., & Krause, A. O. I. (2008). Autothermal reforming of simulated and commercial diesel: The performance of zirconia-supported RhPt catalyst in the presence of sulfur. Applied Catalysis B: Environmental, 84(1-2), 324-331.

Le, T. T., Sharma, P., Bora, B. J., Tran, V. D., Truong, T. H., Le, H. C., & Nguyen, P. Q. P. (2023). Fueling the future: A comprehensive review of hydrogen energy systems and their challenges. International Journal of Hydrogen Energy.

Lee, Y.-L., Kim, K.-J., Hong, G.-R., & Roh, H.-S. (2023). Target-oriented water-gas shift reactions with customized reaction conditions and catalysts. Chemical Engineering Journal, 458, 141422.

Lindermeir, A., Kah, S., Kavurucu, S., & Mühlner, M. (2007). On-board diesel fuel processing for an SOFC-APU-Technical challenges for catalysis and reactor design. Applied Catalysis B: Environmental, 70(1-4), 488-497.

Lindström, B., Karlsson, J. A. J., Ekdunge, P., De Verdier, L., Häggendal, B., Dawody, J., Nilsson, M., & Pettersson, L. J. (2009). Diesel fuel reformer for automotive fuel cell applications. International Journal of Hydrogen Energy, 34(8), 3367-3381.

Liu, D.-J., Kaun, T. D., Liao, H.-K., & Ahmed, S. (2004). Characterization of kilowatt-scale autothermal reformer for production of hydrogen from heavy hydrocarbons. International Journal of Hydrogen Energy, 29(10), 1035-1046.

Martin, S., Kraaij, G., Ascher, T., Baltzopoulou, P., Karagiannakis, G., Wails, D., & Wörner, A. (2015). Direct steam reforming of diesel and diesel-biodiesel blends for distributed hydrogen generation. International Journal of Hydrogen Energy, 40(1), 75-84.

Nowotny, J., & Veziroglu, T. N. (2011). Impact of hydrogen on the environment. International Journal of Hydrogen Energy, 36(20), 13218-13224.

Pereira, C., Bae, J. M., Ahmed, S., & Krumpelt, M. (2000). Liquid fuel reformer development: autothermal reforming of diesel fuel. Argonne National Lab., IL (US).

Permatasari, A., Fasahati, P., Ryu, J.-H., & Liu, J. J. (2016). Design and analysis of a diesel processing unit for a molten carbonate fuel cell for auxiliary power unit applications. Korean Journal of Chemical Engineering, 33, 3381-3387.

Ramantani, T., Evangeliou, V., Kormentzas, G., & Kondarides, D. I. (2022). Hydrogen production by steam reforming of propane and LPG over supported metal catalysts. Applied Catalysis B: Environmental, 306, 121129.

Sahin, Z. (2008). Experimental and theoretical investigation of the effects of gasoline blends on single-cylinder diesel engine performance and exhaust emissions. Energy & Fuels, 22(5), 3201-3212.

Samsun, R. C., Pasel, J., Peters, R., & Stolten, D. (2015). Fuel cell systems with reforming of petroleum-based and synthetic-based diesel and kerosene fuels for APU applications. International Journal of Hydrogen Energy, 40(19), 6405-6421.

Samsun, R. C., Prawitz, M., Tschauder, A., Meißner, J., Pasel, J., & Peters, R. (2020). Reforming of diesel and jet fuel for fuel cells on a systems level: Steady-state and transient operation. Applied Energy, 279, 115882.

Wang, H., Zhao, H., & Zhao, Z. (2021). Thermodynamic performance study of a new SOFC-CCHP system with diesel reforming by CLHG to produce hydrogen as fuel. International Journal of Hydrogen Energy, 46(44), 22956-22973.

JOURNAL OF GAS TECHNOLOGY

Volume 8 /Issue 2/ Winter 2023 / Pages 74-83

Journal Home page: http://jgt.irangi.org

Investigating to Improving the Air-Cooled Condensers Performance (ACC) in Behbahan C.C.P.P

Masoud Dorfeshan[1*], Hamidreza Samipour[2,3]

1. Assistant Professor, Department of Mechanical Engineering, Faculty of Engineering, Behbahan Khatam Alanbia University of Technology, Behbahan, Iran
2. M.Sc. Student, Department of Mechanical Engineering, Faculty of Engineering, Behbahan Khatam Alanbia University of Technology, Behbahan, Iran
3. Senior Mechanical Expert of Behbahan Combined Cycle Power Plant Engineering Unit, Iran

ARTICLE INFO

ORIGINAL RESEARCH ARTICLE

Article History:
Received: 13 October 2023
Revised: 05 December 2023
Accepted: 17 December 2023

Keywords:
Air-cooled condenser
Combined cycle power plant
Efficiency improvement
Cooling system
Heat transfer
Fin tub

DOR: 20.1001.1/jgt.2024.2030988.1041

ABSTRACT

Combined cycle power plants are among the most efficient methods of electricity generation, utilizing a combination of gas and steam cycles to enhance energy efficiency. A crucial component in these power plants is the air-cooled condenser (ACC), which plays a significant role in cooling and converting the exhaust steam from the steam turbine back into water. However, the efficiency of air-cooled condensers is highly influenced by environmental conditions, particularly air temperature, humidity and wind speed, which can lead to a reduction in the overall efficiency of the power plant. This paper examines methods for improving the performance of air-cooled condensers in combined cycle power plants. It first addresses the challenges associated with the design and operation of these condensers under varying environmental conditions. Next, innovative solutions such as changing the angle of the blades, creating water spray paths at the inlet of the blades, and the washing of fin tubes and the evaluation of wind speed reduction methods are analyzed. The findings indicate that by adopting these strategies, it is possible to enhance the thermal efficiency of the power plant, reduce water consumption, and minimize operational costs. Recommendations for future research in the optimization and development of cooling technologies are also provided.

How to cite this article
H.R. Samipour, M. Dorfeshan, Investigating to Improving the Air-Cooled Condensers Performance (ACC) in Behbahan C.C.P.P. Journal of Gas Technology. 2023; 8(2): 74-83. (https://jgt.irangi.org/article_717005.html)

* Corresponding author.
E-mail address: dorfeshan@bkatu.ac.ir, (M. Dorfeshan).

Available online 31 December 2023

1. Introduction

Combined cycle power plants are among the most efficient methods for electricity generation, utilizing both gas and steam cycles to optimize energy use. A key component in these power plants is the air-cooled condenser (ACC), which plays a critical role in cooling the steam exiting the steam turbine and converting it back into water. While air-cooling systems offer significant water-saving advantages, especially in arid regions, their performance tends to decline under specific climatic conditions, particularly during high temperatures and strong winds (Bekker et al. 2022).

The air-cooled condenser of the Behbahan combined cycle power plant, operational since 2015, is designed to function within a temperature range of -4 °C to 50 °C and performs well under normal ambient conditions. However, over time, rising temperatures and strong winds have caused the vacuum pressure in the condenser to increase up to 400 mbar, leading to a reduction in the steam unit's power output. Similar to other power plants with air-cooled condensers, this performance degradation has affected the overall efficiency of the plant (Behbahan CCPP Documents).

Numerous studies have demonstrated that air-cooled condensers experience performance losses when exposed to crosswinds, particularly in areas with high wind speeds. It is evident that the performance of the fan array fluctuates with changing wind conditions, as the inflow and outflow of air through the fans are determined by these external factors. Consequently, both the heat transfer capacity between the turbine exhaust and the ambient air, as well as the back pressure of the power plant, are affected (Duvenhage and Kröger 1996). Due to this sensitivity to wind conditions, the performance of direct air-cooled power plants often deviates from the design specifications during adverse wind conditions. Therefore, it is crucial to investigate the impact of wind on power plant performance and understand the underlying principles of this influence (He et al. 2013 , Marincowitz et al. 2023).

In recent years, to enhance the efficiency of these systems, the use of water spray cooling systems has been proposed as a simple and cost-effective solution (Zeng et al. 2023). This approach, particularly during hot summer days, helps to increase steam turbine efficiency and mitigate the issues associated with high ambient temperatures.

In this paper, to identify an effective and optimal solution for improving the performance of the air-cooled condenser at the Behbahan combined cycle power plant, we investigate the implementation of water spray cooling and fin tube cleaning systems. The results are compared with performance curves, and the economic feasibility of these solutions is evaluated based on the specific conditions of the power plant.

This study aims to enhance the efficiency and stability of electricity generation in combined cycle power plants operating under similar climatic conditions.

2. The Impact of Inlet Airflow Behavior on Cooling System Performances

One of the critical parameters affecting the cooling capacity of the ACC cooling system is the behavior of the air drawn into the ACC fan inlet. While the inlet should be designed to minimize flow separation and ensure uniform distribution, the amount of airflow disturbance increases as wind speed rises. Given the importance of this issue, various studies have been conducted to enhance the cooling capacity of the ACC system by examining the losses in the fan inlet section and analyzing the airflow behavior.

Wind flow (Figure 1) can significantly reduce fan efficiency, leading to a decrease in megawatt output and lowering the reliability of key mechanical components, such as the gearbox, in the moving fans.

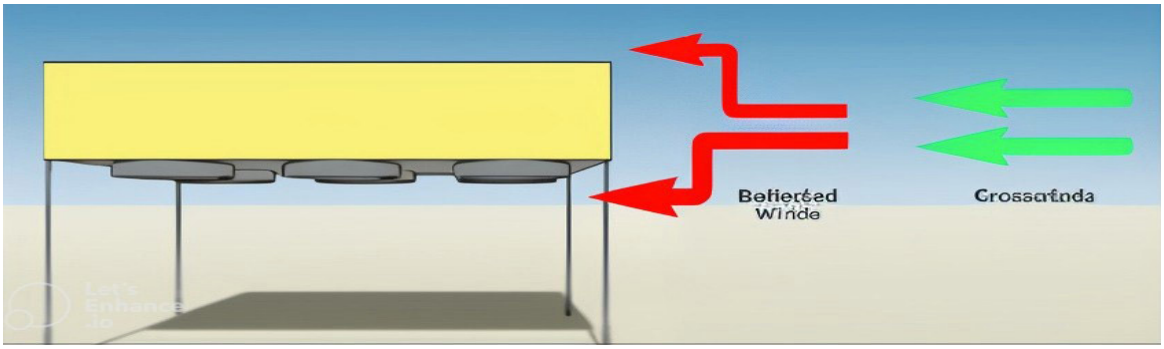

Figure 1. Cross Wind & Deflected Wind

Wind speed fluctuations can cause deviations in airflow, leading to an increase in the acceleration of wind flow. This acceleration causes flow separation at the fan inlet, resulting in an asymmetric distribution of airflow. As wind speed increases, the airflow becomes more turbulent, and the likelihood of the fan experiencing the stall phenomenon rises. Typically, fans are installed at a height of 35 to 40 meters above the ground, and wind power increases with height. For example, when wind speed is 3 meters per second at ground level, it can reach 12 to 15 meters per second at a height of 30 meters.

During normal fan operation, air enters around the fan blades and exits vertically. However, when the fan operates in high wind conditions, the inlet pressure decreases due to the wind direction, reducing the airflow through the fan. This results in increased mechanical stress on the fan and gearbox assembly. As the airflow through the fan decreases, the cooling capacity of the fan-and consequently the condenser-also diminishes. If wind speeds increase further, they can raise the back pressure, reducing the pressure at the fan inlet and impeding airflow. In severe cases, the airflow through the fan can drop to zero, leading to a stall, which can damage the fan and its mechanical components.

In the diagrams below, the operation of the fan is shown under normal conditions (Figure 2), in high wind conditions (Figure 3), and in strong wind conditions (Figure 4). As depicted in (Figure 4), airflow through the fan reaches zero due to strong winds, causing a stall and potential mechanical failure (Maulbetsch and DiFilippo 2008).

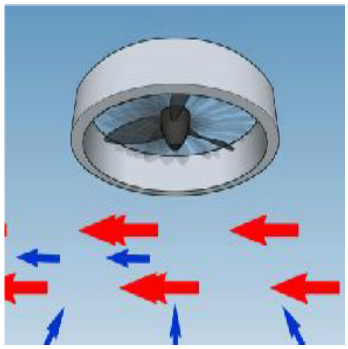

Figure 4- Strong Wind

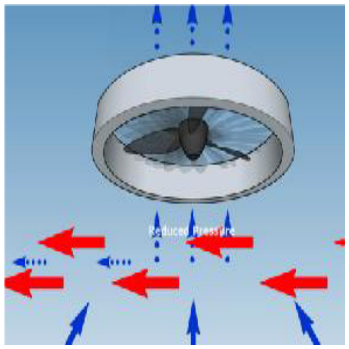

Figure 3- High Wind

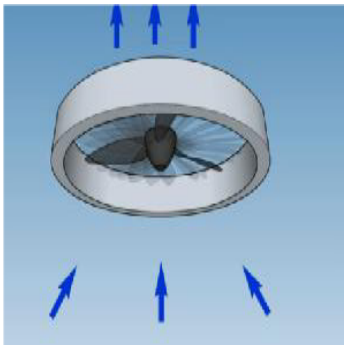

Figure 2- Normal State of the Fan

One solution to mitigate the effects of wind in the ACC system is the use of wind screens (Figure 5). These screens act as barriers against wind flow, reducing wind speed and ensuring a more even distribution of airflow at the fan inlet. Wind screens can be installed in two types: fixed and mobile. Due to their economic viability, wind screens are currently installed in many power plants around the world.

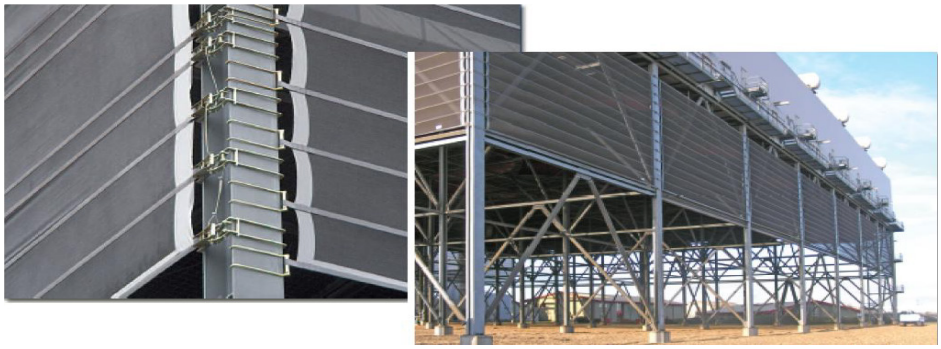

Figure 5. Molile wind Screen Implemented in some European Power Plants

As you can see in the (Figure 6), the back-pressure changes of the condenser are shown in two modes with and without the wind screen in Kings Lynn and Corryton power plants in England. For example, at a wind speed of 14 meters per second, the wind creates a difference in the back pressure of the condenser of approximately 20 millibars.

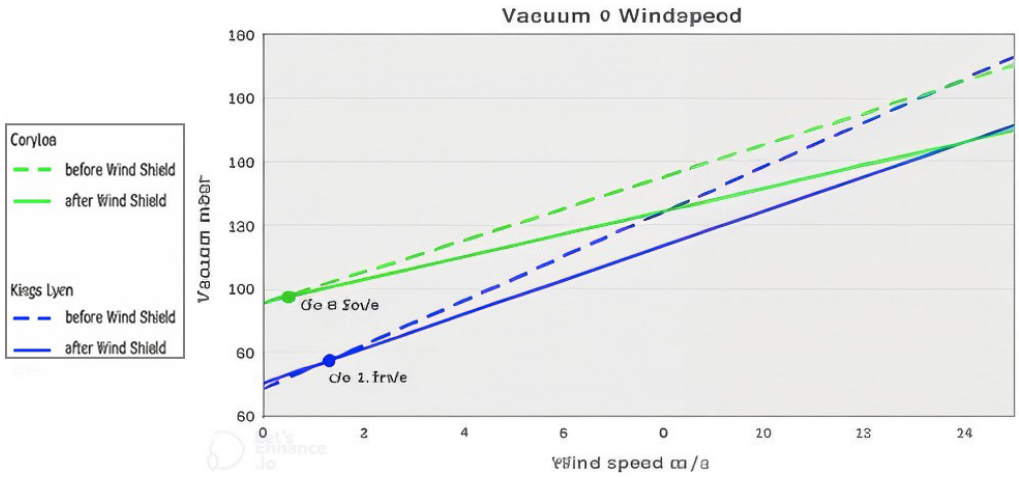

Figure 6. Two Modes for Back-Pressure Changes with and without the Wind Screen

Reducing the effects of increasing wind speed by installing a guide, as mentioned, is one of the major factors affecting the performance of the air condenser system (wind speed and direction), generally, the wind will have a negative effect on the performance of the condenser.

According to (Figure 7), this phenomenon increases the temperature of the air entering the fan, leading to a decrease in the cooling system's performance due to the recirculation of hot air back into the fan. The most significant negative impact of this phenomenon occurs on the fans positioned downstream of the wind flow, particularly along the side walls of the deltas (Yang et al. 2011). Therefore, to enhance the performance of the fans against this issue, the implementation of a retaining wall or guide, as shown in (Figure 8), is recommended.

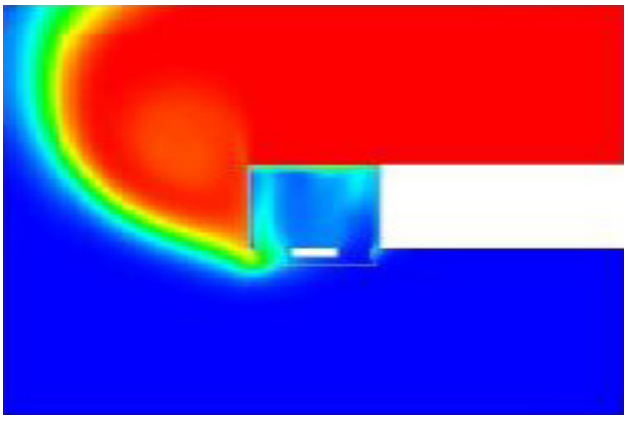

Figure 7. A View of the Thermal Effect on the Fan

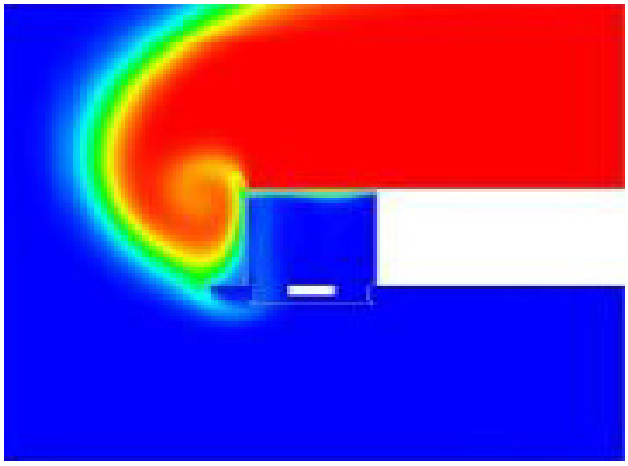

Figure 8. A View of the Thermal Effect on the Fan with a Retaining Guide

3. Comparison of Condenser Performance with the Back-Pressure Curve

As the ambient temperature rises, the subcooling temperature (the difference between the steam input and condensate output temperatures) decreases, leading to a reduction in condenser efficiency. For instance, in (Table 1), the actual operating conditions of the system are compared with the Back-pressure performance curve at 110% of the cycle (where the warranty conditions at 110% of the cycle are set at 12 kPa). Additionally, the gas units are operating in Base Load mode to maintain the steam flow as close as possible to the design conditions.

Table 1. Comparison between Actual Condenser Vacuum and Performance Curve

Deviation of the Vacuum from the Curve	Back Pressure Curve(mbar)	Condenser Vacuum (mbar)	Wind Speed m/s	Temperature	Hour	Date
OK	170	177	2.6	33	08:35	01/09/2021
OK	210	207	1.3	38	10:50	01/09/2021
30 mbar deviation	180	216	5	35	03:10	02/09/2021
50 mbar deviation	300	352	8.3	45	10	27/07/2021
50 mbar deviation	330	386	13	48	12	27/07/2021
30 mbar deviation	270	306	4.8	44	12	26/07/2021
Run Back	300	405	10	45	16:30	04/09/2021

Based on the recorded data and plotting it on the power plant performance diagram (Figure 9) (Behbahan CCPP Document), it is observed that under normal conditions, when the system operates with a wind speed below 4 meters per second, it follows the expected performance curve. However, as wind speed increases, the system's behavior becomes unpredictable, leading to conditions that approach the runback set point (400 mbar) (Li et al. 2018).

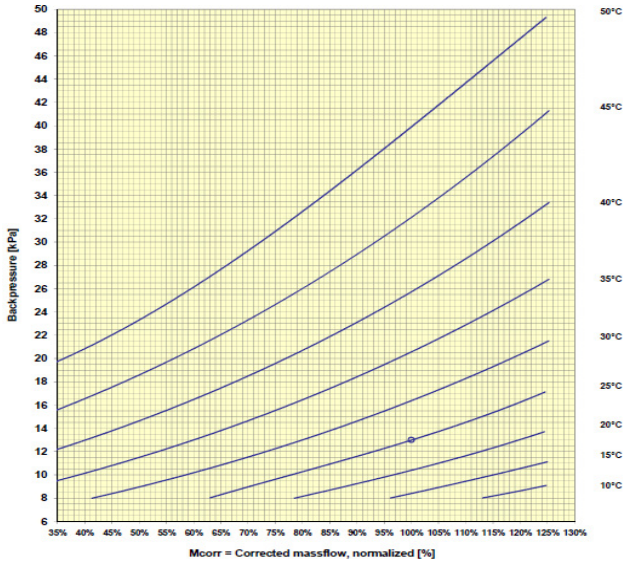

Figure 9. Behbahan CCPP Performance Curve

4. Checking the Implementation of the Water Spray Plan

Due to issues with the main cooling system during hot seasons and specific weather conditions, optimization suggestions were made. One of these suggestions was the implementation of a misting system, which was applied to twelve counterflow fans. This proposal was examined and analyzed from mechanical, electrical, water consumption, and financial perspectives. After performing the necessary calculations, a preliminary design was prepared, and it was decided to implement the misting system on one of the fans using 100 nozzles, each with a size of 0.4 mm.

Upon installation and testing of these 100 nozzles, it was found that at a pressure of 50 bar, the water consumption was approximately 9 liters per minute (Figure 10). Since the ACC washing skid was used for the misting system and this skid could generate a pressure of 50 bar with a flow rate of 180 liters per minute, it was decided to increase the number of nozzles from 100 to 200 and change their size from 0.4 mm to 0.7 mm.

After the misting system was implemented on twelve counterflow fans and tested, the following data (Table 2) were obtained for the system's flow rate and pressure.

Table 2. Water Consumption for the Implementation of the Fogging Plan

Water pressure (bar)	Water consumption (lit/min)
40	130
45	155
47	164
50	180

Considering that the nozzles used at a pressure of 45 bar have the best efficiency, so the tests were tried to be performed at this pressure.

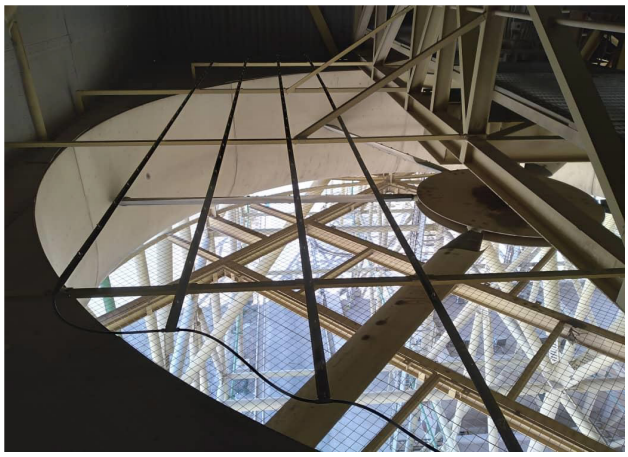

Figure 10. Plan Implemented in Behbahan CCPP

(After repeated tests and data mining in the obtained numbers, this result was obtained:

- Depending on the weather conditions, the temperature inside the fan chamber will decrease between 1.5 and 2.5 degrees Celsius.
- The humidity inside the fan compartment increases between 4 and 20% depending on the humidity of the environment.
- In different conditions, the vacuum pressure of the condenser decreases by 10 mbar (2%) on average.
- According to the formulas presented in the diagram below (Figure 11), in the range between 340 and 400 mbar condenser pressure, with a decrease of 10 mbar, the power of the steam turbine increases by approximately 70 kW.

In addition to the vacuum pressure of the condenser, the speed and direction of the wind also affects the efficiency of the misting system. Therefore, it is suggested to first think about measures to reduce the effect of wind and then focus on the issue of fogging.

In the worst weather conditions, the wind blows from the north and due to the dry nature of this wind, it reduces the humidity to 5% or less. In such a situation, the temperature exceeded 50 degrees, which made the fogging system ineffective (Xiao et al. 2018).

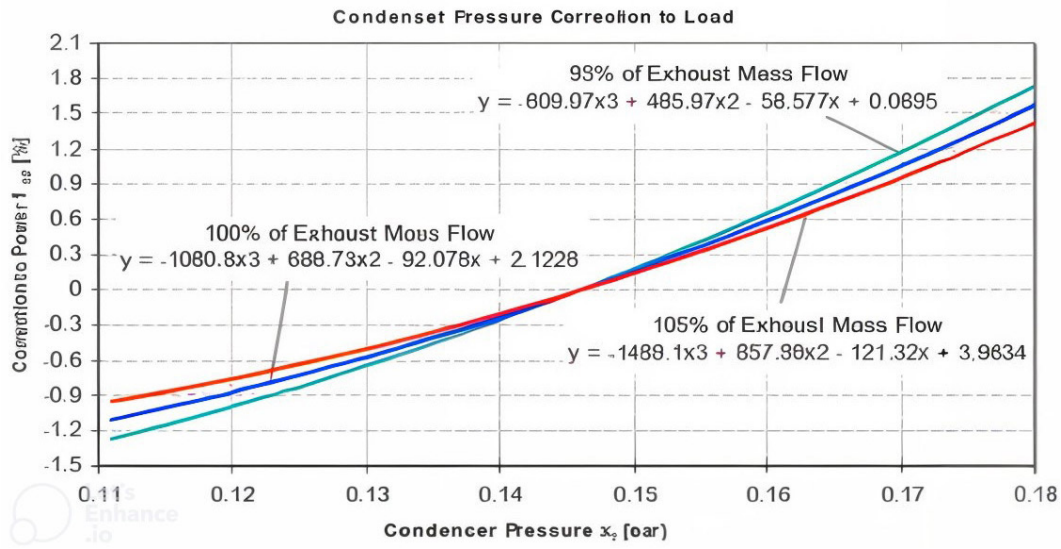

Figure 11. Condenser Pressure Correction to Load

5. Blade Angle Adjustment Testing

A test was conducted on a fan to change the blade angle, adjusting it from 6.4 degrees to 13 degrees based on the manufacturer's recommendation. However, without altering the fan speed, this adjustment was not feasible. It was determined that the limitations of the electric motor, along with the excessive vibration generated, prevented this adjustment from being successfully implemented.

Table 3. Fan Information

After the Change	Before the Change	
13 degrees	6.4 degree	Fan angle
500 m^3/h	500 m^3/h	Air flow rate
1270 rpm	1490 rpm	100% RPM
190 A	190 A	Nominal current of electric motors
180-195 A	140-160 A	Current of electric motors in 110% rotations

6. Investigating the Washing of Fin Tubes

The ACC washing system is commonly implemented in power plants worldwide. This system uses a positive displacement pump, operating at pressures between 40 and 80 bar, in combination with valve controls, to wash fin tubes efficiently and maintain optimal performance. (Figure 12) illustrates the implemented ACC washing system plan in the power plant, demonstrating how this method ensures the desired cleaning quality for the fin tubes.

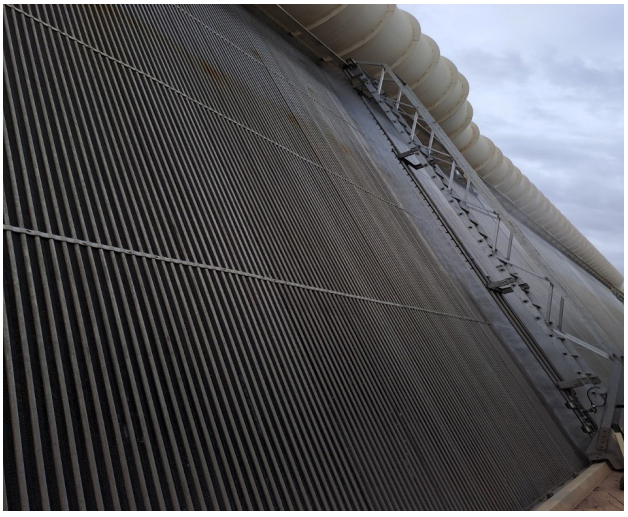

Figure 12. ACC Washing System

To evaluate the impact of ACC washing on condenser pressure, a comparison of the condenser vacuum before and after washing was conducted, using the performance curve as a reference (Table 4). The comparison was made under identical environmental conditions to ensure accuracy and consistency.

Table 4. Comparison Before & After Washing

	Performance Curve	Vacuum conditions at an ambient temperature of 35 degrees	Date	
41 mbar deviation	170 mbar	211 mbar	21/08/2021	Before washing the fin tubes
25 mbar improved	170 mbar	145 mbar	21/10/2021	After washing the fin tubes

7. Conclusion

Based on the investigations and the comparison of condenser pressure at Behbahan power plant with the ACC (Air-Cooled Condenser) system performance chart, it is evident that increased wind speed (both speed and direction) disrupts the system's performance, and under certain conditions, it leads to HRSG (Heat Recovery Steam Generator) runbacks, subsequently reducing the unit's production capacity. If the wind speed remains below 4 m/s, washing the ACC system significantly improves its performance.

Regarding the use of a misting system, tests at the power plant revealed that high water consumption is not a feasible solution given the region's geographical constraints. Additionally, higher wind speeds reduce the misting system's efficiency, leading to its cancellation. Other adverse effects include radiator clogging due to dust accumulation in the area.

Among the problems and challenges caused by changing the blade angle, the following can be mentioned:

- Increased tension in the blades and bolts: Adjusting the blade angle places greater stress on both the blades and the connection bolts, increasing the risk of blade failure under current conditions.
- Increased gearbox stress: The adjustment raises the load on the gearboxes, which presents significant problems due to the high cost of these components and the difficulty of their repair.
- Electric motor current limitations: The system's electric motors become a limiting factor, as increased blade angle demands higher current. While operation can continue up to the system's rated current, there is concern over whether the motors can sustain operation at this level consistently.
- Doubling of vibration levels: Structural vibrations increased by 100%, making it impossible to continue operating the system under these conditions.

Each fan uses 10 U-bolts, and according to the manufacturer's guidelines, new U-bolts must be installed after every adjustment due to the risk of wear and potential blade breakage. With each U-bolt costing $250, the total cost for adjusting a single fan amounts to $2,500. Additional expenses arise from gearbox depreciation, motor bearing replacement, blade failures, and other repairs, which further question the feasibility of this adjustment. While changing the blade angle may seem like a way to enhance performance, it introduces several technical challenges that outweigh the benefits. Combined with the high maintenance and repair costs, adjusting the blade angle is an impractical solution without further modifications to the system's mechanical and electrical components.

In conclusion, the potential benefits of adjusting the blade angle in air-cooled condenser fans are significantly outweighed by the accompanying technical challenges and costs. Increased stress on blades, bolts, and gearboxes, coupled with limitations in motor capacity and heightened vibration levels, pose serious risks to the long-term functionality and reliability of the system. Therefore, this approach is not feasible without major system modifications.

The installation of wind guides and deflectors, which show effectiveness in high wind conditions, lacks economic justification due to the high implementation cost compared to its benefits. Although such solutions to mitigate wind effects are part of modern practices in power plants globally, they have not been implemented in any of the country's plants. Basic studies and relevant calculations by consulting companies are necessary to evaluate the economic feasibility of such plans.

The estimated cost for implementing the project at the power plant is around $4.5 million. This should be weighed against the production losses caused by runbacks during the summer. In 2021, the energy loss due to HRSG runbacks, caused by adverse weather conditions, amounted to approximately 865MW (megawatts), equating to around $2,000 in lost production.

In the summer of 2021, wind speed alone was responsible for the runbacks, though in other cases, both temperature and wind speed contributed to the issue. Washing the ACC system reduced the time the boiler remained in runback conditions. Given that ACC washing improved system performance under the same temperature conditions as before (Table 4), and the total power loss due to temperature and wind speed is estimated at around $2,000, the cost of installing a wind wall ($4.5 million) lacks economic justification.

By analyzing the provided graphs (Behbahan CCPP Performance Curve), it is clear that, despite fewer fans operating after the ACC washing (Table 4), the vacuum improved significantly. This is notable since fewer fans typically result in higher vacuum levels. However, following the washing, not only did the vacuum improve at the same ambient temperature, but it also showed a substantial reduction compared to the ACC's performance curve. Prior to the washing, the condenser pressure was consistently higher than the pressure specified in the performance curve, while after washing, the vacuum level improved markedly.

In conclusion, the implementation of the ACC washing system has successfully reduced the condenser vacuum and enhanced performance, particularly by minimizing the number of HRSG runbacks during the hot season.

References

Baweja, M. and Bartaria, V.N., 2013. A review on performance analysis of air-cooled condenser under various atmospheric conditions. International Journal of Modern Engineering Research, 3(1), pp.411-414.

Behbahan CCPP Documents :

Air cooled condenser system cooling air fan technical data sheet

Air cooled condenser system overall system technical data sheet

Air cooled condenser system performance characteristic curve.

Bekker, G.M., Meyer, C.J. and Van der Spuy, S.J., 2022. Influence of pressure recovery on the performance of an induced draught air-cooled condenser under windless and windy conditions. Applied Thermal Engineering, 213, p.118703.

Duvenhage, K.K.D.G. and Kröger, D.G., 1996. The influence of wind on the performance of forced draught air-cooled heat exchangers. Journal of Wind Engineering and Industrial Aerodynamics, 62(2-3), pp.259-277.

He, W., Dai, Y., Zhu, S., Han, D., Yue, C. and Pu, W., 2013. Influence from the blade installation angle of the windward axial fans on the performance of an air-cooled power plant. Energy, 60, pp.416-425.

Li, J., Bai, Y. and Li, B., 2018. Operation of air cooled condensers for optimised back pressure at ambient wind. Applied Thermal Engineering, 128, pp.1340-1350.

Marincowitz, F.S., Owen, M.T.F. and Muiyser, J., 2023. Multi-objective optimisation for wind resistant air-cooled condenser operation. Applied Thermal Engineering, 218, p.119382.

Maulbetsch, J.S. and DiFilippo, M., 2008. Effect of wind speed and direction on the performance of air-cooled condensers. California Energy Commission: Sacramento, CA, USA.

Xiao, L., Ge, Z., Yang, L. and Du, X., 2018. Numerical study on performance improvement of air-cooled condenser by water spray cooling. International Journal of Heat and Mass Transfer, 125, pp.1028-1042.

Yang, L.J., Du, X.Z. and Yang, Y.P., 2011. Influences of wind-break wall configurations upon flow and heat transfer characteristics of air-cooled condensers in a power plant. International Journal of Thermal Sciences, 50(10), pp.2050-2061.

Zeng, Z., Li, Y., Shang, T. and Zhan, H., 2023. Effects of the atomisation spray on heating transfer in evaporative condensers: A numerical study. Thermal Science and Engineering Progress, 42, p.101923.

استفاده از یک سیستم خبره در انتخاب کاندیداهای مناسب برای عملیات اسیدکاری و مشاوره در زمینه آسیب‌های سازندی

- احمد ریگی[1]، محمد نوروزی دلاویز[1]، سامان جهان‌بخشی[2*]

۱. کارشناسی ارشد مهندسی نفت، شرکت مدیریت پروژه‌های صنعتی ابدال، مرکز فناوری مپصا، تهران، ایران

۲. استادیار، دانشکده مهندسی معدن، دانشکدگان فنی، دانشگاه تهران، تهران، ایران

(ایمیل نویسنده مسئول: jahanbakhshi@ut.ac.ir)

چکیـــــــده

درطول عمر یک چاه، عوامل متعددی نظیر کاهش فشار، مشبک‌کاری ناقص، جریان آشفته و آسیب سازندی، می‌توانند بهره‌وری چاه را به‌شدت تحت تأثیر قرار دهند. شناسایی و رسیدگی به این مشکلات، به‌ویژه آسیب‌سازندی، بسیار حیاتی است. عملیات اسیدکاری به‌طور معمول برای کاهش چنین آسیب‌هایی به کار گرفته می‌شود و معمولاً پس از انجام این عملیات، بهره‌وری چاه افزایش می‌یابد. عموماً، انتخاب چاه‌ها برای انجام اسیدکاری و شناسایی آسیب‌های سازندی بر پایه تجزیه و تحلیل‌های گسترده زمین‌شناسی و مهندسی استوار بوده است. این روش‌های سنتی، هر چند کامل، زمان‌بر هستند و شامل بررسی داده‌های پیچیده ژئوشیمیایی، ژئوفیزیکی و زمین‌شناسی می‌شوند. به همین علت، این مطالعه یک سیستم خبره را برای ساده‌سازی این فرآیندها معرفی می‌کند. سیستم‌های خبره به‌صورت خودکار و سریع به تجزیه و تحلیل داده‌ها پرداخته که موجب سرعت بخشیدن به تصمیم‌گیری و بهبود کارایی می‌شود. سیستم خبره توسعه‌یافته در این تحقیق، توانایی قابل‌توجهی در پردازش مجموعه‌های داده‌های پیچیده نشان می‌دهد و در نتیجه بهره‌وری را افزایش می‌دهد و احتمال خطاها را کاهش می‌دهد. توانایی پیش‌بینی سیستم‌های خبره همچنین امکان مدیریت پیشگیرانه چاه‌ها را فراهم می‌آورد. این تحقیق از یک سیستم خبره برای تحلیل ده چاه استفاده می‌کند و شش مورد را به‌عنوان نامزدهای مناسب برای عملیات اسیدکاری شناسایی می‌کند. این سیستم به‌طور مؤثر آسیب‌های احتمالی سازندی در این چاه‌ها را شناسایی می‌کند و دقت آن در تشخیص و تصمیم‌گیری را نشان می‌دهد. استفاده از سیستم‌های خبره در سناریوهایی با عدم قطعیت بالا که نیازمند تحلیل دقیق هستند، امیدوار کننده است. با بهره‌گیری از الگوریتم‌ها و مدل‌های ریاضی بیشتر معمول یا استاندارد، این سیستم‌ها می‌توانند فرآیندهای تصمیم‌گیری، دقت پیش‌بینی و کارایی عملیاتی در مخازن نفت و گاز را به‌طور قابل‌توجهی بهبود بخشند. بهبود تصمیم‌گیری یک مزیت کلیدی است زیرا این سیستم‌ها، با داده‌های جامع و تحلیل شده، امکان تصمیم‌گیری‌های آگاهانه‌تر و مؤثرتر را فراهم می‌آورند. در این مطالعه، یک سیستم خبره برای انتخاب چاه‌های مناسب برای عملیات اسیدکاری و تشخیص نوع آسیب‌های سازندی توسعه یافته است. از ده چاه تحلیل شده، شش مورد برای عملیات اسیدکاری مناسب شناخته شدند. توانایی این سیستم در شناسایی آسیب‌های احتمالی سازندی در هر چاه، کارایی آن را نشان می‌دهد. استفاده از این سیستم‌ها در مواردی با عدم قطعیت بالا و نیاز به مدل‌سازی دقیق، ارزشمند است و به بهبود کارایی عملیاتی و بهره‌وری در بخش نفت و گاز کمک می‌کند

واژگان کلیدی: سیستم‌های خبره، اسیدکاری خمیره، آسیب سازند، انتخاب کاندیدای اسیدکاری، بهره‌وری چاه

تولید غشای کامپوزیت پلی‌اترایمید/ZIF-8 برای جداسازی دی‌اکسید کربن از متان

- شیوا فلاحتی[1]، امید علیزاده[2*] و مسعود مختاری[3]

۱. دانشجوی کارشناسی ارشد، گروه شیمی و مهندسی شیمی، واحد رشت، دانشگاه آزاد اسلامی، رشت، ایران

۲. استادیار، گروه شیمی و مهندسی شیمی، واحد رشت، دانشگاه آزاد اسلامی، رشت، ایران

۳. استاد، گروه شیمی و مهندسی شیمی، واحد رشت، دانشگاه آزاد اسلامی، رشت، ایران

(ایمیل نویسنده مسئول: alizadeh@iaurasht.ac.ir)

چکیـــــــده

در این مطالعه، غشای کامپوزیت پلی‌اترایمید/ ZIF-8 به روش ریخته‌گری حلال تولید شد. طیف‌سنجی فوریه تبدیل مادون‌قرمز - بازتاب کاهش‌یافته (FTIR-ATR) غشای تهیه‌شده تأیید کرد که گروه‌های عاملی پلی‌اترایمید وجود دارند. پراش اشعه ایکس (XRD) نشان داد که ذرات افزودنی به‌خوبی در پلیمر پخش شده است که منجر به کاهش بلورینگی غشا شد. پراش اشعه ایکس پراکنده انرژی (EDAX) وجود و پخش مناسب ذرات روی در غشا را تأیید کرد. در نهایت، نتایج آزمون‌های عبور نشان داد که افزودن ZIF-8 به غشا به‌طور قابل‌توجهی میزان عبور و انتخاب‌پذیری آن را افزایش داده است. عبور غشای کامپوزیت برای گاز دی‌اکسید کربن GPU ۵/۹۱ بود، بیش از دو برابر غشای پلی‌اِتریمید خالص. علاوه بر این، عبور گاز متان GPU ۰/۳۱ بود که نشان‌دهنده بهبود قابل‌توجهی نسبت به نفوذیت غشای خالص با عبور GPU ۰/۱۷ بود. همچنین، انتخاب‌پذیری دی‌اکسید کربن/متان هم از ۱۵/۳ در غشای خالص به ۱۹/۱ در غشای کامپوزیت افزایش یافت. در نتیجه، این مطالعه نشان داد که افزودن ZIF-8 به ماتریس پلی‌اِتریمید می‌تواند کارایی غشای کامپوزیت حاصل را در جداسازی CO_2 از CH_4 بهبود بخشد. این بهبود انتخاب‌پذیری را می‌توان بیش از همه به افزایش ضریب حلالیت دی‌اکسید کربن نسبت به متان در غشای کامپوزیت ارتباط داد.

واژگان کلیدی: پلی‌اترایمید، غشای ماتریس آمیخته، ZIF-8، جداسازی گاز

شبیه‌سازی و ارزیابی اقتصادی بازیافت گاز مشعل با استفاده از نانوجاذب‌ها

- میثم بیژنی خو[1]، زهره سعادتی[2*]، افسانه ملکی[2]

۱. دانشجوی دکتری، گروه شیمی، واحد امیدیه، دانشگاه آزاد اسلامی، امیدیه، ایران

۲. دانشیار، گروه شیمی، واحد امیدیه، دانشگاه آزاد اسلامی، امیدیه، ایران

(ایمیل نویسنده مسئول: zo.saadati@iau.ac.ir)

چکیـــــــده

صنعت نفت و گاز با انتشار روزافزون گازهای مشعل که ناشی از گسترش جهانی صنعت و افزایش مصرف سوخت فسیلی در پالایشگاه‌ها و کارخانه‌های پتروشیمی است، با چالشی حیاتی مواجه است. اثرات زیست محیطی قابل توجه این انتشار گازهای مشعل، نیاز مبرمی به توسعه استراتژی‌های مؤثر برای به حداقل رساندن خطرات زیست محیطی مرتبط ایجاد کرده است. با این حال، پیاده‌سازی فن‌آوری‌هایی برای کاهش انتشار گازهای مشعل، موانع اقتصادی و زیست‌محیطی را به همراه دارد. در این مطالعه، ما کاربرد نانوجاذب‌ها را در برج‌های آکنده به‌عنوان یک رویکرد امیدوارکننده برای بازیابی و استفاده مجدد از گازهای مشعل بررسی کردیم. با استفاده از نرم‌افزار MATLAB، دو مطالعه موردی را برای ارزیابی عملکرد جاذب‌های مختلف، از جمله ژل‌های سیلیکا Ws، H و همچنین یک غربال مولکولی 4Å، برای بازیابی و تبدیل گازهای مشعل ترش به گاز شیرین و مرطوب انجام دادیم. تجزیه و تحلیل نشان داد که مدل ایزوترم لانگمویر مناسب‌ترین نتایج شبیه‌سازی را ارائه می‌کند که امکان‌سنجی فنی و اثربخشی این رویکرد را نشان می‌دهد..

واژگان کلیدی: جاذب، ژل سیلیکا، غربال مولکولی، شبیه‌سازی مشعل، گاز طبیعی

طراحی و شبیه‌سازی تولید هیدروژن از ریفرمینگ دیزل برای کاربردهای پیل سوختی

- مصطفی جعفری[۱]، مجید خورشیدیان[۲*]، مظاهر رحیمی اسبوئی[۳]، وحید کرد فیروزجائی[۲]، علی وطنی[۴]

۱. پژوهشگر، موسسه گاز طبیعی مایع (I-LNG)، دانشکده مهندسی شیمی، دانشکده فنی، دانشگاه تهران، تهران، ایران

۲. پژوهشگر، دانشگاه صنعتی مالک اشتر، پژوهشکده علوم و فناوری شمال، فریدونکنار، ایران

۳. استادیار، دانشگاه صنعتی مالک اشتر، پژوهشکده علوم و فناوری شمال، فریدونکنار، ایران

۴. استاد، موسسه گاز طبیعی مایع (I-LNG)، دانشکده مهندسی شیمی، دانشکده فنی، دانشگاه تهران، تهران، ایران

(ایمیل نویسنده مسئول: khorshidian@mut.ac.ir)

چکیـــــــده

تولید هیدروژن با چالش‌های قابل توجهی در حمل و نقل و ذخیره‌سازی مواجه است، مانند نشت، ایمنی در حین انتقال و نیاز به شرایط ذخیره‌سازی کارآمد. تولید در محل از طریق ریفرمینگ سوخت دیزل یک راه‌حل امیدوارکننده به شمار می‌رود به دلیل مقرون‌به‌صرفه بودن، دسترسی آسان و سهولت حمل و نقل دیزل. با این حال، گوگرد و مونوکسید کربن موجود در دیزل باید حذف شوند تا از کاتالیزورهای دخیل در این فرآیند محافظت شود. این مطالعه یک فرآیند مفهومی برای ریفرمینگ دیزل حاوی گوگرد به‌منظور تولید ۳۰۰ کیلووات برق در یک سیستم پیل سوختی را با استفاده از روش داگلاس طراحی می‌کند، که طراحی فرآیند شیمیایی را به یک سلسله مراتب تصمیم‌گیری سازماندهی می‌کند. این سلسله مراتب با ساختار ورودی-خروجی شروع می‌شود و فرآیند را با جزئیات دادن به جریان‌های ورودی و خروجی بر اساس متغیرهای طراحی تعیین شده خلاصه می‌کند. ساختار جریان بازیافتی فرآیند را به بخش‌های راکتور و جداسازی تقسیم می‌کند، که هر کدام جریان‌های بازیافتی تعریف شده‌ای را در برمی‌گیرند. در نهایت، ساختار کلی بخش جداسازی، سیستم‌های بازیافت گاز و مایع را ادغام می‌کند و یک استراتژی جامع برای طراحی واحدهای جداسازی ارائه می‌دهد. نمودار جریان فرآیند (PFD) ابتدا توسعه یافت و سپس از طریق شبیه‌سازی با استفاده از نرم‌افزار Aspen HYSYS به‌دقت تحلیل شد. نتایج نشان می‌دهد که تولید ۳۰۰ کیلووات برق به ۱۷ کیلوگرم در ساعت هیدروژن خالص نیاز دارد که مستلزم ۴۷ کیلوگرم در ساعت دیزل بدون گوگرد است. به‌طور کلی، ۶۰ کیلوگرم در ساعت دیزل مورد نیاز است. تحقیقات آینده باید بر بهینه‌سازی حذف گوگرد، کاهش سطح مونوکسید کربن، بهبود واکنش تغییر آب-گاز، به حداکثر رساندن بهره‌وری انرژی و ارزیابی قابلیت اقتصادی، از جمله بازگشت سرمایه و دوره بازپرداخت، متمرکز شود.

واژگان کلیدی: دیزل، ریفرمینگ، هیدروژن، سلول سوختی، برق، اسپن هایسیس

بررسی بهبود عملکرد کندانسورهای هوا خنک (ACC) در نیروگاه سیکل ترکیبی بهبهان

- مسعود درفشان[1*]، حمیدرضا سمیع پور[2,3]

۱. استادیار، گروه مهندسی مکانیک، دانشکده فنی و مهندسی، دانشگاه صنعتی خاتم الانبیاء بهبهان، بهبهان، ایران

۲. دانشجوی کارشناسی ارشد، گروه مهندسی مکانیک، دانشکده فنی و مهندسی، دانشگاه صنعتی خاتم الانبیاء بهبهان، بهبهان، ایران

۳. کارشناس ارشد مکانیک، واحد مهندسی، نیروگاه سیکل ترکیبی، بهبهان، ایران

(ایمیل نویسنده مسئول: dorfeshan@bkatu.ac.ir)

چکیـــــــده

نیروگاه‌های سیکل ترکیبی یکی از کارآمدترین روش‌های تولید برق هستند که از ترکیب چرخه‌های گاز و بخار برای افزایش بهره‌وری انرژی استفاده می‌کنند. یکی از اجزای مهم در این نیروگاه‌ها کندانسور هوا خنک (ACC) است که نقش مهمی در خنک سازی و تبدیل بخار خروجی از توربین بخار به آب دارد. با این حال، راندمان کندانسورهای هوا خنک به شدت تحت تأثیر شرایط محیطی، به ویژه دمای هوا، رطوبت و سرعت باد است که می‌تواند منجر به کاهش راندمان کلی نیروگاه شود. این مقاله روش‌هایی را برای بهبود عملکرد کندانسورهای هوا خنک در نیروگاه‌های سیکل ترکیبی بررسی می‌کند. ابتدا به چالش‌های مرتبط با طراحی و عملکرد این کندانسورها در شرایط محیطی متفاوت می‌پردازد. در ادامه راه‌حل‌های ابتکاری مانند تغییر زاویه تیغه‌ها، ایجاد مسیرهای پاشش آب در ورودی تیغه‌ها و شستشوی لوله‌های پره و ارزیابی روش‌های کاهش سرعت باد مورد تجزیه و تحلیل قرار می‌گیرد. یافته‌ها حاکی از آن است که با اتخاذ این استراتژی‌ها می‌توان بازده حرارتی نیروگاه را افزایش داد، مصرف آب را کاهش داد و هزینه‌های عملیاتی را به حداقل رساند. توصیه‌هایی برای تحقیقات آینده در بهینه‌سازی و توسعه فناوری‌های خنک کننده نیز ارائه شده است.

واژگان کلیدی: کندانسور هوا خنک، نیروگاه سیکل ترکیبی، بهبود بهره‌وری، سیستم خنک‌کننده، انتقال حرارت، لوله پره‌دار

JOURNAL OF GAS TECHNOLOGY
VOLUME 8 • ISSUE 2 • WINTER 2023
EISSN: 2588-5596

Contents